2-1-2016

# A sustainable complex fenestration system using recycled plastics

Islam Ayman Mashaly

THE AMERICAN UNIVERSITY IN CAIRO
الجامعة الأمريكية بالقاهرة


# A SUSTAINABLE COMPLEX FENESTRATION SYSTEM USING RECYCLED PLASTICS

**A Thesis Submitted to**

**Sustainable Development Program**

**In partial fulfilment of the requirements for the degree of**

## Master of Science in Sustainable Development

by

**Islam Ayman Mashaly**
B.Sc. in Building Engineering, Ain Shams University

**Under the Supervision of:**

**Dr. Khaled Nassar**
Associate Professor, Construction Engineering Department
The American University in Cairo

**Dr. Salah El Haggar**
Professor and Chairman, Mechanical Engineering Department
The American University in Cairo

**July 2016**

*To my amazing family,*

*My wonderful wife Yussra*

*& my best friends.*

# Acknowledgements

First, I would like thank my advisors Dr. Khaled Nassar and Prof Salah El-Haggar for their tremendous effort in all the phases of my thesis. Dr. Khaled Nassar directed me and helped me to stay focused on the thesis topic, I attribute the level of my Master's degree to his encouragement and effort. Prof. Salah El-Haggar greatly supported me in bringing my thesis work to live by allowing me to use the Waste Management lab and guided me patiently through my research until I managed to create a successful prototype.

I would also like to thank my thesis examination board, Dr. Ahmed Fekry and Dr. Khaled Tarabieh who ,with their passionate participation and advice, ensured that my thesis work is well presented.

I would also like to thank the AUC Waste Management lab associate Eng. Mohamed Saeed for his keen work and practical advice which helped in producing a physical prototype as a proof of concept for my thesis work.

Moreover, I must express my deepest gratitude to my parents and family for providing me with unfailing support and encouragement throughout the period of research and writing this thesis. In particular, I would like to thank my sister Sarah for proof reading my thesis writing.

Finally, I must profoundly express my gratitude to my wife and best friend, Yussra Rashed, without whose love, encouragement and editing assistance, I would not have finished this thesis. She has been my main source of motivation.

# Abstract

## A Sustainable Complex Fenestration System using Recycled Plastics

Daylighting in built spaces has several benefits. It helps in reaching satisfactory levels of energy consumption by reducing the usage of artificial lighting. Furthermore, daylighting is also a major contributor in altering the visual comfort of occupants. Consequently, it boosts occupants' concentration and productivity, which affects their performance in work tasks. However, an inadequately designed daylighting scheme leads to excessive solar heat gain, especially in hot and arid climates, increasing the temperature of interior spaces. In addition, due to the high solar altitudes in summer, the direct sunlight may fall right beneath the fenestration system and will not reach the depth of the space this phenomena is known as the "cave effect". Many proposed designs of blinds, louvers, shades and low emitting glass panels, tackled the side effects of the summer sun; on the other hand, a few of the proposed solutions incorporated the use of recycled materials, for an added sustainable value.

The aim of this thesis is to achieve a sustainable complex fenestration system (CFS) design that can diffuse and redirect the direct daylight component through an optimized pattern on its translucent layer. The CFS will comprise recycled plastic waste, which results from the conventional household waste. The recycled plastic waste will be used as a translucent material, with an optimized prismatic array design, to ensure adequate daylighting in hot climate desert areas.

An optimization model for designing a prismatic panel is developed to meet the objective of minimizing sun light near the window and redistributing the sunlight to the depth of the space, while a ray tracing program is used to validate the developed model's results. Furthermore, Radiance, a validated ray tracing simulation program, is used to produce accurate analysis with detailed hourly illuminance measurements throughout the year for the proposed CFS design using the five-phase method. Finally, a physical small scale model is developed to prove the viability of the CFS using three different recycled plastics, polystyrene (PS), polycarbonate (PC) polypropylene (PP).

The proposed design succeeded to improve the daylight performance by redirecting an average of 50% of the direct light to an upward direction, thus levelling the daylight within the room depth. The physical prototype exhibits great performance in the redirection of daylight into deep areas of the room especially at high solar altitudes. Polycarbonate proved to be the best of the three tested recycled plastic followed by the polystyrene, while polypropylene needs further research to develop a more feasible product.

# Contents

# List of Figures

# List of Tables

# List of Abbreviations

The following defines the connotation of various abbreviations and acronyms used throughout the thesis.

| | |
|---|---|
| **ASE** | Annual Sunlight Exposure |
| **BRDF** | Bidirectional Reflectance Distribution Function |
| **BSDF** | Bidirectional Scattering Distribution Function |
| **CAD** | Computer Aided Design |
| **CFS** | Complex Fenestration System |
| **CIE** | Commission Internationale de l'Eclairage (Int. Commission of Illumination) |
| **DA** | Daylight Autonomy |
| **$DA_{con}$** | continuous Daylight Autonomy |
| **DF** | Daylight Factor |
| **EA** | Evolutionary Algorithm |
| **EPS** | Expanded Polystyrene |
| **HDPE** | High-Density Polyethylene |
| **$I_{crit}$** | Critical Angle Of Incident |
| **IES** | Illuminating Engineering Society |
| **LEED** | Leadership in Energy and Environmental Design |
| **PC** | Polycarbonate |
| **PET** | Polyethylene Terephthalate |
| **PMMA** | Polymethyl methacrylate |
| **PP** | Polypropylene |
| **PS** | Polystyrene |
| **RPC** | Recycled Polycarbonate |
| **RPP** | Recycled Polypropylene |
| **RPS** | Recycled Polystyrene |
| **SA** | Solar Altitude |
| **sDA** | Spatial Daylight Autonomy |
| **SEM** | Standard Error of the Mean |
| **SHGC** | Solar Heat Gain Coefficient |
| **TIR** | Total Internal Reflection |
| **Tvis / VT** | Visible Transmittance |
| **UDI** | Useful Daylight Illuminance |
| **USGBC** | United States Green Building Council |

# **CHAPTER 1:**
# INTRODUCTION

# Chapter 1: Introduction

## 1.1 Importance of Daylighting

Daylighting is considered one of the most effective components in building and architecture sustainable design processes (Ihm, Nemri, & Krarti, 2009). It is a passive strategy to regulate the illumination inside spaces and improve energy performance within any living space (Lim, Kandar, Ahmad, Ossen, & Abdullah, 2012). Since daylight spectrum is the most adequate for human visual response, it contributes to the humans' health productivity and comfort (Cheung & Chung, 2008). Daylighting is believed to have a more positive effect than artificial daylighting in terms of psychological comfort (Cuttle, 1983). It is believed that daylighting can lower the risk of many human diseases such as skin diseases as well as psychological conditions like jetlag, seasonal affective disorder (SAD), circadian rhythm sleep disturbances and depression. (van Hoof, et al., 2012).

Not only does daylighting improve occupants' health, but it also remarkably lowers the energy consumption of buildings through its light and thermal energy. Around 20% to 40% of developed countries' energy consumption is dedicated to both commercial and residential buildings. This energy is used in space cooling and heating (in residential buildings) and illumination (in commercial building) (Bülow-Hübe, 2001) (Perez-Lombard, Ortiz, & Pout, 2008), both energy consuming elements can be improved by effective daylight design.

Windows and fenestration systems largely contribute to the energy consumption and illumination of buildings where it is believed that around 20-40% of energy gained is sourced from the buildings' envelope openings (Hee, et al., 2015), while 60% of energy loss from the building is through the envelope openings (Fabric energy efficiency for zero carbon homes - A flexible performance standard for 2016, 2014).Therefore it is crucial to carefully design and develop the fenestration system of a building envelope to ensure maximum energy saving and optimum comfort environments for occupants.

## 1.2 Excessive Daylighting Issues

Although daylighting plays an essential role in energy saving and increasing the illumination inside the built space, daylighting has its drawbacks if excessively present within a space, especially in hot arid climates and low solar altitude regions such as Egypt.

Due to the inconsideration of some designers to proper daylight design, lateral illumination in summer results in non-uniform distribution of light all over the room. This results from large fenestration openings, which allows excessive sunlight within the room and causes acute contrast between the source of light and the surrounding surfaces, or small opening designs that it causes high difference in illumination intensity between the area near from the light source and the area far from the source. The latter is known as the cave effect, which results in glare. The glare is described as visual discomfort that affects the performance of the occupants.

In summer, the sun tends to have higher radiation levels, therefore more heat gain passes through the windows increasing the heat load within the space, to neutralize, high cooling loads are needed, and therefore more energy consumption is needed.

Therefore it is crucial to adequately design our fenestration systems in order to ensure proper daylighting and benefit from the presence of daylight rather than preventing it. Unfortunately, many common practices in Egypt tend to overlook the benefits of daylighting and design an inadequately small fenestration area that doesn't allow proper sunlight and causes the previously illustrated effects. The Egyptian energy code recommends the window to wall area ratio should not exceed 30% in northern facades, and 18-22% in southern facades, which is considerably a small value to illuminate large spaces (Housing and Building Research Center, 2006).

## 1.3 Recycling plastic in Egypt

"Plastic recycling is still a relatively new and developing field of recycling. The post-consumer items made from PET and HDPE resins have found reliable markets within the US and in ASIA" (Connecticut Metal Industries Inc., 2005).

The volume of plastic wastes from the Egyptian household, mainly as packaging wastes, constitutes about 50% of the total national plastic waste from all sectors. Around 80%-90% of those consumer products' plastics are (1) PET (polyethylene terephthalate), (2) HDPE (high-density polyethylene), (3) V (vinyl), (4) LDPE (low-density polyethylene), (5) PP (polypropylene), (6) PS (polystyrene), and (7) PVC (poly-vinyl chloride).Milk and detergent bottles are the most popular products produced from postconsumer HDPE. Polypropylene is used as transparent food containers. While PET is used in making mineral water, cooking oil bottles and Soda.

Recycled PET is the most commonly utilized type of plastic in some industries and markets. One of the important markets are the textiles, carpet manufacturing companies use up to 100% recycled resin in their polyester carpets. (El Haggar, 2007)

The Zabbaleen area is one of the most influential areas in recycling in Cairo, their economy mainly depends on wastes from all over Cairo. The Zabbaleen area recycling system is highly efficient with an 80% recovery rate that economically benefits more than 40,000 individuals in Cairo. (Iskandar, 2003) However, with recent policies and regulations that forced relocation of the Zabbaleen communities to remote areas, the government's contract with international collectors and the presidential decree ordering the cull of the entire pig-raising in waste treatment herd, due to the rise of the H1N1 influenza global epidemic (Furniss, 2015), the Zabbaleen business has been going downstream. This affected all waste collection, treatment and recycling processes in greater Cairo, eventually leading to more plastic waste.

## 1.4 Limitation of using state-of-the-art technology fenestration systems in Egypt

Although many innovative solutions, that will be discussed in the literature review section, have been created to provide adequate illumination in rooms and prevent thermal heat losses/gains, most of those solutions

require complex designing and manufacturing processes. Moreover most of the materials used in such systems are either synthesized or uneconomical to use in Egypt. Therefore, most of those solutions, despite their positive environmental impact, are not considered sustainable to the Egyptian environment due to their low economic value.

## 1.5 Thesis Significance

This thesis aims to contribute to the implementation of a low cost glazing system with high quality of indoor environment and illumination. Focus will be on the design development of the system, taking into consideration the Egyptian conditions which comprise the economic state, material availability, social and environmental aspects. The intent is to contribute to the development of the glazing systems in Egypt, where lack of designing adequate systems and resources utilization is present. With the significance of energy scarcity in Egypt and the presence of limitless amounts of unutilized plastic waste, it is opportunistic to investigate creating a solution targeting both problems.

## 1.6 Thesis Hypothesis

The objective of this research project, however, has to be defined in more specific and operational terms to be pursued in a scientific manner. Therefore, a hypothesis has to be developed in order to verify the success of the attempt of creating a sustainable complex fenestration system. In order to pursue the fore mentioned aim and objective, the following hypothesis is being drawn up:

*The aim of the thesis is to achieve a **sustainable** complex fenestration system (CFS) design that can **diffuse** and **redirect** sunlight deep inside rooms through an **optimized prismatic panel** on its **translucent layer**.*

From the hypothesis above, the certainty of the outcome can be confirmed. Either the research will succeed in reaching a concrete measurable solution verifying the hypothesis, or it may run on contrary to the predictions of the hypothesis.

## 1.7 Thesis Methodology

The following points review the methodology to be used in pursuing the objective of the thesis:

1. Studying previous literature concerning daylighting solutions and determining the drawbacks of the studied systems.
2. Establishing the problem statement and setting the objectives of the thesis.
3. Developing a mathematical model along with an objective function suitable for the research conditions. Generation of an optimized prismatic shape from the mathematical model and producing the output light behaviour of the selected shape.

4. Verification of the mathematical model via a ray-tracing software.
5. Enhancement of the output by adding the power factor to the exiting light rays using the ray tracing software.
6. Using Radiance for a comprehensive daylighting analysis using the Five-Phase Method, which calculates hourly illuminance throughout the year.
7. Constructing and manufacturing a physical prototype to test the panel design.

The following figure, Figure 1, visualizes the methodology used and the relation between the different activities and their importance in shaping the methodology of this thesis.

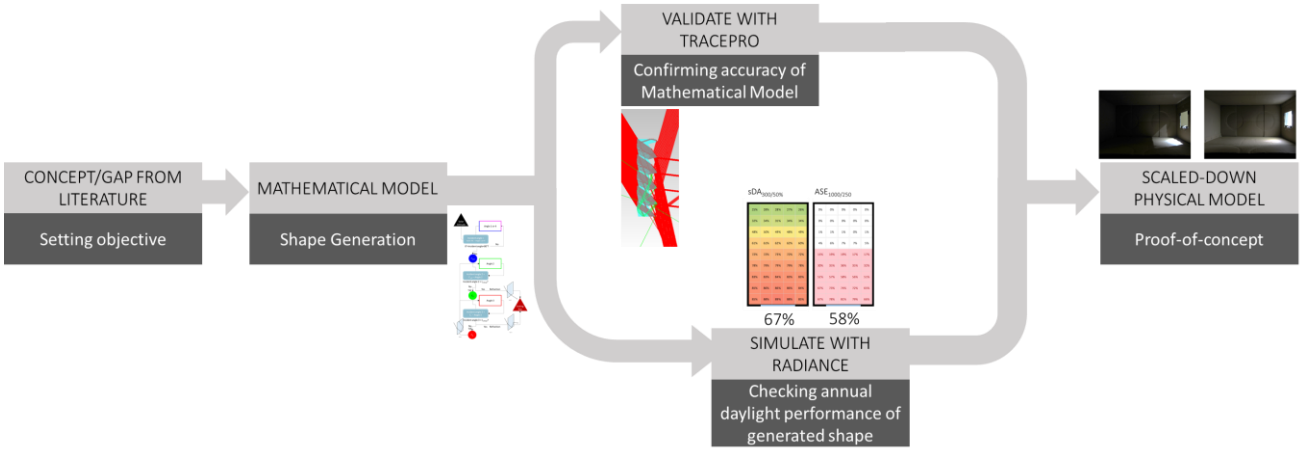


**FIGURE 1 FLOWCHART OF THE METHODOLOGY USED IN THE THESIS**

## 1.8 Thesis Outline

This thesis consists of 6 chapters including literature review, research work done over the course of the thesis, as well as results and conclusions concerning the proposed design. The thesis also includes recommendations and diverse test procedures upon dealing with complex fenestration systems, as well as, recommendations for commercializing and mass production of the proposed design. The first chapter is an introduction about daylighting and its benefits, current challenges, state of the art technology to tackle daylighting common problems and research gaps. Afterwards, a literature review is done in chapter 2, covering the latest daylight measuring techniques, the different research done in testing different glazing properties and the general effect of those properties, as well as potential material to use in the proposed design. In chapter 3 the development of an optical mathematical model is discussed, where optimization of the prismatic surfaces using genetic algorithm is used. Subsequently, it is validated using a 3D raytracing tool TracePro®, where not only the deflection angle of light would be measured, but the power of transmission of sunlight is measured as well. In chapter 4, a tool for CFS optimization through annual simulation using Radiance is defined along with a range of challenges and trials. As for chapter 5, a physical model setup, fabrication and measurements are clarified, as well as the results of the physical model measurements. In the end, the conclusions, further research and limitations are described in chapter 6.

# CHAPTER 2:
# LITERATURE REVIEW

# Chapter 2: Literature Review

## 2.1 Daylight measures

Since daylighting performance is an intangible measure as well as a subjective matter where it depends on each human's perception personally, it is considered one of the most difficult measures facing architects when designing any space. Through the past century many researchers and building rating systems established various performance metrics, whether those metrics are illumination metrics or thermal metrics, to measure the performance of daylighting.

To improve our understanding for daylighting, to have a relative measurable outcome from the illuminance and benchmark our measurements, a Daylight Factor (DF) has been created. The DF is a ratio between the horizontal illuminance of a standard CIE sky with no clouds and the internal illuminance of a space and it is represented in a percentage disregarding the absolute values of the measurements (Hopkinson, 1963).Early versions of the USGBC, LEED rating systems required a Daylight Factor (DF) of 2% in at least 75% of the task zones to achieve the credit of the Indoor Environmental Quality 8.1

Point in time illuminance is a measure of the illuminance inside a space with static sky conditions, however it takes into consideration the actual sky conditions depending on: the location of the building, the orientation of the façade of the building where the analysis takes place and the sky conditions at the exact time of the analysis.

Since daylight's only source is the sun and the sun's position changes in the sky throughout the day the illumination of a space, in reality, is a dynamic measure where illumination intensity and light scattering pattern changes throughout the day. (Mardaljevic, Heschong, & Lee, 2009) Therefore the point in time illuminance is not a true representation of the daylighting measurements in a space for the purpose of designing. Consequently, measures such as Useful Daylight Illuminance (UDI) (Nabil & Mardaljevic, 2005), and Daylight Autonomy (DA) (Reinhart & Walkenhorst, 2001)and continuous Daylight Autonomy ($DA_{con}$) were created by researchers in the past decade. Nevertheless, those measures still had some limitations in their measurement criteria

The US Illuminating Engineering Society lately published the LM-83-12 document "Approved Method: IES Spatial Daylight Autonomy (sDA) and Annual Sunlight Exposure (ASE)", which presents the sDA and the ASE, two new daylight performance indicators (Illuminating Engineering Society, 2013).

The sDA indicates the amount of lighting a space receives. In detail, sDA describes "the percentage of floor area that receives at least 300 lux for at least 50% of the annual occupied hours". While the ASE is how much direct sunlight the space receives, that can cause visual discomfort, known as glare, or increase cooling loads to neutralize its effect. Specifically, ASE measures "the percentage of floor area that receives at least 1000 lux for at least 250 occupied hours per year. Combining both measurements give an indication about daylighting adequacy and visual comfort. (Illuminating Engineering Society, 2013)

## 2.2 Glazing properties effect

The fenestration system's efficiency and effectiveness is associated with certain glazing properties. The glazing properties determine the effectiveness of the system in transmitting light and/or heat transfer through the glazing panel.

### 2.2.1 Thermal Behavior

The main glazing thermal properties are solar heat gain coefficient (SHGC) and U-value which affects the heat transfer from the exterior to the interior.

In the windows application, various types of window materials are used. Low-E, for instance, are spectrally selective coatings on the glass that prevents infra-red, and sometimes ultra-violet, light waves to pass by reflecting them back without comprising the amount of visible light transmitted .Electro-chromatic material is another application, where it is able to adjust the optical properties of the glass through running voltage. (Granqvist, 1995) (Papaefthimiou, Leftheriotis, & Yianoulis, 2001)

Another way to decrease the U-value of a glazing system is through using more than one layer of glazing and adding different gaseous mediums in between the layers of glazing panels. Sullivan et. al analyzed different design combinations in a residential building in California. The single, double and triple-glazed windows were observed against their energy efficiency in different climatic conditions (Sullivan & Selkowitz, 1985). While Rousseau observed that having a layer of inert gas or air between multiple panes result in higher thermal resistance than single glass panes, which determines that gaseous layers have more thermal impact on the overall U-value than the glass itself. (Rousseau, 1988). One of the recent technologies, the vacuum glazing, is considered to achieve low U-values, it was successfully fabricated in the 1980s (Robinson SJ, 1989)although it was first introduced as a concept in 1913 (German Patent No. 387655, 1924)and consequently more researchers started developing in this novel technology reaching relatively low U-values (Cuce & Riffat, 2015)

### 2.2.2 Visual Properties

As for the visual properties, the visible transmittance and reflectance are considered the most important properties, since they determine the illumination intensity inside a space, as well as the view to the outside.

## 2.3 Building and Window Orientation

Building orientation plays an important role in the glazing selection and design process. Since the sun's position changes with time and the amount of solar radiation varies throughout the day, the window's orientation should be carefully considered when designing the fenestration system. As proper designing standards, the window's orientation will conclude a change in the window's size visual and thermal properties, moreover changing the window's orientation means a change in the shading technique used, if available. For example, a window in the south orientation has to be comparatively smaller in area than a window in the northern direction, since the northern façade should not receive any direct daylighting throughout the day (Hee, et al., 2015). As well as the duration of daylight penetration into the space will change with each orientation (Hee, et al., 2015). (Sherif A. , et al., 2015) identified the effect of designing different window to wall ratios at different orientations on a hospital room. (Sherif A. , Sabry, Wagdy, & Arafa, 2015) discussed the

optimization of a façade design in order to improve the daylight performance by slightly changing the window orientation.

## 2.4 Conventional Techniques in optimizing daylighting performance

Using shading devices or internal blinds within a room proved to be an effective way to prevent excessive daylighting inside the room. (Sherif A. , Sabry, Wagdy, Mashaly, & Arafa, 2016) developed a brute-force algorithm to test 77 slat shapes for window blinds for their daylight and view performance, while (Sabry, Sherif, & Gad Elhak, 2012) addressed the optimization of a combination of light shelves and solar screens to achieve high daylighting performance in spaces.

## 2.5 State of the art technology

The advancement in glazing systems has been occurring since the early 20$^{th}$ century, starting with the conventional window type, the single pane of clear glass, which constitutes of several pane thicknesses and reaching complex design systems that include advanced state of the art technology.

Mainly, the glazing system strategies can be categorized according to the following:

1- Improvement of conventional techniques and retrofitting
2- Developing of new glazing systems by changing chemical or physical structure of the glazing system
3- Innovations in light guiding systems

Each system tends to have diverse effects and treats daylighting issues using different methods and techniques. For instance, shading systems have been the most conventional treatment strategy that blocks direct sunlight from entering and admits diffused indirect lighting whilst conserving the same window to wall ratio. However, some shading systems inhibit other functionalities such as redirecting and diffusing light (Kischkoweit-Lopin, 2002). A combination of two or more functionalities are more to occur, for instance, a combination of a horizontal shading device and lighting shelves are commonly used in classrooms to prevent direct sunlight and diffuse it through the depth of the room.

Other systems do not include shading devices, such as diffuse light guide systems, direct light guide systems, scattering systems and light transporting systems (Kischkoweit-Lopin, 2002). A quick review of the previous systems is shown in the following table (Kischkoweit-Lopin, 2002):

**TABLE 1 DAYLIGHT SYSTEMS**

| System type | Name | Description |
|---|---|---|
| **Diffuse Light Guide** | Light Shelves | Doesn't block the view to the outside |
| | Fish System | Gives uniform illumination / Control light entering |
| **Direct Light Guide** | Laser Cut Panel | Optimized shape of glass that redirects and diffuse the light |
| | Prismatic Panels | giving a diffused view to the outside / Gives Uniform illumination / Redirect light according to the design |

| | | |
|---|---|---|
| **Scattering** | Frosted Glass | Coating on a clear glass pane which makes the view unclear to the outside / Uniform illumination |
| **Light transport** | Heliostat | A group of mirrors directed in a certain manner to ensure light reaches dark areas / Light guiding to the depth of room |
| | Light Pipe | Tubes of reflective material which allows the light to pass through to reach enclosed areas from the vertical elements |
| | Solar Tube | Tubes of reflective material which allows the light to pass through to reach enclosed areas from the ceiling |

### 2.5.1 Advancements in the Complex Fenestration Systems

As for Complex fenestration systems (CFS), they refer to any light transmitting window technology that features at least one non-transparent layer or one layer with switchable properties (Bueno, Wienold, Katsifaraki, & Kuhna, 2015).

At the present time, the advancement of fenestration systems, due to high effort in research and development, had made a wide variety of options and effects to fit different environments. Such advancements include change in the micro, as well as the macro, structure of the glazing panel. (Rubbert, 1999) demonstrated a commercial design in cooperation with the Institute for Light and Building Technology (ILB) called LUMITOP® which is a set of macro structured acrylic lamellas that guide the light within a certain angle, see Figure 2. The panel succeeded to direct light upwards at both low and high solar altitudes as shown in Figure 3.

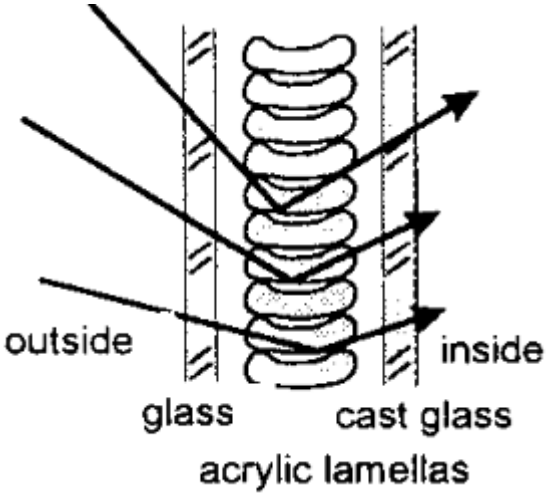


**FIGURE 2 TYPICAL SECTION OF THE LUMITOP PANEL WITH THE LAMELLAS OBVIOUSLY REDIRECTING LIGHT TO UPWARDS (KISCHKOWEIT-LOPIN, 1997)**

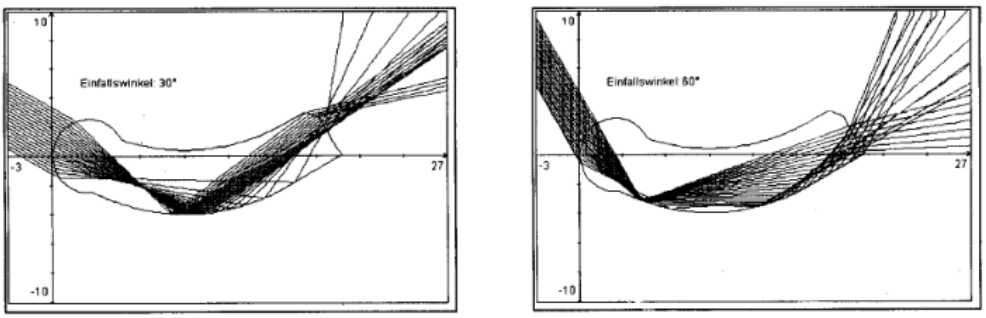


**FIGURE 3 AN UP CLOSE VIEW ON THE STRUCTURE IN A RAY TRACING SIMULATION REDIRECTING LIGHT UPWARDS IN BOTH ANGLES 30° (LEFT) AND 60° (RIGHT) (KISCHKOWEIT-LOPIN, 1997)**

(Edmonds & Pearce, 1999) used a macro prismatic structure in crop illumination by placing the panels horizontally and controlling the tilt angle. Other researches focused on different regions that are in the higher latitudes, such as micro-structured panels that uses hybrid polymers developed by the institute of Solar Energy Systems in Frieburg (Walze G. , et al., 2005). (Klammt, Neyer, & Muller, 2012) combined a micro-prism array with lens-like geometry in order to increase the efficiency of redirection of light. The micro-prism structure, see Figure 4, was made of acrylic and the upward and downward transmission were measured against a wide range of solar altitudes.

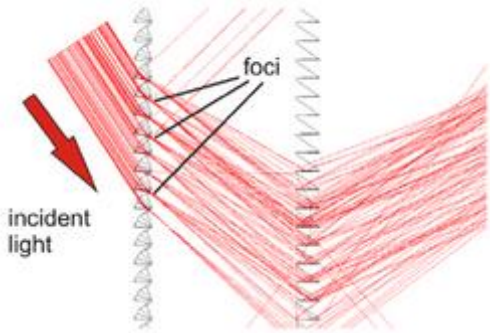


**FIGURE 4 (KLAMMT, NEYER, & MULLER, 2012) MICRO-PRISM ARRAY DESIGN DIRECTING RAYS UPWARD**

Moreover, (Vlachokostas, 2012) used a “liquid filled prismatic structure” to redirect light within deep areas in a room. While (Buß, Teisseire, Mazoyer, & Sondergard, 2013) used “silica sol-gel nano-imprint lithography” in order to form nano-scale gratings for optical diffraction. Recently, (Huang, et al., 2015) manage to lower the energy consumption and achieve uniform daylighting at solar altitudes 40° to 70° by 70% by designing a prismatic array microstructure that redirects light and reduces infrared rays through a silver coating.

(El-Henawy, et al., 2014) proposed a panel based on a sine wave structure for horizontal fenestration, which works on low latitude regions, the structure works on diverging direct sunlight towards dark areas. Further proposed work on vertical fenestration was conducted with other structural shapes such as the saw tooth with optimized angles to ensure maximum daylight penetration into the depth of rooms (Nassar, et al., 2014).

The following, Table 2, summarizes all the previous researches stating features used in the designs or objectives

**TABLE 2 SUMMARY OF THE STATE OF THE ART RESEARCHES IN CFS**

| Publications / Features | Rubbert, 1999 LUMITOP® | (Edmonds & Pearce, 1999) LCP | Walze et. al., 2005 | Vlachokostas et. al., 2012 | (Padiyath, 2013) 3M™ Film | Buß et. al., 2013 | Klammet et. al., 2013 | (Thanachareonkit, Lee, & McNeil, 2013) | ElHenawy et. al., 2014 | Nassar et. al., 2014 | (Huang, et al., 2015) |
|---|---|---|---|---|---|---|---|---|---|---|---|
| **Targeted Solar Altitude** | Low | Low | Low | Low | N/A | N/A | Low | Low | High | High | Medium |
| **Prism Structure Scale** | Macro | Macro | Micro | Macro | Micro | Nano | Micro | Micro | Macro | Macro | Micro |
| **Manufacturing Sophistication** | High | High | High | High | High | High | High | High | Low | Low | High |
| **Controlled Angular Redirection** | | ● | | ● | | | | | ● | | |
| **Commercial** | ● | ● | | | ● | | | ● | | | |
| **Use of Additive/coating** | | | ● | ● | | ● | | | | | ● |
| **Ray-tracing** | ● | ● | ● | | | | ● | | ● | ● | ● |
| **Radiance/Illuminance Simulation** | | | | ● | ● | | | | ● | ● | |
| **Fabrication (large scale)** | ● | ● | | | ● | | ● | ● | ● | | |

## 2.6 Potential Materials to be used in CFS

It is widely common to use glass as the main material in any fenestration system, (Nicholls & Dennis Hall, 2004) recommend that it is preferable to add a multi-layer glass window in order to get better thermal performance. (Carmody, 2007) studies different glazing types using wood or vinyl frame in a typical American house in two different climates, and runs an annual energy performance. He utilizes solar heat gain coefficient including the frame effects ($g_{tot}$), and the visible transmittance (VT).

Table 3 summarizes the effect of each of the tested glazing types by (Carmody, 2007)

**TABLE 3 TESTED GLAZING TYPES AND THEIR PROPERTIES (CARMODY, 2007)**

| Window | Glazing type | *U*-value ($W/m^2 K$) | SHGC | VT |
|---|---|---|---|---|
| A | Single, clear | 0.84 | 0.64 | 0.65 |
| B | Single, tint | 0.84 | 0.54 | 0.49 |
| C | Double, clear | 0.49 | 0.56 | 0.59 |
| D | Double, tint | 0.49 | 0.47 | 0.44 |
| E | Double, high performance tint | 0.49 | 0.39 | 0.50 |
| F | Double, high solar gain, low-e | 0.37 | 0.53 | 0.54 |
| G | Double, moderate solar gain, low-e | 0.35 | 0.44 | 0.56 |
| H | Double, low solar gain, low-e | 0.34 | 0.30 | 0.51 |
| I | Triple, moderate solar gain, low-e | 0.29 | 0.38 | 0.47 |
| J | Triple, low solar gain, low-e | 0.28 | 0.25 | 0.40 |

Advanced glazing materials intend to offer solar gain control, high performance thermal insulation, daylighting solutions or a combination (Sadineni, Madala, & Boehm, 2011)

The following table, Table 4, summarizes different materials that can be used in CFS:

**TABLE 4 SUMMARY OF DIFFERENT GLAZING TECHNOLOGIES**

| Category | Name | Material Used | VT (%) | U-value |
|---|---|---|---|---|
| **Multilayer Glazing** | (Han & Kim, 2011) | multilayer film($TiO_2/SiO_2/TiO_2$) | N/A | N/A |
| | (Hasan, Abdul Malek, Haseeb, & Masjuki, 2010) | $TiO_2$and Ag | N/A | N/A |
| | (Asdrubali & Baldinelli, 2009) | silicon nitride or carbon nitride | N/A | N/A |
| **Suspended Films** | (Frost, Eto, Arasteh, & Yazdanian, 1996) | Serious materials – 1125Picturewindow | 0.23 | 0.28 |
| | | Vision wall Solutions Inc. - Series 204 4-Element Glazing System | 0.50 | 0.62 |
| **Vacuum Glazing** | (Fang, Hyde, Arya, & Hewitt, 2013) | Air gap & low-e coating. | N/A | 0.24 |
| | (Han, et al., 2012) | Stainless steel support pillars & 4 low-e coatings | N/A | 0.2 |

#### 2.6.1.1 General optical properties of plastics

Generally the optical properties of any plastic material are defined in terms of transparency, specular and diffuse transmission, and refractive index. Mainly, both transparency and refractive index of the material determine the output light propagating through its medium, where transparency mainly affects the power of light, while the refractive index determines the final output angle of the light beam depending on the incident angle and surface composition and structure. (Tripathi, 2002)

#### 2.6.1.2 Recycled Plastic in raytrace simulation

Recycled plastic is often mixed with other foreign parts which results in some deformation in the inner structure of the final recycled product, often called recyclate. The mechanical and structural properties of the recyclates are influenced by the degree of mixed polymeric fractions in recycled plastics. Polymers residue mixed within the recyclates negatively affects the macroscopic properties of the final product. (Vilaplana & Karlsson, 2008)

Therefore it is hard to predict an accurate mathematical model for such product. On the other hand, modelling a geometrical prototype with the random deformities can give a prediction to the optical behaviour of such materials.

# **CHAPTER 3:**
# PRISM DESIGN

# Chapter 3: Prism Design

## 3.1 The concept of forming a mathematical model

In general, having a mathematical model will give the basic foundation for developing a scientific-based design even though some limitations might emerge. To develop a mathematical model for an optics problem there are certain laws and formulae that are taken into consideration to provide the basic behaviour of light and deliver an accurate model to build upon using other tools and methodologies. Mainly, the optical behaviour depends on the law of reflection and law of refraction. The following chapter will discuss the development of the mathematical model in order to design a prismatic panel to meet a certain objective.

As shown in Figure 5, there are some inputs regarding the sun's position and the material's refractive index, which are the variables of the model. As well as, a clear indication of the constraints in the design of the prismatic panel, since the surfaces' tilt angles are confined to the maximum possible boundaries of the shape. Furthermore, the objective is defined and fed into the algorithm, which is to be discussed in this chapter, and an output design is created from the algorithm.

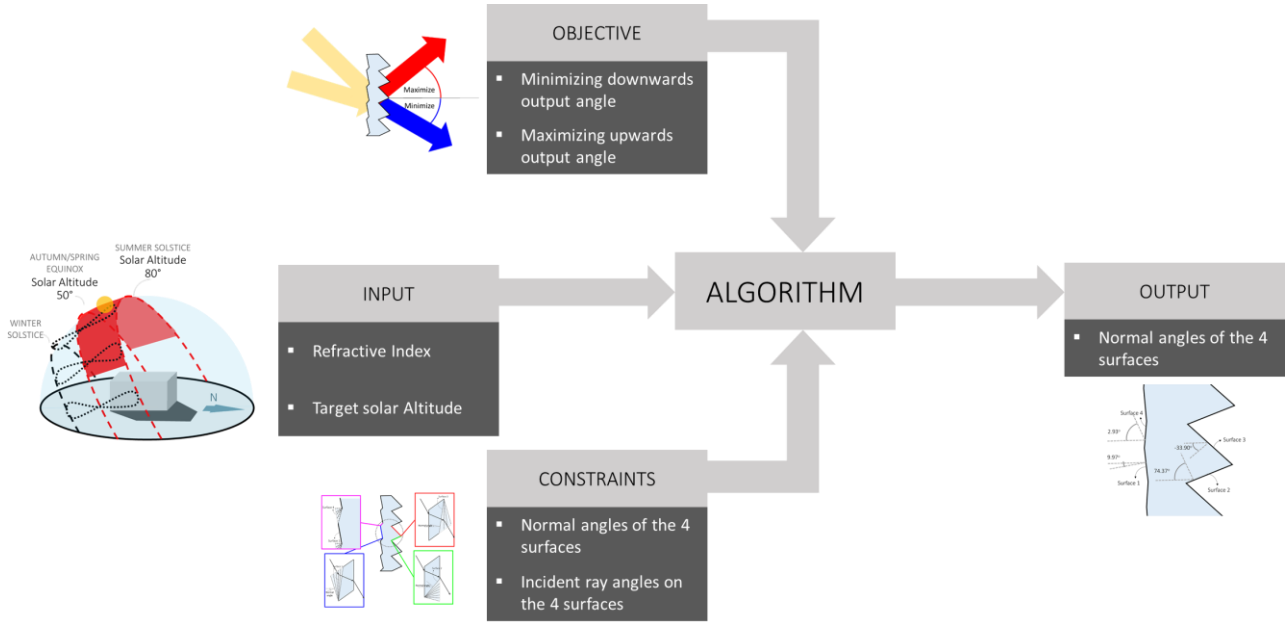


**FIGURE 5 FLOWCHART OF THE MATHEMATICAL MODEL COMPONENTS**

## 3.2 Shape Creation

The objective is to create a prismatic shape with certain angles that can reflect incident light from the high solar altitude upwards within any space and maximize this angle, on the other hand, minimize the angle of the direct daylight concentrated under the window as shown in Figure 6.

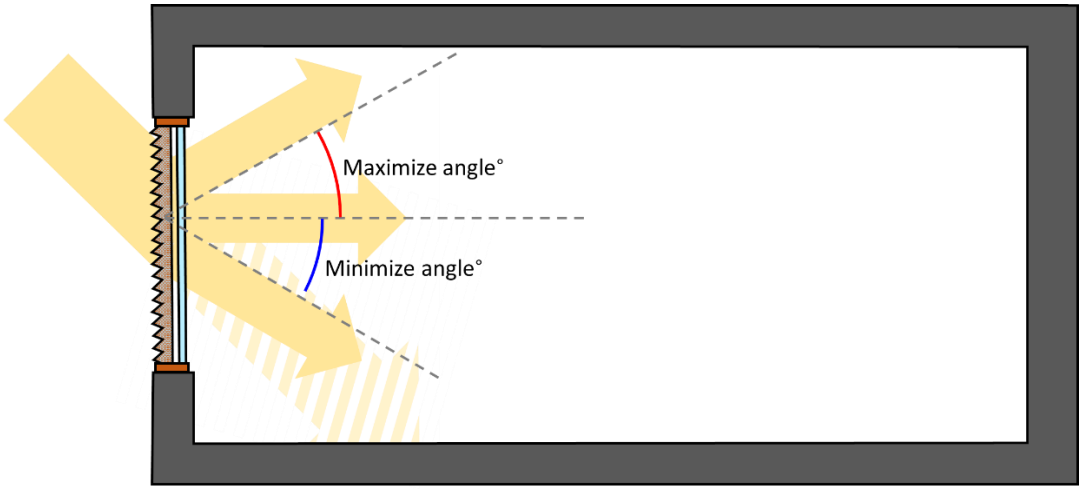


**FIGURE 6 THE OBJECTIVE FUNCTION OF THE OPTIMIZATION PROCESS**

### 3.2.1 Using a mathematical model

Using the formulae explained in appendix B, a simple 2-bounce ray tracing model is created. This model consists of 3 connected surfaces which represents the cross section of the glazing panel. A vector ray is directed towards the left hand side surface, see Figure 8, and passes within the space enclosed by the 3 surfaces. The incident angle of the ray entering the glazing panel is determined by the solar altitude angle of the sun in the desired observation times and the glazing surface tilt angle.

#### 3.2.1.1 Cases Description

A series of probable rays' behaviour were observed in order to predict the exiting ray's angle, as illustrated in Figure 7 and Figure 8.

- **Case1**: Refraction at both surfaces 1 and 3, where the ray does not fall on surface 2
- **Case2**: Total internal reflection (TIR) inside the glazing at surface 2 and exits the boundaries through the right hand side surface (surface 3).
- **Case3**: The ray exits from surface 2 by refraction
- **Case4**: The ray experiences TIR at both surface 2 and 3

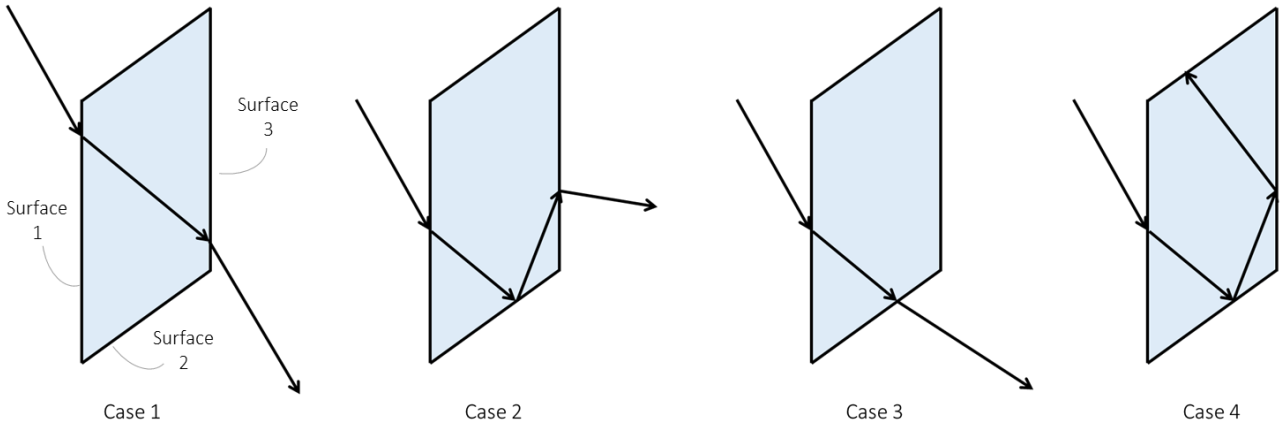


**FIGURE 7 DIFFERENT CASES OF LIGHT BEHAVIOR**

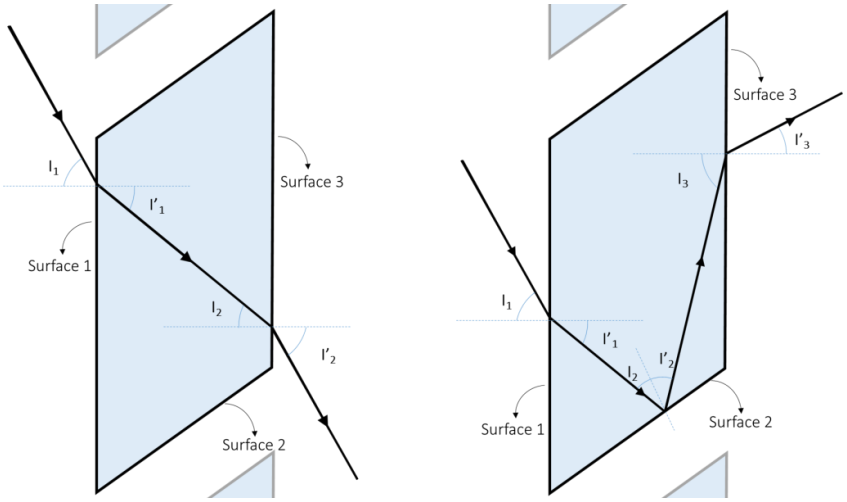


**FIGURE 8 A CROSS-SECTION SHOWING THE RAY BEHAVIOR AND DIFFERENT INCIDENT ANGLES FOR 2 CASES**

## 3.3 Cases Observation

For Case 1, light enters through surface 1 and exits from surface 3, this is considered a normal glass pane behaviour since both surfaces 1 and 3 are parallel to each other; therefore, the angle of incidence at the outer side of surface 1 is equal to the output angle at surface 3

As for case 4, the ray never exits the glazing system from surface 3, and this results from the high incident angles at both surfaces 2 and 3, where both angles are higher than the material's critical angle ($I_{crit}$) creating total internal reflection (TIR) inside the material's boundaries.

In both cases 2 and 3, the ray exits the panel from the right hand side. In case 2 the ray bounces from surface 2 and refracts as it passes through surface 3. While in case 3 the ray misses surface 3 and projects directly to surface 2, resulting in a refraction of the ray upon exiting.

Cases 1 and 4 are unwanted cases to fulfil our objective, since case 1 results in an output angle similar to the input angle. Whereas cases 2 and 3 produce different output angles that results in a lower incident angle ($I^{iv}$), thus leading to a greater dispersion of light throughout the space.

#### 3.3.1.1 Definition of Constrains and Variables

In order to ensure a lower angle of incidence, a number of variables are set up and defined for the mathematical model explained previously. Initially the angle between surfaces 1 and 2 and the angle between surfaces 2 and 3 were considered the main variables that control the angle of the exiting ray.

Solar altitude is the condition the design is optimized upon. Initially the target sun position is intended for the summer sun in mid-day time, since at this time, the light enters inside the space with a high angle near the fenestration system. Moreover, the direct solar radiation at summer is extremely high introducing more heat, with the sunlight, entering the space.

The refractive index is one of the essential optical properties of any material. It determines the refraction value for any incident angle on the surface of the material, it also determines the total internal reflection within the material. The higher the refractive index, the greater the deflection value, however a high refractive index means a smaller critical angle which helps in the occurrence of TIR inside the material. The refractive index value for virgin polypropylene is around 1.49 and polystyrene is around 1.56 while polycarbonate is 1.60 (Scientific Polymer, Inc., 2013) and since the materials intended to be used have different refractive index, an average refractive index of 1.55 is assumed throughout the initial optimization process.

The critical angle, which is calculated from equation (28) , is one of the crucial factors in the optimization equation; where after a ray's incident angle inside the material exceeds the critical angle on the surface Total Internal Reflection (TIR) will occur. This phenomena resulted in constraints on the incident angle on surface 3 of the optimization problem.

**TABLE 5 LIST OF VARIABLES AND CONSTRAINTS DEFINED IN THE OPTIMIZATION PROCESS**

| Parameter | Constraint |
|---|---|
| **Refractive index** | 1.55 |
| **Critical Angle** | 40.18° |
| **Incident angle on surface 1** | 0° - 80° |
| **Incident angle on surface 2** | 0° - 80° |
| **Incident angle on surface 3** | 0° - 40° (critical angle) |
| **Variables** | |
| **Average targeted solar altitude** | 50°- 80° |
| **Normal of surface 1 range** | -60° - 0° |
| **Normal of surface 2 range** | 0° - 90° |
| **Normal of surface 3 range** | -60° - 60° |
| **Normal of surface 4 range** | 0°-60° |

Rays falling on both surfaces 2 and 3 can experience TIR, therefore rays incident on surface 3 should not be allowed to exceed the critical angle of the material, and otherwise case 4 will occur. However, rays incident on surface 2 will be allowed to internally reflect, since the ray will still bounce from surface 2 to surface 3. In order to control the incident angle of rays on surfaces, the normal angles of the surfaces will be a variable parameter.

The optimization process will undergo two parallel processes in which scenario 1 will involve the entering ray incident on surface 1 and scenario 2 will involve the ray entering incident on surface 4.

Changing the normal angle of surface 1 will induce a change in the exiting incident angle from it. This change in angle will afterwards affect the behaviour of the ray incident on the next surface, whether it is surface 2 or 3. As the normal angle of surface one is tilted towards a negative angle (rotated counter clockwise) the incident angle will increase thus resulting in a smaller exiting incident angle from the surface.

Another possibility is the incident rays entering from surface 4, which is a “complementary surface” that is needed to complete the prism design. The rays from surface 4 will mainly fall on either surface 2 or 3 and will exit in a downwards direction. Figure 9 illustrates the change in tilt angles of all 4 surfaces for a single prism.

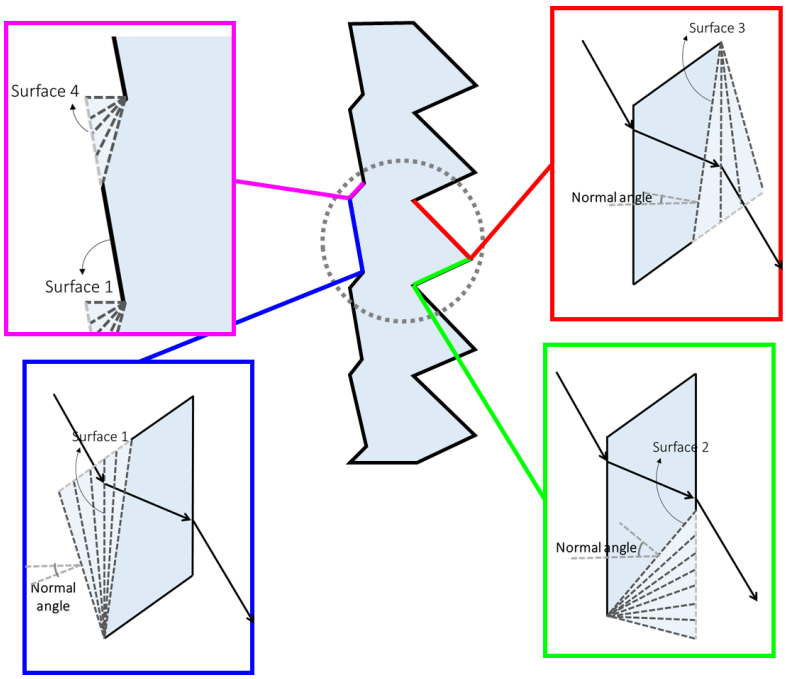


**FIGURE 9 CHANGING THE TILT ANGLES OF SURFACES 1, 2, 3 AND 4 FOR THE OPTIMIZATION PROCESS**

### 3.3.2 Using Evolutionary Algorithm in determining the optimized tilt angles for the panel’s surfaces

One of the fast and effective ways of determining the initial optimum tilt angles is using evolutionary algorithm. Evolutionary Algorithm (EA) is based on a simplified form of the evolution and natural selection concept, where evolution helps species adapt to their environments. Basically, EA revolves around creation of an environment in which latent solutions can evolve. The environment is formed by the parameters of the problem and promotes the evolution of suitable solutions. It is important to note that the accuracy of the results of such algorithm depends mainly on the right definition of variables, constrains and the objective function. The variables and constrains are mentioned in Table 5. Each variable is constrained with maximum and minimum boundaries in order to limit the solutions to fit one of the 3 cases of ray behaviour within the material as previously mentioned. After defining constrains and variables of the problem, a fitness function is determined. In that case, the fitness function of the optimization problem was to minimize the output angle absolute value.

### 3.3.3 Running the optimization

The optimization process took several iterations and modifications to reach the optimum solution. The evolutionary method was used since the problem was non-smooth and nonlinear, where changing a single variable would affect the optimum value of the other variables in the equation. The convergence was set to 0.01% while the mutation rate was 7.5% and the population consisted of 100 chromosomes. The optimization logic was as follows in Figure 10:

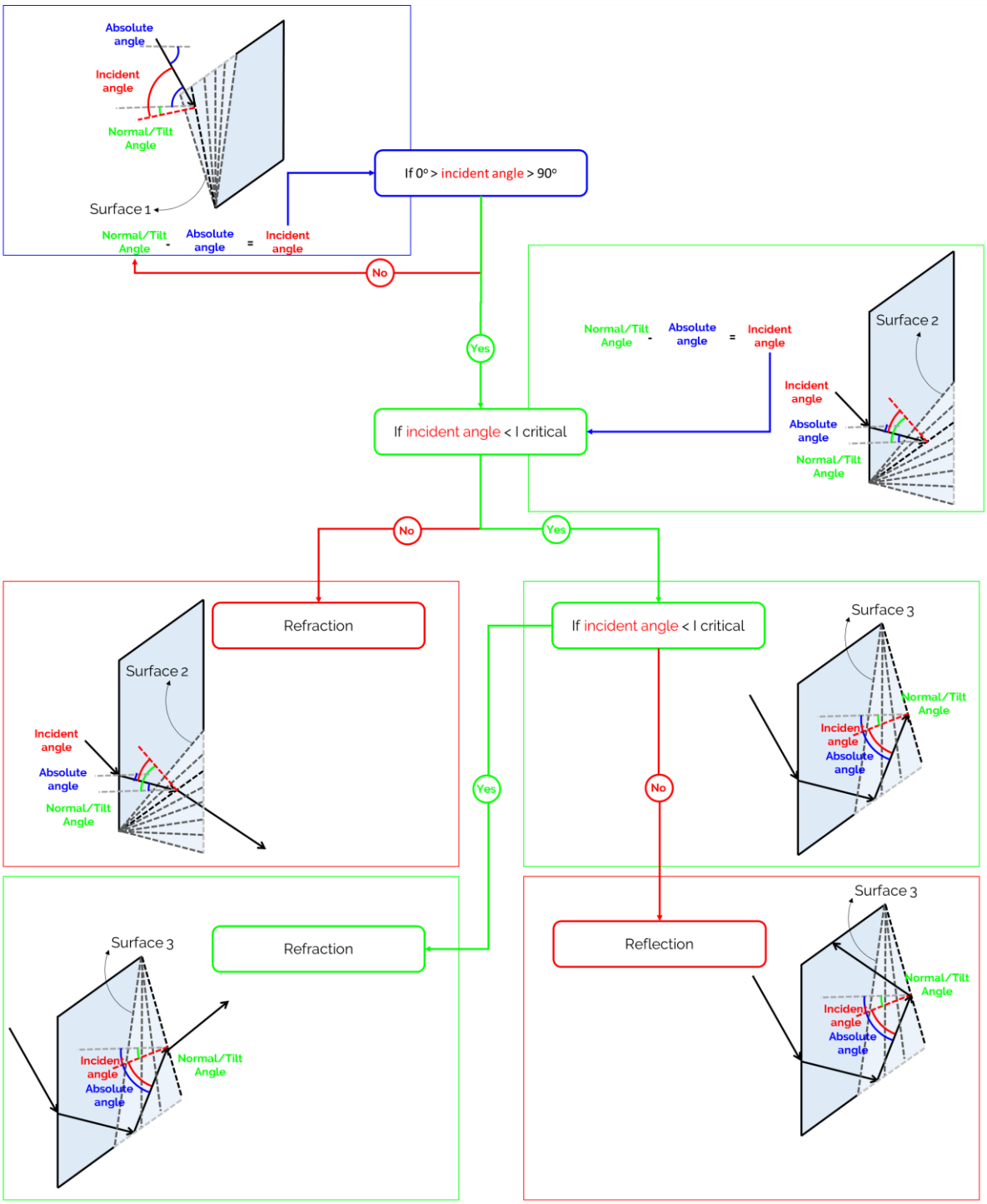


**FIGURE 10 FLOWCHART OF THE OPTIMIZATION PROCESS CARRIED OUT**

A random tilt angle for surface 1 is generated and processed with the solar altitude, or the input ray angle. Afterwards the incident angle of the two angles is calculated and checked if it is between 0° and 80°. If the check was positive, it goes on to the other stage where a refraction formula calculates the refracted angle from surface 1 according to the refractive index of the material and incident angle $I_1$. Surface 2 tilt angle is generated randomly between the constrains set previously, see Table 5, and this tilt angle is processed with incident angle exiting from surface 1 to calculate the incident angle on surface 2.

At this point the incident angle on surface 2 is checked with the critical angle of the material. If the value exceeds the critical angle, total internal reflection occurs and the process carries on to surface 3; however, if the incident angle does not exceed the critical angle, the ray will refract outside the boundary surfaces of the panel. If the ray continues inside the glazing panel, it will be incident on surface 3 which by turn has a tilt angle that is compared with the reflected ray incident angle. Similar to the previous process, ray 3 is checked for total internal reflection according to the same critical angle. If the ray reflects inside again, it would be considered a fail case. If it refracts, the angle of refraction is calculated and checked with the objective function of the optimization process.

The process will continue until reaching an optimum solution which will result minimizing the downward angle and maximizing the upward angle.

### 3.3.4 The optimization results

An optimum solution was obtained after a number of iterations, the 4 surfaces tilt angles were obtained.

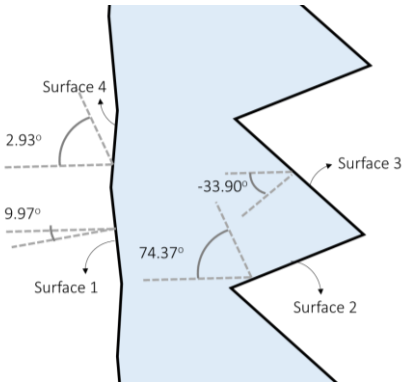


**FIGURE 11 FINAL SURFACES' TILT ANGLES FROM THE OPTIMIZATION PROCESS**

The final result's process included all 4 surfaces in determining the exiting ray angle, as presented in Figure 11. Where the behaviour of the ray of the first scenario (when a ray enters from surface 1) depended on the TIR from surface 2 and refraction of surface 3 with a minor consideration of the cases where the light ray exits from surface 2. On the other hand, the ray which enters from surface 4 (second scenario) tends to exit the prism from surface 2 by refraction directed downwards. The final tilt angles are a result of the optimization process which worked on maximizing the upward angle and minimize the downward angle of the exiting ray, as shown in Figure 12.

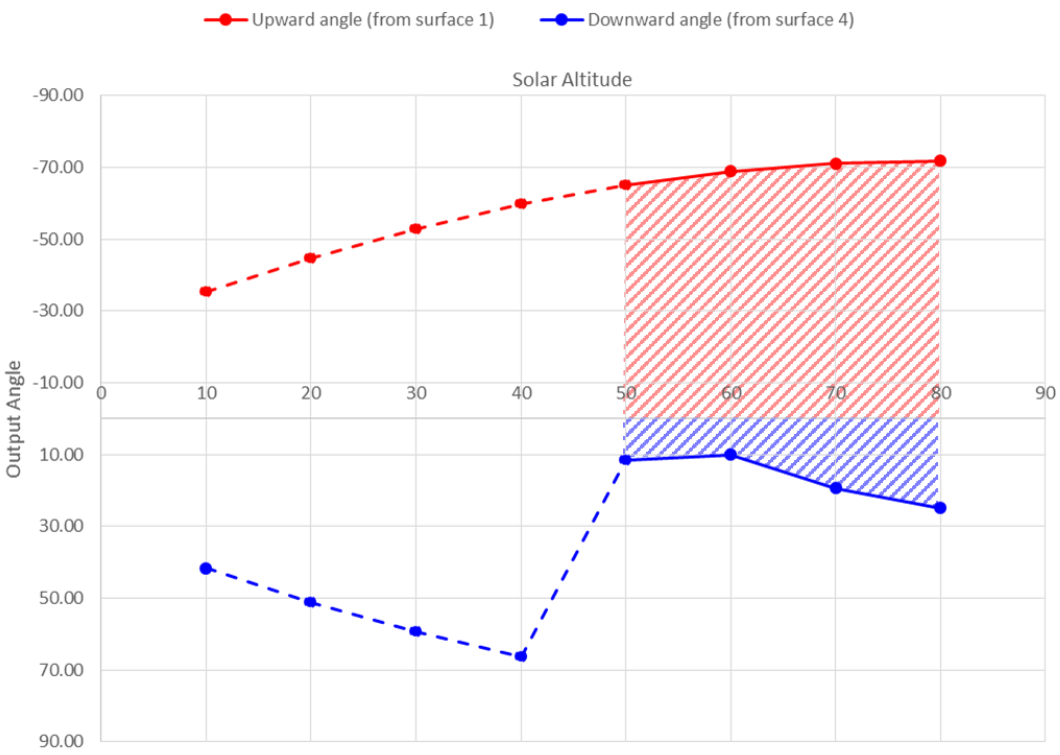


**FIGURE 12 THE FINAL DESIGN EXITING ANGLES VERSUS SOLAR ALTITUDE**

### 3.3.5 Testing limitations for the design using the mathematical model

However, certain ray tracing behaviour cannot be processed using the given equations such as ray splitting, blockage of neighbouring surfaces and decrease in power of ray when refracted. Both behaviours would not determine the final direction of the ray; however, they would affect the power of the ray exiting. Therefore, further analysis should include the previous indicators within the design.

## 3.4 3-Dimensional Raytracing Model Development

In order to come up with a more accurate analysis than the previously developed two dimensional mathematical model developed, more factors should be considered in the design process. Factors such as the ray splitting phenomena and blockage of some rays can affect the final output result of the analysis. Certain software, such as, TracePro® (TracePro), ZEMAX (Zemax), OSLO (OSLO) and CODE V (CODE V Optical Design Software) take into consideration different factors other than the refraction and reflection of light in the ray tracing process. Most of those are commercial software with competitive features; however, two software packages would stand out. TracePro® and ZEMAX are both pioneers in lens and prisms design, however,

Another feature that ZEMAX lacks is the importing of external geometry within the program. This feature can be used with TracePro® extensively where the geometry is imported as objects and surfaces. Both imported objects and surfaces can have independent properties. Table 6 summarizes the important features of the mentioned software.

**TABLE 6 SELECTED FEATURES IN OPTICAL DESIGN SOFTWARE**

| Features \ Software | TracePro | ZEMAX | OSLO | CODE V |
|---|---|---|---|---|
| **Prism Design** | ● | ● | | |
| **Interactive GUI** | ● | | | |
| **Geometry Importing** | ● | | | ● |
| **Optical Optimization** | | ● | ● | ● |

## 3.5 Trace pro in prismatic panel design

TracePro® is considered a validated software in lighting design. The software has been used in numerous research work as a part of the design process such as (García-Fernández, Vázquez-Molini, & Fernández-Balbuena, 2011) and (Fernandez-Balbuena, Vázquez-Moliní, Garcia-Fernandez, Garcia-Botella, & Bernabeu, 2009) used the software in prismatic designs, while (Shell, Brown, Schuetz, Davis, & French, 2011) used TracePro® in designing reflectors and concentrators. On a more related research topic, (El-Henawy, et al., 2014) used TracePro® in optimizing the sine wave period and amplitude design, in order to ensure wider refraction angles to be applied in narrow streets and dark wells. While (Nassar, et al., 2014) succeeded in determining the surface tilt angle of a prismatic design to redirect light upwards inside a room, the proposed design will attempt to refine the results using a different prismatic pattern.

TracePro® is a visual software where 3D modelling is allowed. Despite of the presence of different geometrical objects, such as lenses, cones and spheres, the program lacked the flexibility in designing prismatic panels. Therefore, the design was modelled on a more flexible modelling software called Rhinoceros 5.0 and imported to TracePro® as geometry. Afterwards, the geometry's properties were defined on Trace Pro, using a material with a refractive index of (n=1.55).Then a light source is set up to simulate the sunlight, where light is represented as individual rays each with a defined flux. The flux which is the power of the light ray is set to 1 Watt while the source light is set to emit a light beam of 200 rays with a wavelength of 0.5461 μm. The incident rays were measured before entering the panel medium and were found to have a total flux of 200 W and flux per angle 51,440 W/sr for each solar altitude.

For an accurate simulation, a wide range of solar altitudes is to be tested with the ray tracing software. A range of 10° to 80° degrees is tested with 10° degrees increments to mimic the sun's position at different times of the year. The light source is directed on the panel's prismatic surface, with the different proposed solar altitude angles.

### 3.5.1 Ray tracing Simulation Results

The results for the TracePro® simulation are represented in the final exit angles of the light rays including their flux and the total output flux as well as the efficiency of the whole system. In Figure 13, starting with solar altitudes from 50° to 80° degrees, the solar altitudes range that the optimization was based on, showed similar behaviour as the mathematical model used in the optimization. For instance, at input angle of 60° degrees, the output angle was recorded 75° degrees upwards. However, this was one of the 2 main output angles, as another output angle was analysed at 80°degrees downward. The downward angle was the result of the rays entering from the 4$^{th}$ surface resulting from the prism design and exiting the medium at surface 2.

At solar altitude 80° there was no output rays directed upwards at all, since the rays would enter from surface 1; however, they do not reach either surface 2 or 3. Whereas at solar altitude 70° the rays directed upwards have less power than the ones directed downwards due to the high refraction of light which decreases the power of the rays.

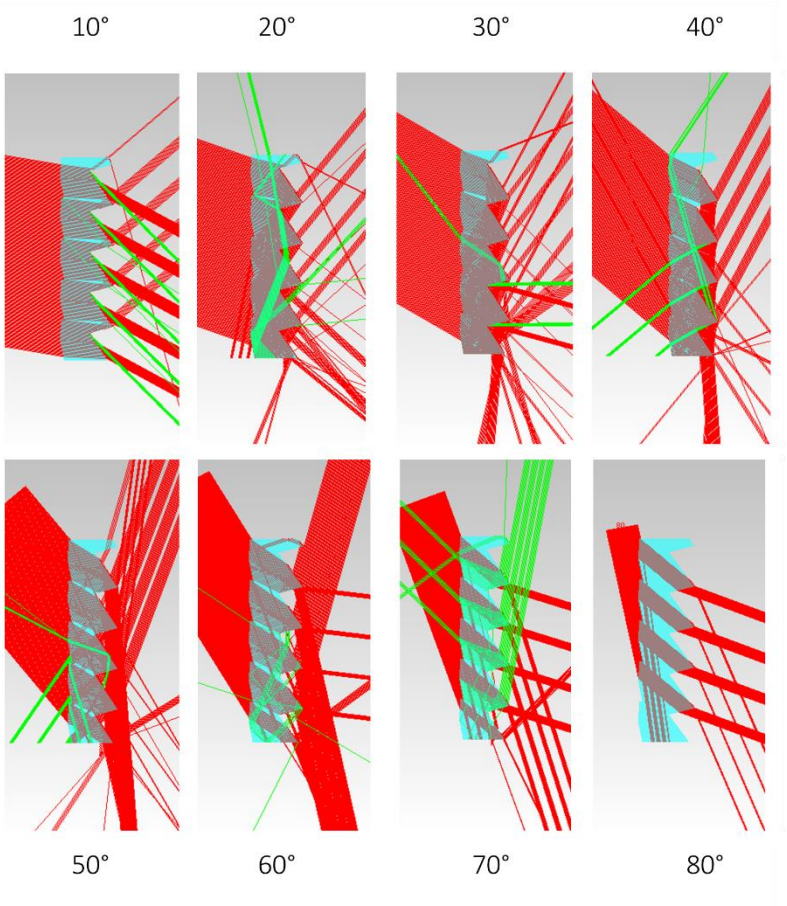


**FIGURE 13 TRACEPRO® RAYTRACING VISUAL RESULTS FOR BOTH THE DIRECTION AND POWER OF RAYS AT TILT ANGLES RANGE FROM 10°- 80° (RED RAYS: STRONG POWER, GREEN RAYS: WEAKER POWER)**


**FIGURE 14 TRACEPRO® RAYTRACING POLAR CANDELA RESULTS AT TILT ANGLES RANGE FROM 10°- 80° INDICATING THE POWER OF EACH ANGLE**

As for lower solar altitudes, the output angles showed promising deflection of light upwards, which could mean less direct sunlight and more light reflected upwards on the ceiling giving a more uniform daylighting pattern. Another observation was that at solar altitudes 10°, 30°, 60° and 70° the exiting rays had 3 exiting angles not just 2 as the rest of the solar altitudes. This 3rd output angle was due to the rays refracted at surface 1 while entering the medium and experience a TIR at surface 3, then exiting the medium from surface 2 by a slight refraction, due to the low incident angle with the surface.

In Figure 14 and Figure 15 the power of the different output angle is clearly indicated. There is no clear pattern for the power output at different incident input angles, however the upward rays are characterized by higher power compared to the downward rays at each corresponding solar altitude. This is observed in all cases except for solar altitude 10° and 70° where the downward ray's power was more dominant.

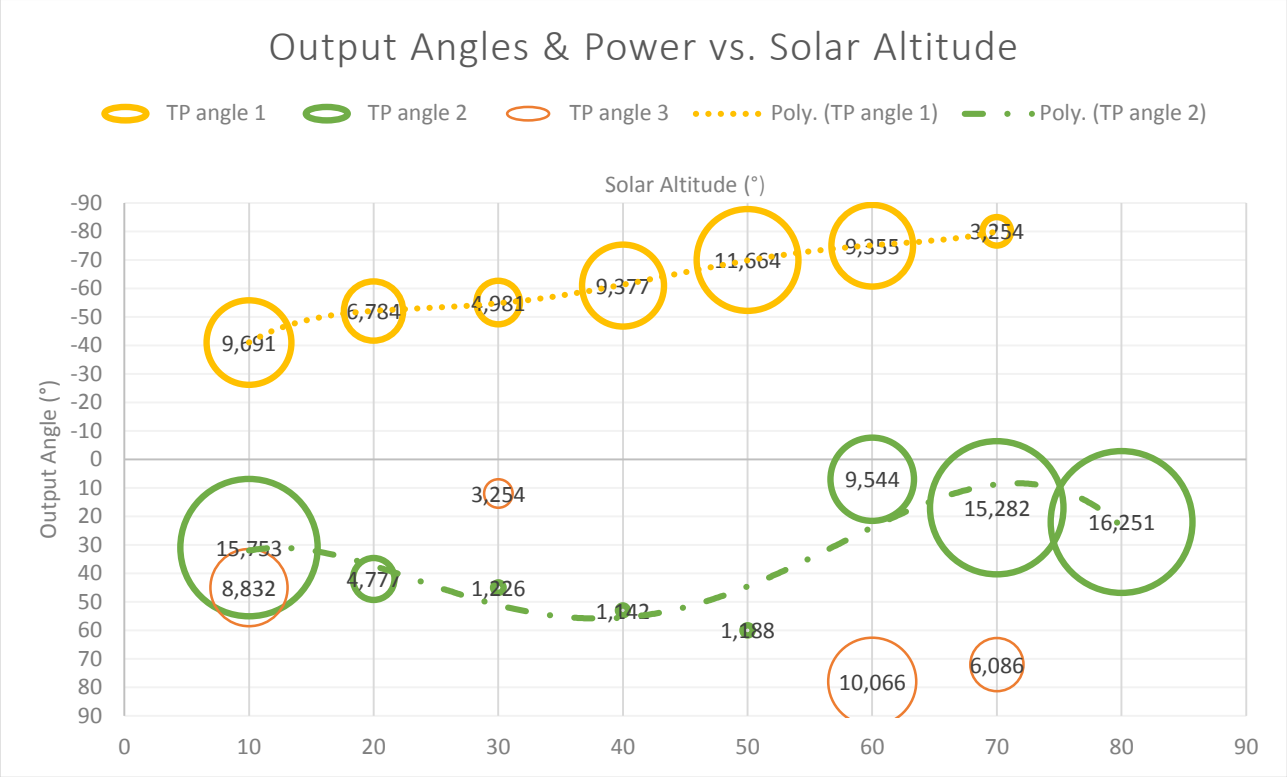


**FIGURE 15 OUTPUT ANGLES & THEIR POWER VERSUS THE INPUT ANGLES**

As for the efficiency, which is the measure of total output flux against the total input flux, the proposed design showed a variation in the values. The efficiency was measured regardless the downward or upward direction of the light. There was a fluctuation along different solar altitudes as shown in Figure 16, however this fluctuation was between 35% and 68% efficiency. The peak was at the target solar angle where it reached %68 efficiency with a total flux of 136 W. While at the least and highest solar altitude the design resulted in similar efficiencies of 42% and 45% respectively. Another local peak was observed at solar altitude 30 where it jumped to 51% and then fell down back to 35% at solar altitude 40°.

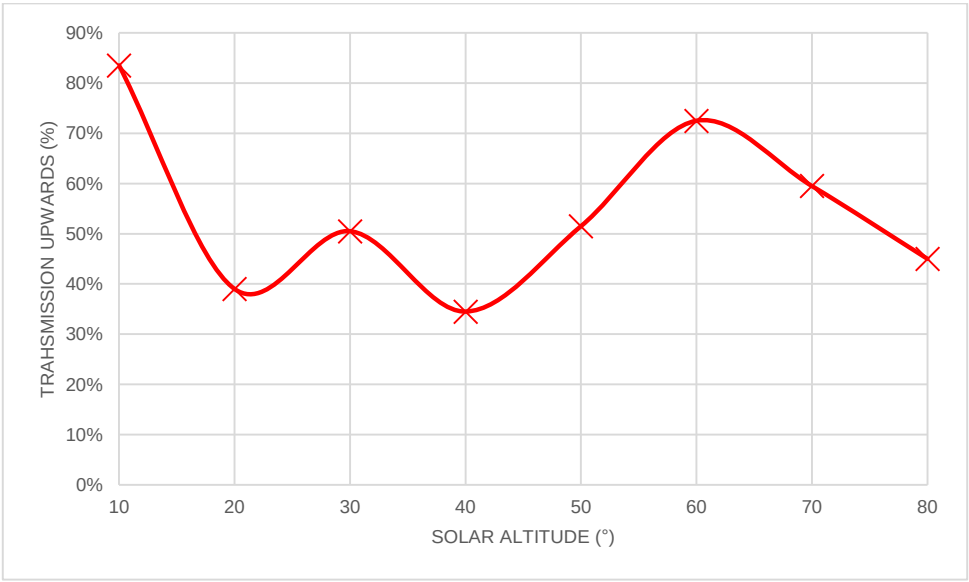


**FIGURE 16 OVERALL EFFICIENCY OF THE PROPOSED DESIGN VERSUS THE SOLAR ALTITUDE**

### 3.5.2 Relative Displacement of the prisms

The proposed design has parameters other than changing the surface tilt angle. Since the prismatic shape is found on both sides of the panel, the relative displacement of the pattern is considered an effective parameter to experiment with. (Klammt, Neyer, & Muller, 2012) discussed that prismatic structures would have great variance if a shift between the surfaces occurred.

Therefore, to test the shift displacement of the 2 surfaces, another design was created with the same surface tilt angles and different relative displacement of the right and left surfaces as in Figure 17. The results were also observed on TracePro®.


**FIGURE 17 SURFACE SHIFT OF THE PRISM**

The displacement of the surfaces resulted in a change in the power of the output beam. The displacement was measured against the power output at all solar altitudes as illustrated in Figure 18. As the displacement between the left and right surfaces increased the power output decreased until reaching a lower peak. Afterwards the power increased again till reaching the end of the cycle and returning to the original phase shift.

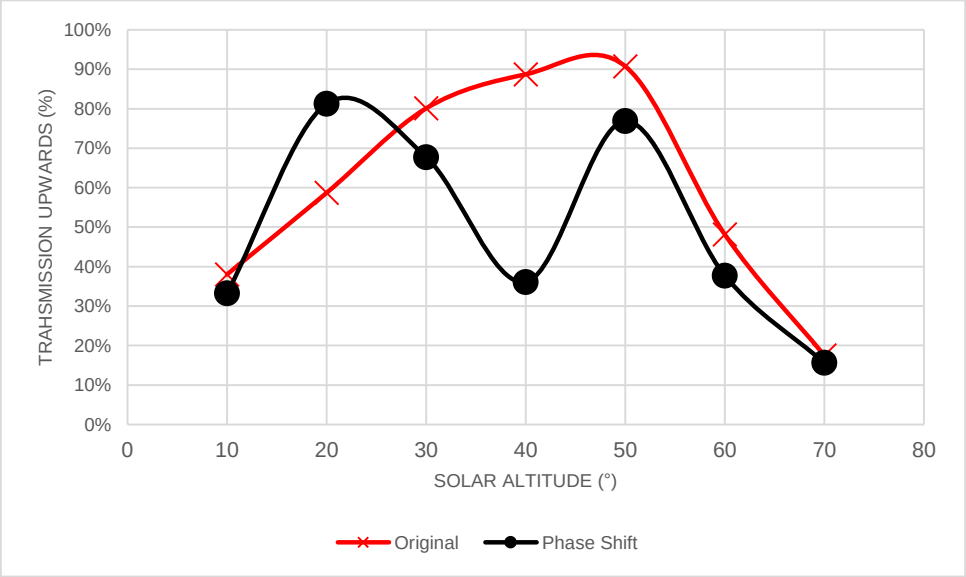


**FIGURE 18 UPWARD TRANSMISSION CHANGE IN COMPARISON WITH THE PHASE SHIFT**

## 3.6 Comparison with other models

The final design's ray trace output was compared with other model designs in order to evaluate its potential strengths as seen in Figure 19. The design was weighed against 3 of the most relevant and significant design in the literature in terms of efficiency. The assessment criteria was the percentage of light power directed upwards at solar altitudes 10° to 75°.

The proposed design showed high power transmission above 80% at solar altitudes 22° till 52°, while it was higher than 50% from solar altitude 12° till 58°. However, the transmission upwards decreased dramatically from 60° to 75° reaching 20%. Compared to other designs, the proposed design transmission is higher than LUMITOP® at all solar altitudes, while it exceeds Muller's design at solar altitudes 20° to 55° and Nassar's design from 10° till 40°.

Overall the proposed design has a higher area under the curve which means that it has an overall higher percentage of light redirection upwards.

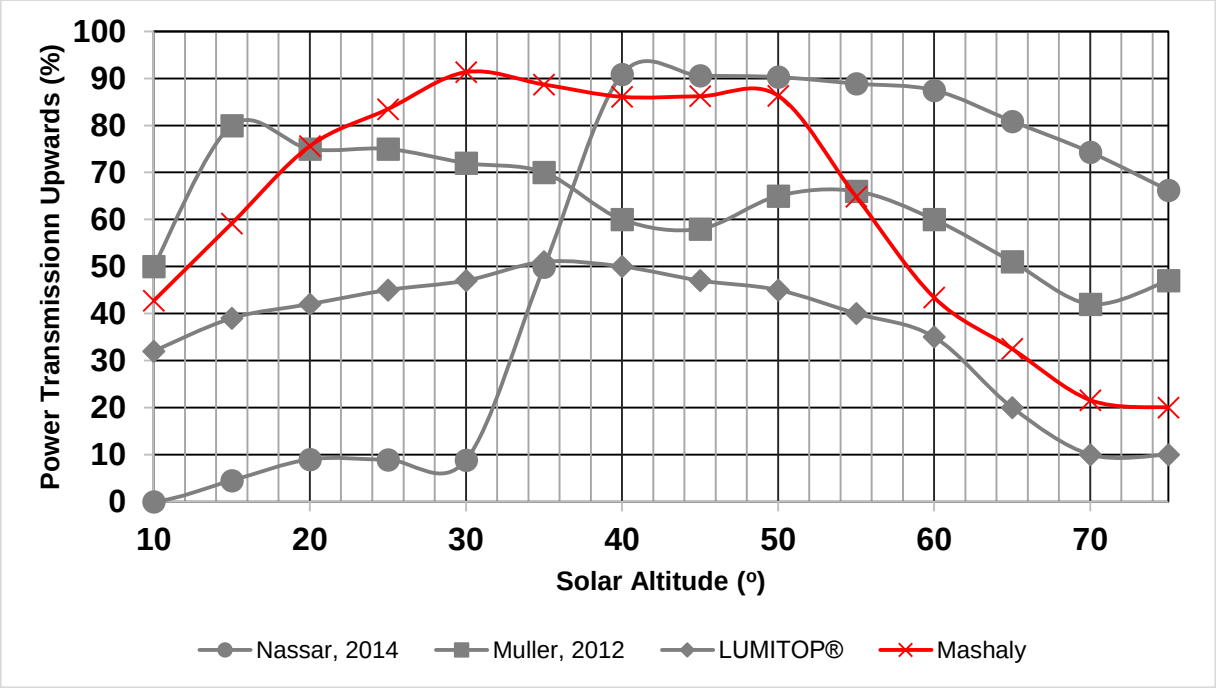


**FIGURE 19 POWER TRANSMISSION UPWARDS COMPARISON**

## 3.7 Conclusion

An optimum solution was developed through several iterations and processes using both the mathematical model and the 3D ray trace software. The proposed design produces desirable output angles at high solar altitudes, as well as low solar altitudes, with an acceptable power output. Both TracePro® results and mathematical model results showed great resemblance with an average error of ±5°.

It is important to note that ray tracing was the key factor in forming the final shape. Furthermore, the power output, calculated through TracePro®, gave an initial indication for the expected illumination if such design was to be used commercially.

# CHAPTER 4:

# DAYLIGHT SIMULATION OF CFS

# Chapter 4: Daylight Simulation of CFS

## 4.1 Daylight simulation methods

### 4.1.1 Computer aided tools for daylight assessment in buildings

The assessment of daylight performance can be accurately carried out using real scale facilities ready for measurement of daylight performance. On the other hand, using small scale models is more economic, however, specialized equipment such as a Heliodon or a sky simulator should be used (Scartezzini, 1994) (Thanachareonkit, Comparing physical and virtual methods for daylight performance modelling including complex fenestration systems, 2008). Although the previous methods would produce highly accurate results, researchers, nowadays, tend to rely more on the use of computational simulation and daylight assessment software, due to the high cost of manufacturing of CFS, difficulty in installation and setting up the complete model, sophistication of measurement equipment and the availability of the devices.

The first computer aided simulation were first developed in the 1970s (Thanachareonkit, Comparing physical and virtual methods for daylight performance modelling including complex fenestration systems, 2008), where creating geometrical 3-dimensional shapes and analysing their shadows was possible; however, they were recognized more in the early 1990s as PCs were readily available. In 2006, 79% of researchers, evaluators, engineers and designers used computer simulation with their daylight related work (Reinhart & Fitz, 2006).

Figure 20 summarizes the areas of lighting simulation using computer, the chart was developed by (Dávila, 2014) referenced from (Ward & Shakespeare, Rendering With Radiance: The Art And Science Of Lighting Visualization, 2004) and (Ochoa, Aries, & Hensen, 2011):

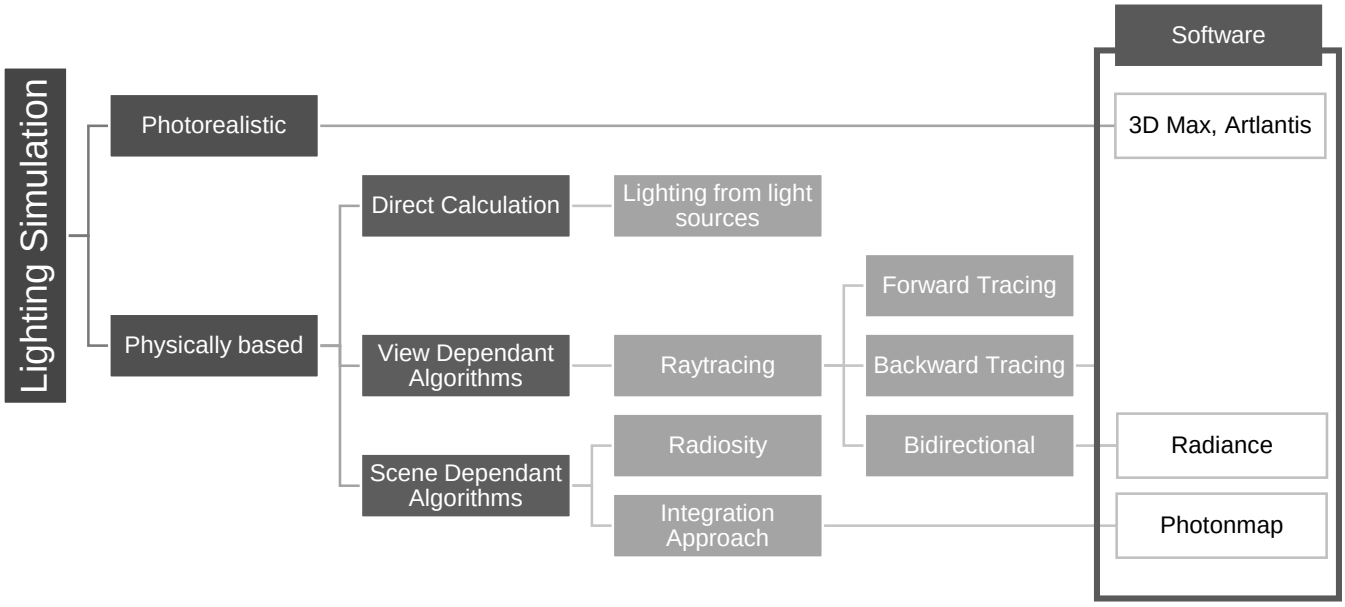


**FIGURE 20 SUMMARY OF AREAS OF LIGHTING SIMULATION USING COMPUTER**

There are two main areas in the lighting simulation field, the first is photorealistic rendering and the second one is physical-based visualization or predictive rendering (Ochoa, Aries, & Hensen, 2011) (Moeck & Selkowitz, 1996). Although photorealistic rendering is far more attractive than the physically based rendering, however, they do not represent the behaviour of lighting in real life. Some of the famous photorealistic rendering software are 3Ds Max, Architect 3D and Artlantis (Dávila, 2014). Nonetheless, one study by (Reinhart & Breton, 2009) proved the reliability of 3Ds Max in daylight simulation design in comparative settings with a physically based daylight simulation reliable software called Daysim.

Computer algorithms are used in daylighting simulation tools to solve the light distribution within or outside buildings; techniques used in prediction are classified into 3 main types as seen in Figure 21: scene-dependent algorithms (radiosity method), view dependant algorithms (ray-tracing technique) and direct calculations. The view-dependent algorithms are then divided according to the direction of the rays' computation (backward tracing or forward tracing), while the scene-dependent algorithm are not able to deal with specular reflections.

Ray-tracing algorithms are used in cases where the surfaces have ideal specular properties, while radiosity-based models are more convenient when having surfaces with diffused properties (Lambertian surfaces are used in the assumption (Chan & Tzempelikos, 2012)).

The algorithms that combine both ray-tracing and radiosity are considered as a more efficient way for calculating the global illumination (Ochoa, Aries, & Hensen, 2011).

**TABLE 7 LIGHTING SIMULATION ALGORITHMS CURRENTLY AVAILABLE (CARLOS, MYRIAM, & JAN, 2012)**

| Algorithm | Value |
|---|---|
| **View-dependent** | forward ray tracing |
| | backward ray tracing |
| | bi-directional ray tracing |
| **Scene-dependent** | Radiosity |
| | Photon map |
| | Integrative approaches |
| | Multi-pass approaches |
| **Direct Calculation** | For artificial lighting, follows national standards |
| **Calculation Aids** | Deterministic methods |
| | Statistical Sampling methods (Monte-Carlo) |

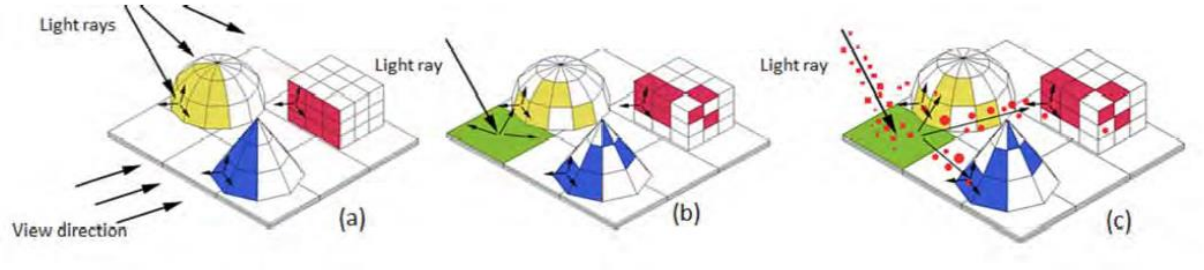


**FIGURE 21 SCHEMATIC ILLUSTRATIONS OF THE 3 COMMONLY APPLIED LIGHTING SIMULATION ALGORITHMS: (A) RAY TRACING (B) RADIOSITY (C) PHOTON MAP (CARLOS, MYRIAM, & JAN, 2012)**

### 4.1.2 Programs comparison

**TABLE 8SUMMARY OF THE RECENT LIGHTING SIMULATION TOOLS (CARLOS, MYRIAM, & JAN, 2012)**

| Tool | Algorithms used | Purpose | Availability |
|---|---|---|---|
| **AGi32** | Direct calculation<br>Radiosity<br>Limited raytracing | Luminaire design<br>Daylight integration | Paid |
| **DIALux** | Direct calculation<br>Daylight calculation<br>POV raytracer for images | Luminaire design,<br>Daylight integration | Free<br>Proprietary software |
| **Inspirer** | Bidirectional raytracing | General purpose | Paid |
| **mental ray** | Photon map<br>Radiosity principles<br>Raytracing principles | General purpose | Found within paid modelling software |
| **Radiance*** | Backward raytracing<br>Scene radiance | General purpose | Free<br>Open source |
| **Relux** | Direct calculation<br>Radiosity and modified Radiance raytracing | Luminaire design,<br>Daylight integration | Free<br>Proprietary software |
| **Velux Daylight Visualizer** | Photon map<br>Bidirectional raytracing | Conceptual stages in daylight application | Free<br>Proprietary software |

### 4.1.3 Radiance's Backward and Bidirectional tracing techniques

Radiance software is established upon the concept of "backward ray-tracing algorithms". It is considered one of the most influential tools in the daylighting industry (Ward and Shakespeare, 1998). Radiance is used to calculate accurate and highly-detailed illuminance distributions. "Backward raytracing" depends on what the spectator perceives by emitting rays from the reference point or the eye back to the light source.

A sophisticated sampling method, named the Monte-Carlo method, was usually merged with ray-tracing calculations in ray sample generating process (Tsangrassoulis et al., 2002). Moreover, a “forward ray-tracing algorithm” is used to deliver a more spontaneous full-scale results of illumination distribution in a room (Campbell and Whittle, 1997).

Pure ray tracing has its drawbacks. For instance, it requires a heavy duty processor and a vast amount of computational memory, on top of that it is extremely time-consuming, particularly for surfaces rich with information about diffuse characteristics “large amount of rays should be sampled to accurately model anisotropic effects in the ray-tracing process”. Faster algorithms, for instance, radiosity based techniques are preferred in various situations (Athienitis and Tzempelikos, 2002) (Lehar and Glicksman, 2007).

Radiance is considered as one of the most influential and accurate software in the world of lighting simulation, since it uses both backward ray-tracing and bi-directional transmission distribution functions (BTDFs).Accordingly, the specular and direction diffuse components of a radiance scene are calculated accurately (Dávila, 2014).

The program, Radiance, is very flexible in terms of geometry and material selection, modification and creation. Its advantages, nevertheless, comes with the price of complexity in running the program and handling, since radiance is an open source program and has no interface. However, many developers succeeded in reshaping the open source software Radiance and embed its engine within other daylight simulation software that have friendly user interface. An overview of some of the notable software using Radiance as their daylight simulation engine are demonstrated in the table below:

**TABLE 9SUMMARY OF THE LIST OF PROGRAMS THAT USE RADIANCE SOFTWARE AS THEIR SIMULATION ENGINE**

| Tool | Purpose | Sky modelling | Availability |
|---|---|---|---|
| **DAYSIM** | Annual illuminance values | CIE standard skies | Free |
| | Annual glare risks | | |
| | Electric lighting energy demand for dynamic systems | | |
| | Dynamic facades | | |
| **LIGHTSOLVE** | Exploration of different design options | ASRC/CIE Perez model | Free |
| | Illuminance on yearly basis using a time segmentation method | | |
| **DIAL+** | Lighting, cooling and ventilation in buildings | CIE overcast sky | Paid |
| | Daylight factor, daylight autonomy and the electricity demand of office rooms | | |
| | Advanced fenestration systems such as blinds, overhangs | | |
| **DIVA for Rhino** | Daylighting and energy modelling in buildings | Multiple sky types (overcast and clear skies) | Free & Paid versions |
| | Environmental performance including “climate-based daylighting metrics” | | |
| | Individual and Annual time step glare analysis | | |
| | Single-thermal zone energy | | |
| | Materials type can be used including BSDF data only in point in time simulation | | |

| | | | |
|---|---|---|---|
| **GERONIMO** | Perform CFS daylighting calculations | Multiple sky types (overcast and clear skies) | Free |
| **Relux Pro (Relux Informatik 2010)** | Electric light calculations mainly | CIE standard skies | Free |
| | Photometric data from luminaire manufacturers is linked to the programme | | |
| | Radiosity method mainly but an enhanced version of RADIANCE has been implemented lately | | |
| | CFS simulations (only 4 are available in the EPFL/LESO-PB DB) | | |

(Reinhart & Wienold, DAYSIM, 2016) (Perez, Seals, & Michalsky, 1993) (Andersen, et al., 2008) (Paule, Flourentzou, & Bauer) (Alstan, 2014) (Kämpf, Basurto, & Scartezzini, Visualization of the impact of complex fenestration systems based on Radiance, 2011) (Kämpf & Scartezzini, GERONIMO: the CFS Daylighting Wizard, 2011) (Validation case test CIE-171-2006, 2013)

## 4.2 Simulation of daylight behavior through a Complex Fenestration System (CFS)

### 4.2.1 Three-Phase Method

Numerous modelling and simulation strategies are proposed in the recent years to exemplify the light behavior of Complex Fenestration Systems CFS. Mainly the “Bi-directional Scattering Distribution Function” (BSDF) is the most common and validated scheme to simulate the optical characteristics of a complex model. Klems established a calculation method to produce “BSDF data of multi-layered complex glazing systems from the angularly set data of single layers”, that can be independently calculated and measured (Klems, 1994). Physically, a goniophotometer can be used to measure the BSDF data of complex fenestration systems, however the measurement instrument is not widely available. Therefore an alternative, less cheap and easier way, is using computer based simulation ray tracing. GenBSDF, a Radiance-based program, calculates the datasets from the geometry of macroscopic surfaces and surface properties of the base materials (McNeil A. , Jonsson, Appelfeld, Ward, & Lee, 2013). Radiance, as a ray tracing based software, can deal with the BSDF data to simulate the daylighting performance. With the purpose of accurately simulating the behavior of a CFS and relying on the outcome, there are certain methods on Radiance that can do that (Ward, Mistrick, Lee, McNeil, & Jonsson, 2013). The three-phase method is an approach based on the daylight coefficient method, in the three-phase method the light transport from the outside to the inside environment is separated into three phases: exterior light transport, fenestration light transmission through a BSDF dataset and interior light transport (Ward & Shakespeare, Rendering With Radiance: The Art And Science Of Lighting Visualization, 2004).

The "three-phase method" is considered an effective method for performing annual simulations of complex fenestration systems (CFS) and dynamic fenestration systems. Figure 22 illustrates the matrices used in the 3 phase method. The flux transfer is categorized into 3 independent simulation stages as the following:

1. Sky dome to the exterior of window system
2. Transmission by BSDF through window fenestration system
3. Inner part of window into the simulated room

Instead of simulating daylight behavior in a specific point in time, “the three-phase method computes normalized coefficients that link flux input to output for each phase” (Mcneil, The Three-Phase Method for Simulating Complex Fenestration with Radiance, 2013).

$$I_{3ph} = VTDS \tag{1}$$

Where;
I= Illuminance matrix, in a form of time series
V= View matrix, involving outward directions on window to desired points at the interior space
T= Transmission matrix, connecting incident fenestration system directions to exiting directions (BSDF)
D= Daylight matrix, linking sky patches to incident directions on window
S= Sun Matrix, a collection of sky vectors represented by direction patches in the sky

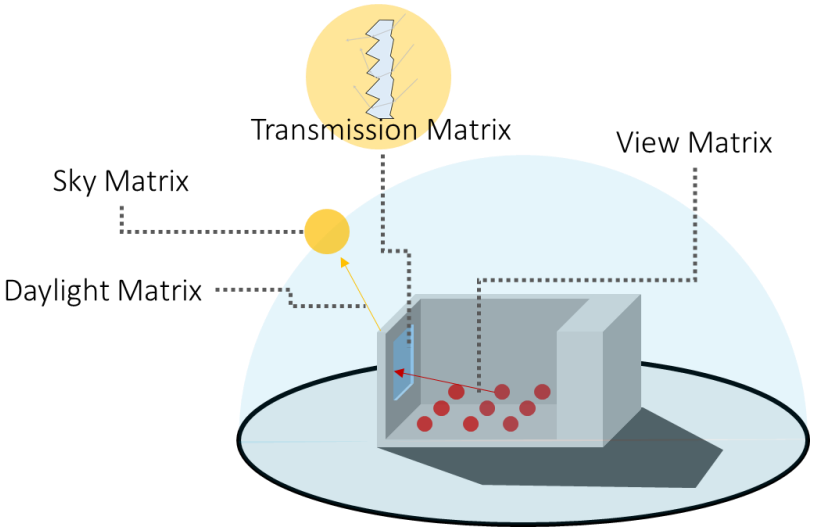


**FIGURE 22 ILLUSTRATION OF THE COMPONENTS OF THE THREE-PHASE METHOD**

Both the view matrix and daylight matrix are created with Radiance simulation, as for the sun matrix, it is mainly extracted from a weather file of a specific location. While the transmission matrix is mainly a BSDF that can be created using radiance’s genBSDF command or TracePro®.

“A result for a specific daylight condition is computed by multiplying the coefficient matrices by the input values (sky luminance values). Matrix calculation can be performed very quickly enabling the user to simulate many sky conditions and fenestration transmission properties.” (Mcneil, The Three-Phase Method for Simulating Complex Fenestration with Radiance, 2013)

#### 4.2.1.1 Flux Transfer Phases

##### 4.2.1.1.1 SKY

The sky matrix is the input of the 3 phase method, it is not considered one of the three phases since it describes the quantity and origin of flux. The command *genskyvec* generates a sky description that converts it to sky vectors in case of point in time situation, or sky matrix in case of an annual simulation.The sky matrix is created from a weather data file (.wea), it holds 8760 direction vectors for the year's hourly values.

The sky vector is a record of RGB radiance values for every individual sky patch, the patches are in either Tregenza or Reinhart division schemes.

##### 4.2.1.1.2 TRANSMISSION MATRIX (BTDF)

The transmission component processes directions of incident flux on a fenestration system and calculates the outgoing flux. The transmission matrix contains all the possible directions incident on a certain fenestration system, giving all possible output directions on Klems divisions which are 145 patches projected on a hemisphere with numbered subdivisions.

##### 4.2.1.1.3 DAYLIGHT MATRIX

It consists of the coefficients of luminous flux transfer resulting from sky patches to the fenestration system's incident divisions. The sky divisions light source is derived from the sky matrix, explained above, where each hour in the year is represented and calculated by each patch of the 145 Tregenza sky division.

##### 4.2.1.1.4 VIEW MATRIX

The view matrix component describes the relation involving the light exiting the fenestration from inside a space, or room, and falling on a specific point in space within the room. Since each matrix is simulated independently, the light source in this scene is considered the window from inside and it is assigned a *glow* material in order to characterize the relationship between the exiting rays from the window and the points inside the space. It is important to set the normal location of the surface of the window inside the room, since glow material is unidirectional, otherwise light would be emitted outside the space.

##### 4.2.1.1.5 COMPLATION OF ALL MATRICES

After obtaining the four matrices files independently with correct relationships between each matrix and the other, a compiler programming code multiplies all the matrices together to come up with the final illuminance values at each defined point in space at the 8760 timestep hours of the year. The irradiance values are produced in an RGB value form, therefore it should be converted using the following equation to show the illuminance values (Stokes, Anderson, Chandrasekar, & Motta, 1996) (IEC 61966-2-2, 2003) (International Telecommunication Union, 2015):

$$[(Red \times 0.26507412) + (Green \times 0.67011463) + (Blue \times 0.06481124)] \times 179 = Illuminance \quad (2)$$

The 179 is the luminous efficacy in lumens per watt used by Radiance

### 4.2.2 Five-Phase Method

Further effort has been placed in developing the Three-Phase Method in the recent years.The development of the Three-Phase method has led to a better accurate representation to a model that follows the dynamic daylight simulations standard daylight coefficient model that was offered by Bourgeois et al. More particularly,

the 5-phase method computes the component of the direct solar independently from the interreflected solar component and sky to attain higher precision of the scattering of direct solar rays in a space for CFS. The five-phase method is utilized in the state-of-the-art review on different CFS systems done by (Basurto, Kampf, & Scartezzini, 2015)

The equation employed for the three-phase method is adjusted for the five-phase method:

$$I5ph = VTDS - V_dTD_dS_{ds} + C_{ds}S_{sun} \quad (3)$$

Where:
$V_d =$ Direct only view matrix
$D_d =$ Direct daylight matrix only
$C_{ds} =$ Coefficient matrix for direct sun relating radiance of many sun positions to direct illuminance at a sensor point using a BSDF with proxy geometry or a variable resolution BSDF material.
$S_{ds} =$ Sky matrix containing only the sun luminance (no sky luminance)
$S_{sun} =$ Direct sun matrix containing the radiance and position of the sun

The principal approach of the five-phase method is as following:

1. Execute a normal simulation using the three-phase method.
2. Remove the contribution of the component of the direct solar.
3. Add the direct solar component that is simulated more accurately.

#### 4.2.2.1 $V_dTD_dS_{ds}$ - Isolating the three-phase direct sun contribution

The VdTDdSds term recreates the 3 phase scene with the computation of the direct sun contribution only. It is essential to calculate the previous component in order to separate the direct sun in order to subtract it from the 3 phase method result preceding to introducing a more precise direct sun contribution.

##### 4.2.2.1.1 $S_{DS}$ – DIRECT SUN MATRIX

$S_{ds}$ is the sky matrix which consists only of the more accurate direct solar radiance. It is generated with the -d constraint of *genskyvec* or *gendaymtx.*

##### 4.2.2.1.2 $D_D$ – DIRECT DAYLIGHT MATRIX

The direct daylight component matrix contains light coming from the sky that falls on the fenestration system without any reflections. The -ab 0 can be used.

Even with using ambient bounces (-ab) equal zero to avoid the inter-reflections, if the light ray falls on a surface with a non-zero specularity and roughness less than 0.002, a mirror-like reflection ray will be bounced (even with -ab 0) that would then fall back on the surface dome of the sky's.

In order to prevent the previous mirror specular reflections, a new material file with materials of zero specularity has to be created; however, changes has to be made later to all materials to black for similar reasons.

##### 4.2.2.1.3 $V_D$ – DIRECT VIEW MATRIX

The direct view matrix contains light that goes straight from the fenestration system to a light sensor node or a surface, in the case of a rendering. The direct view matrix is produced in the same manner of the view matrix,

but to avoid rays from reflecting surfaces, using -ab 1 is a must and having black material on all surfaces to avoid specularity.

#### 4.2.2.2 $C_{ds}S_{sun}$ - Calculating the direct sun contribution

##### 4.2.2.2.1 CREATING $C_{DS}$

This run uses a sky with various suns in the sky. In order to simulate the suns' positions only without any ambient lighting or reflected flux from other surfaces. The radiance scene, in normal practice, is set to zero ambient bounces, in a way that the rays simulated are the ones that do not bounce and goes directly to the source.

The command *–ab* 0 cannot be used since the surface is a BSDF material. The BSDF material needs to be sampled from all directions, which can be made with ambient sample rays. The *–ab* 1 is used to create ambient samples. Nevertheless, the reflected sunlight component should be suppressed using an all-black model.

BSDF is used to calculate the direct sun component, it can be done using proxied geometry or without. All other materials should be black as well.

##### 4.2.2.2.2 CREATING $S_{SUN}$

*Gendaymtx* is used in creating the sun matrix coefficient. "*Gendaymtx* has the currently undocumented option '-5' for the 5-phase method direct sun matrix generation. This option creates a direct only sky with all the sun's energy in a single patch. Additionally, the energy is adjusted to suit the solid angle of the sun instead of a full sky patch (since suns are used in the simulation)." (McNeil, The Five-Phase Method for Simulating Complex Fenestration with Radiance)

#### 4.2.2.3 Combining the components

In order to come up with the final result of the five phase method, all 3 main terms have to be combined together. First, the three-phase result is obtained and the direct component is subtracted from it, while the third term of the more accurate sun component is added to compute the five-phase method. The method of combining the results depends on the type of result. rcalc is used for an illuminance sensor result while pcomb is used for a rendered result.

## 4.3 Modelling a BSDF on Radiance for the CFS

In order to create a representative complex fenestration system on Radiance and to accurately simulate the behaviour of the light propagating through it, a genBSDF function has to be used. The radiance command genBSDF generates a BSDF which acts in a form of a surface with a forward and backward transmission behaviour similar to the CFS in reality.

Generating this BSDF requires first accurate modelling of the whole geometry of the CFS, not just the glazing part. Therefore, the prismatic panel, normal glazing panel and the fenestration frame were modelled on Rhinoceroses 5.0 with the right dimensions. However, the modelled fenestration exterior face normal was oriented parallel to the Z+ while the whole fenestration had to be within the negative side of the Z axis since

the flux source for the BSDF is on Z=zero while the light direction is with the -Z direction. Therefore the CFS room facing side normal is directed towards the negative Z. The modelled CFS is independent from the Radiance Scene that will come afterwards. As Radiance considers the horizontal plane the XY plan, while the genBSDF command considers the XZ the horizontal plane as shown in Figure 23.

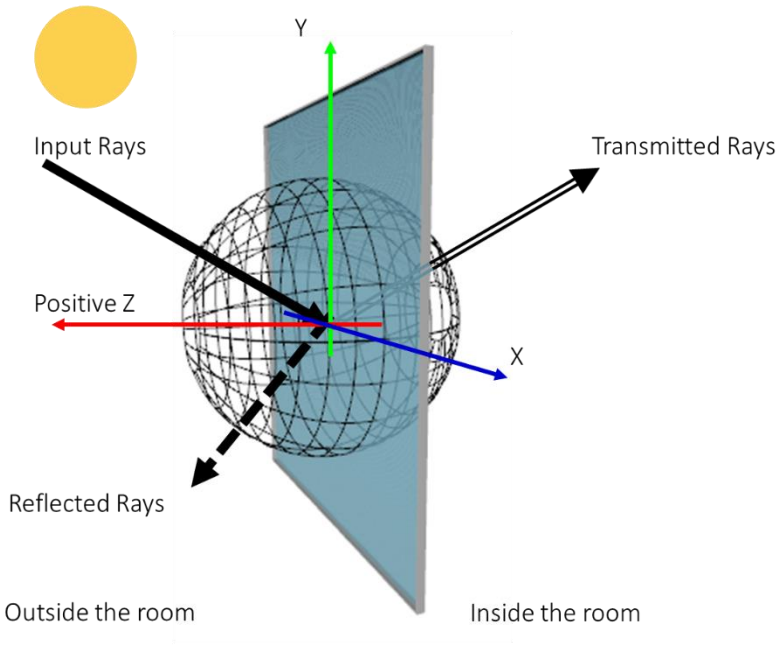


**FIGURE 23 SCHEMATIC DIAGRAM REPRESENTING INTERIOR AND EXTERIOR VECTORS OF A BSDF**

### 4.3.1 GenBSDF results on Klems patches

The Klems patches viewing mode is one of the principal methods of viewing the results of a BSDF file generated by Radiance or Window6. The viewer contains both the incident rays, which are input by the user and transmitted rays, which are acquired from the XML file generated from genBSDF Radiance command. The 2 circles represent the hemispheres of incident rays (or reflection) and transmission. Each hemisphere is divided into 145 patches where each patch represents a specific angle as shown in Table 10 and Figure 24.

**TABLE 10 THE PATCHS DIVISIONS & THE ANGLE RANGE OF EACH THETA BAND IN THE KLEMS PATCHS IN BSDF**

| Theta Band | Number of phi | Patch Numbers | Theta Range | Solid Angle | Average Cosine Theta | BSDF value for specular patch |
|---|---|---|---|---|---|---|
| **1** | 1 | 1 | 0°-5° | 0.0239 | 0.9981 | 41.9043 |
| **2** | 8 | 2 -9 | 5°-15° | 0.0238 | 0.9811 | 42.8764 |
| **3** | 16 | 10 - 25 | 15°-25° | 0.0234 | 0.9361 | 45.6281 |
| **4** | 20 | 26-45 | 25°-35° | 0.0274 | 0.8627 | 42.333 |
| **5** | 24 | 46-69 | 35°-45° | 0.0293 | 0.7631 | 44.6724 |
| **6** | 24 | 70-93 | 45°-55° | 0.035 | 0.6403 | 44.6724 |
| **7** | 24 | 94-117 | 55°-65° | 0.0395 | 0.4981 | 50.7996 |
| **8** | 16 | 118-133 | 65°-75° | 0.0643 | 0.3407 | 45.6281 |
| **9** | 12 | 134-145 | 75°-90° | 0.1355 | 0.1294 | 57.0215 |

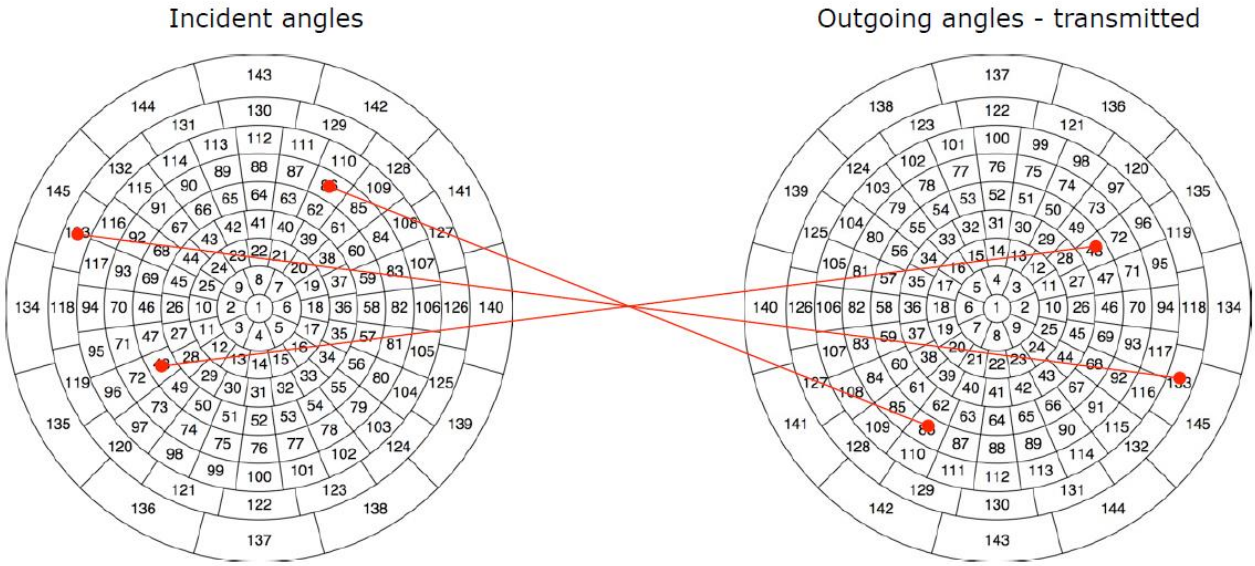


**FIGURE 24 NUMBERED KLEMS PATCHES EXPLAINING HOW TO READ THE BSDF VIEWER (MCNEIL, JONSSON, & APPELFELD, VALIDATION OF GENBSDF, 2011)**

### 4.3.2 Modelling the proper material properties

Polypropylene (PP) natural is opaque/translucent because it contains crystals of PP. The crystals have a different refractive index than the amorphous (non-crystalline) part and are of the right size to scatter light, this makes the material cloudy. Additives can be used in order to make the crystals smaller so that they don't scatter light giving PP that is close to transparent.

PP homopolymer is normally translucent. Light can pass through it but is scattered for the reasons previously mentioned. PP copolymers are inherently more transparent.

Due to the diversity in the types of the polypropylene and the ways of manufacturing and applications, it is difficult to standardize the optical properties of this translucent material. PP can range from being a transparent material to solid and opaque. Therefore, for the purpose of this thesis research, the polypropylene used will be assumed to have high transmittance value and glossiness.

### 4.3.3 Defining Translucent Plastics in Radiance

In a study published by Reinhart and Andersen entitled “Development and validation of a Radiance model for a translucent panel” it was demonstrated that modelling translucent materials in Radiance is possible with an overall mean bias errors (MBE) below 9% and root mean square errors (RMSE) below 19%, which is considered to have greater accuracy than those demonstrated in earlier validation studies for the plastic, metal, and glass material types (Reinhart & Andersen, 2006).

So as to model translucent material, Radiance’s library includes materials that take into account translucency, specularity and transmission. This material is defined by the modifier *Trans* within Radiance’s material definitions (Building Technologies Program, 2014).

The trans primitive is defined as follows:

```
modifier   trans identifier
Ø
Ø
7     R     G     B     ◀     (Colour)
      spec  rough       ◀     (specularity & roughness)
      trans tspec       ◀     (transmission & transmitted specularity)
```

#### 4.3.3.1 Defining Recycled Plastics

As for recycled plastics, it is highly probable that the recycling process would not be 100% pure PP and any type of impurities will affect the optical properties of the final product. Moreover, the impurities are randomly present within the medium of the panel. Therefore, to represent those impurities during simulation the prismatic panel material should contain a "*FunctionFile*" replicating those impurities. The most sutiable function file done in radiance for the previous circumstances is the"*Noise.cal*". In order to use the *Noise.cal* function file, another material definition should be used, the *transfunc*. The *transfunc* is a unique material definition script that is used for arbitrary (BRDF). The arguments to this material are the data file in this case the *Noise.cal* coordinate index functions, in addition to specular transmission and reflectance. The only modifier that is not available in this material definition is roughness, which is not required since the BRDF data is dominant. The *transfunc* parameters is defined as follows:

```
modifier   transfunc  identifier
2+    brtd        funcfile        transform
Ø
6     R     G     B     ◀     (Colour)
      rspec             ◀     (specularity)
      trans tspec       ◀     (transmission & transmitted specularity)
```

## 4.4 Applying the Five-Phase Method

The five-phase method will be used afterwards in generating data sets and illumination results for the forms that are going to be generated, the data will be used to optimize the forms' shape in order to produce an adequate shape suitable for the current environment. The testing's location will be Cairo, Egypt in a room model based on the standard office reference room for assessments of façade and light technologies. (Reinhart, Jakubiec, & Ibarra, Definition of a Reference Office for Standardized Evaluations of Dynamic Façade and Lighting Technologies, 2013). The dimensions of the room modelled are 3.6 m x 8.2 m x 2.8 m. The window dimensions are to be determined within the procedure of the research.

### 4.4.1 Room Location

The location of the experiment will take place in Cairo, Egypt, hot-arid environment, located at latitude 31 degrees at the northern hemisphere. The location is characterized by its high temperatures in summer, and clear sky with less than 10% cloud cover in the year. Cairo is considered an optimum location to test the efficiency of the designed CFS due to the high altitude sun in the summer days. Table 11 shows the values of the solar altitudes at its highest and lowest.

**TABLE 11 LOCATION-BASED VARIABLES**

| Variable | Date | Value |
|---|---|---|
| **Latitude** | | 30.13° |
| **Longitude** | | 31.40° |
| **Location** | | Cairo |
| **Highest Solar Altitude** | 21st June, 12:00 | 82° |
| **Lowest Solar Altitude** | 21st December 12:00 | 36° |

## 4.4.2 Room Parameters

The room will be based on the “reference office” room for evaluation of façade and light technologies developed by Reinhart et. al in 2013, see Figure 25 and Figure 26. The optical properties of the reference room were extracted from the study (Reinhart, Jakubiec, & Ibarra, Definition of a Reference Office for Standardized Evaluations of Dynamic Façade and Lighting Technologies, 2013) , except for the glazing which was based on the local usage of glazing, and the recommended by the Egyptian Energy Efficiency Building Code ECP 306-2005 (Egyptian Energy Effeciency for Building Code Comittee, 2006)

According to table 3-4 in the ECP 306-2005, which includes data concerning the building external envelope, the minimum required solar heat gain coefficient (SHGC) of a window in order to have a 20% window to wall ratio is 0.64. However, due to lack of reinforcement of the code in Egypt, the common practice involves using a single glazing panel with no thermal insulation or less transmission of light.

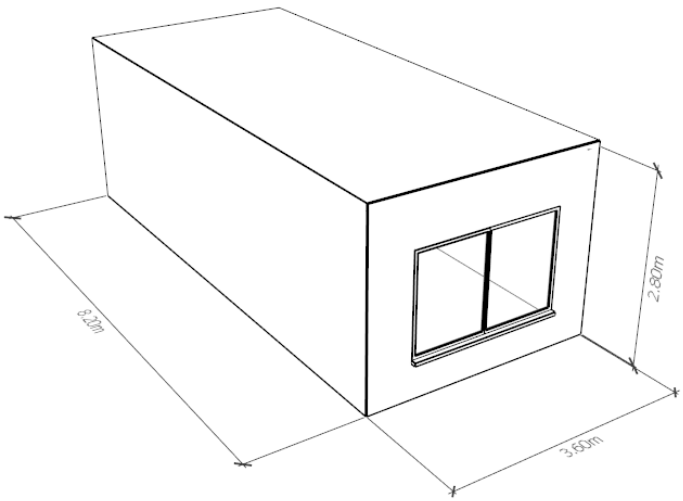


**FIGURE 25 REFERENCE OFFICE ROOM DIMENSIONS**

Input parameters for the case study are summarized in Table 12.

**TABLE 12 INPUT PARAMETERS AND ASSUMPTIONS FOR THE FIVE PHASE METHOD MODEL**

| Interior Room Surface | Parameter | Value |
|---|---|---|
| **Interior Walls** | Reflectance (%) | 0.50 |

| | | |
|---|---|---|
| **Floor** | | 0.50 |
| **Ceiling** | | 0.80 |
| **Window Frame** | | 0.50 |
| **Internal Glazing** | Transmission (%) | 0.88 |
| | SHGC | 0.64 |
| **Window to wall ratio** | Ratio (%) | 0.20 |
| **Windows Dimensions** | Length x Width (m) | 2.0 x 1.8 |
| **Shading Device** | Y/N | No |
| **Illuminance sensor point** | Height (m) | 0.75 |
| | Distance in-between (m) | 0.50 |
| | Number of points | 45 |
| | Distribution (L x W) | 8 x 5 |
| **Sky Condition** | Clear/Overcast/uniform | Clear Sky |

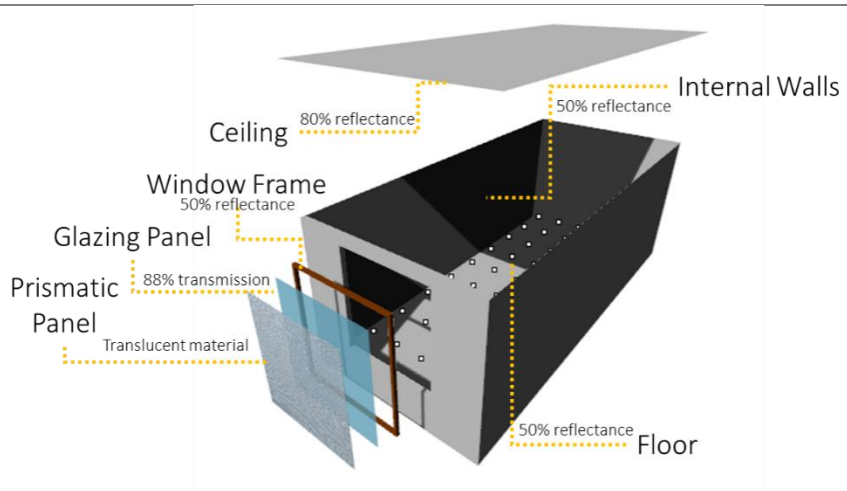


**FIGURE 26 ILLUSTRATION OF THE ROOM MATERIAL'S PROPERTIES**

## 4.5 Simulation Procedure

### 4.5.1 Five Phase Method

The simulation method used will be the five-phase method which is adequate with the modelling of CFS. The steps that will be taken into account while proceeding with the simulation are in appendix B.

## 4.6 Results & Discussion

Taking a first look at the results, the five phase method produces a list of all the hourly illuminance values throughout the year for each illumination sensor node. The total number of nodes were 45 nodes in an array of 8x5, see Figure 27. The 45 nodes were numbered according to the following illustration starting with1 in the left corner near the window and ending with the right corner in the deepest part of the room.

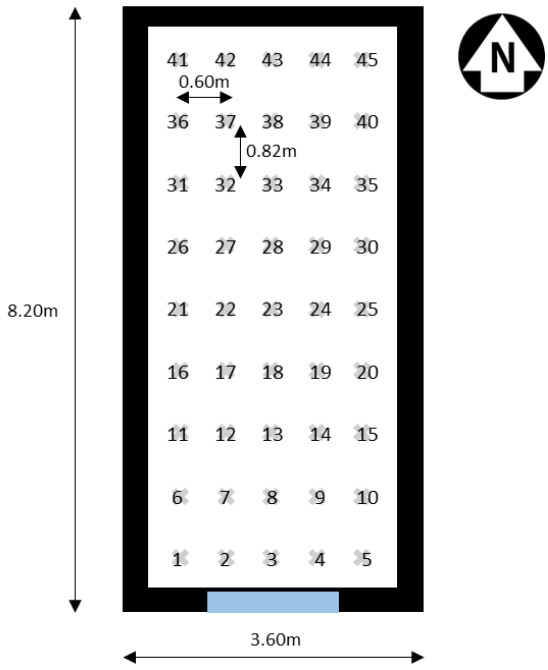


**FIGURE 27 NODES NUMBERING, POSITIONING AND DISTANCES FOR THE ROOM**

They were arranged with 0.82 meters between each row and 0.60 meters between each column. The total values for each node is 8760, which represents the number of hours per year. The value of each node corresponds to the illuminance at that point, ranging from 0 lux, at night time to 17,460 lux at mid-day time right in front of the fenestration system.

Generally, a comparison between both a window with glass only (Room 1) and the same window but with adding the proposed prismatic CFS (Room 2) would reveal the effect of adding the CFS on the general illumination in the room.

The simulation process was broke down into 4 independent trials, to test the different effects of changing some crucial parameters in the simulation procedures.

### 4.6.1 First trial

In the first simulation round, the model was set up as stated in the methodology above; however, due to the long generation time of a BSDF for a translucent material can take, it was initially assumed as a glass material panel but with the main optical property, which is the refractive index that was determined to be 1.56.

Therefore, the initial BSDF contained the prismatic panel with a material definition of glass as following:

```
void  glass CFS
0
0
4     0.96  0.96  0.96  1.56
```

This was done to check the validity of the prismatic panel behavior, which was tested before with both the mathematical model and TracePro® raytracing simulation, see Figure 28. Moreover, the upcoming results would be beneficial in case of the need for a reference model for testing other types of material to replace the recycled plastics.

#### 4.6.1.1 Comparison of mathematical model, TracePro® and Radiance's genBSDF Results

Figure 28 shows the output angles of the mathematical model, TracePro® and BSDF. Both the mathematical model and TracePro have the similar pattern where in angle 2 the output angle increases to reach the maximum angle at solar altitude 60°, then decreases with a steady rate similar in both the mathematical model and TracePro® results. While in angle 1 (upward angle) the both the TracePro® and the mathematical model sets of results show great resemblance; however, a shift of around an average of 5° is noticed between the TracePro® and Mathematical model. The standard error of the mean (SEM) for the upward angle was ±1.03 while the downward angle was ±2.47.

The BSDF model exhibits different behaviors at different incident angles, for angle 2 the values between 15° and 45° are nearly similar to the mathematical model; however, a shift in the values of around 10° is observed. Moreover, the difference between the values of the genBSDF and the mathematical model increases at both the start and end of the curve. As for angle 1, it takes a steadily increasing pattern in a rate higher than TracePro® and mathematical model with some variation in values at the high and low angles. The standard error of the mean for the BSDF results versus the mathematical model was ±3.70 for the upward redirection, while for the downward redirection the SME was ±5.83.

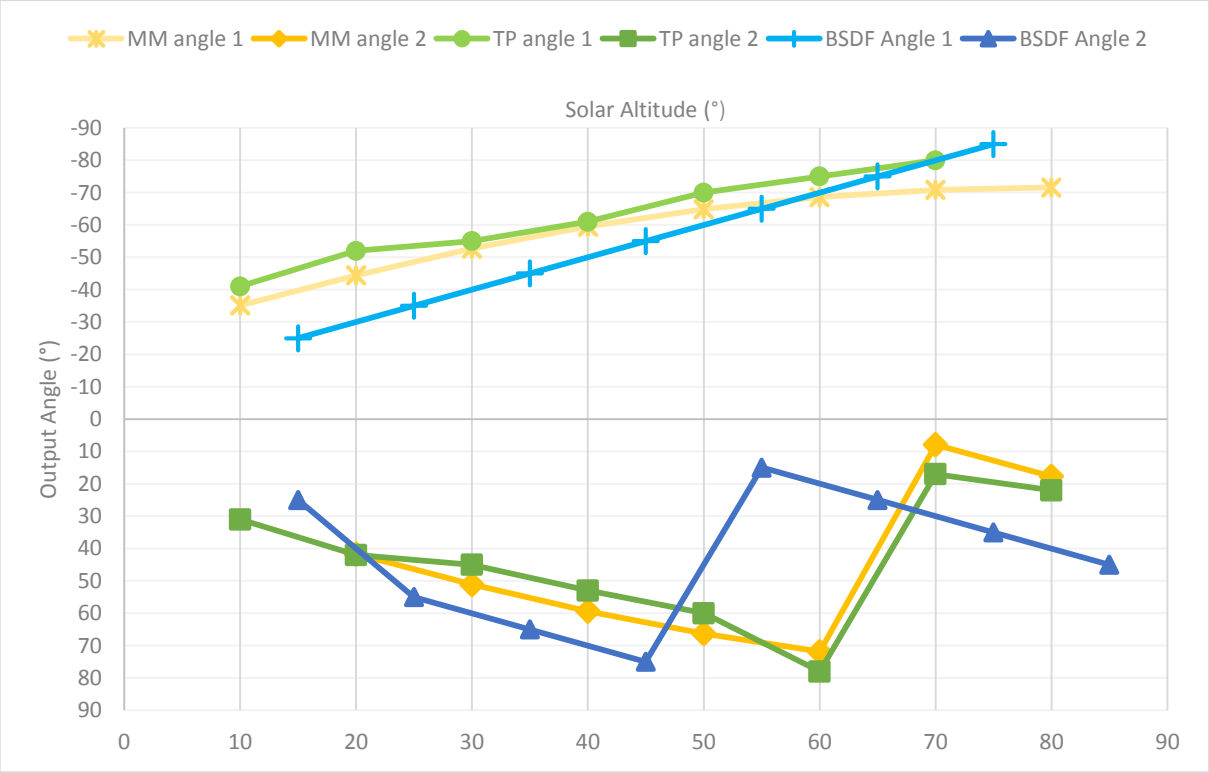


**FIGURE 28 COMPARISON BETWEEN THE MATHEMATICAL MODEL (MM), TRACEPRO® (TP) AND BSDF VIEWER OUTPUT ANGLES**

As for the power, in Figure 29, a great resemblance in the curve shape however the BSDF has higher power peaks than the TracePro®.

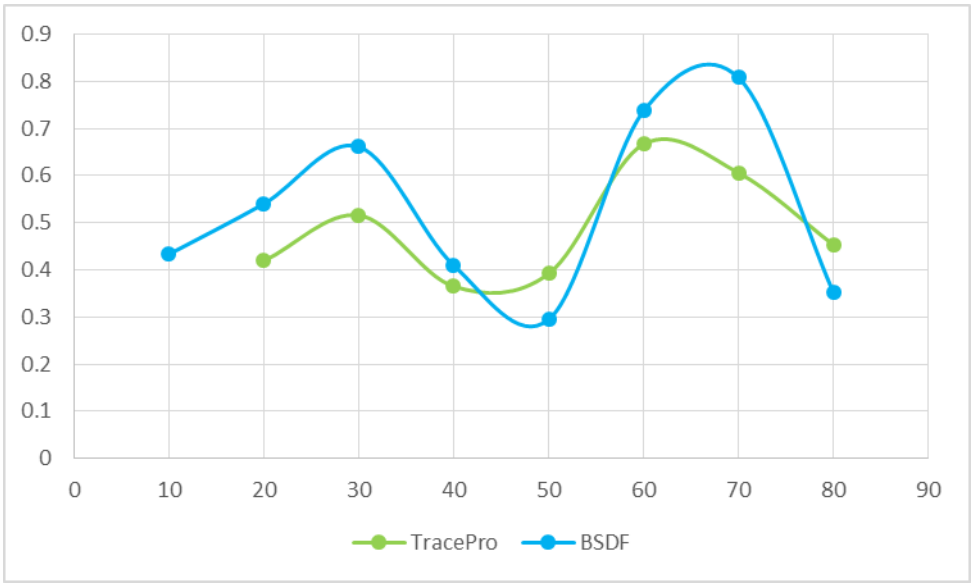


**FIGURE 29 NORMALIZED POWER FOR BOTH TRACEPRO® AND BSDF**

The proposed design considers the material used as a perfect material with flawless properties within its composition; however, plastics are versatile material that can have different properties according to the way of manufacturing. For example, polypropylene is a semi crystalline thermo plastic, unlike acrylic, the internal structure of the material might contain deformities and haziness depending on the catalyst used in the resin of PP. (Tripathi, 2002). Therefore it is crucial to test the effect of the different optical properties on the overall direction and power of light.

#### 4.6.1.2 Basic measurements

In room 1, the room with a glass only window, high illumination values were observed at sensors near the window. Those illumination values slightly decrease in the summer time, near June, and increase at the beginning and end of the year, around the spring and autumn equinoxes. Moreover, the total number of daylight hours increases in the summer reaching 14 hours per day, while in winter the number of daylight hours reaches a minimum value of 10 hours per day. Conversely, as the distance of the sensor point from the window is indirectly proportional with the illumination and decreases dramatically at the depth of the room, this leads to a great difference between the illumination values at nodes near the window and nodes further away from the window. The illumination values at the deeper parts of the room would reach values as low as 105 lux and maximum 900 lux in midday time, at hours between 10 am and 2 pm.

Similarly, room 2 had high illumination values at the spring and autumn equinoxes, with a maximum of 17,460 lux near spring equinox (09 March). Consistently, the illumination values decreases as the distance from the window increases reaching a minimum value of 146 lux and a maximum value of 820 lux at the hours between 10 am and 2 pm.

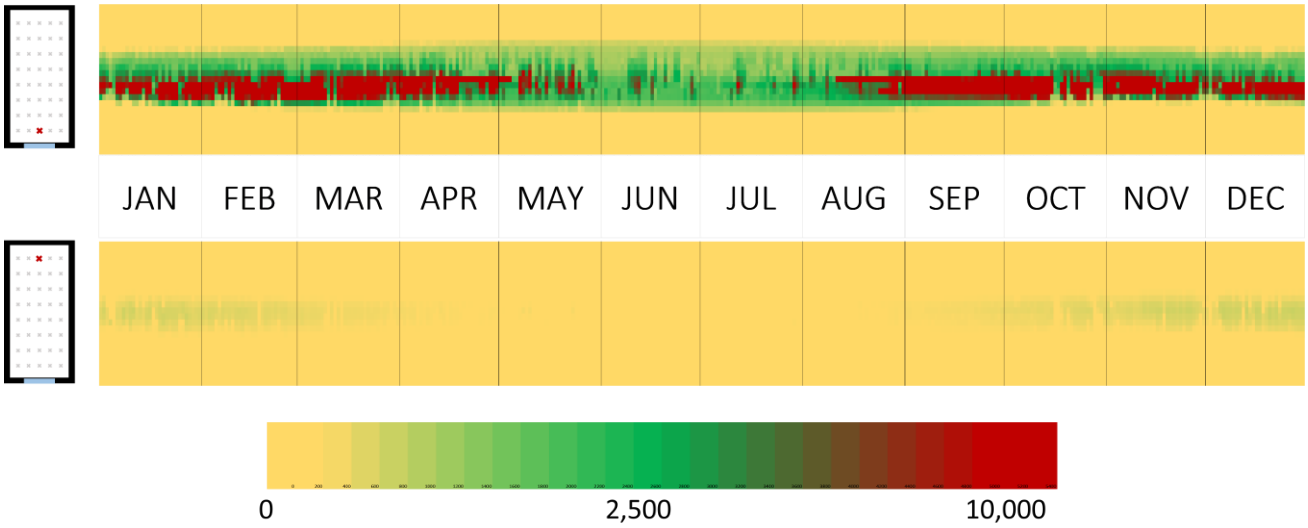


**FIGURE30 ILLUMINATION VALUES FOR THE SENSOR POINTS 3 AND 43**

It was noticed that the values of the sensors closest to the window achieved higher values than the sensors of room 1. However, the percentage increase in illumination at those sensors is considered a minor; around 9%, in the summer, and 14% in the winter, improvement in illumination. Contrariwise, a great percentage increase was noted at the illumination nodes further from the window especially at spring, autumn and summer days. Where for instance, in autumn (21st September), a 28% increase was observed, while a significant 34% increase was observed in the summer (21st of June).

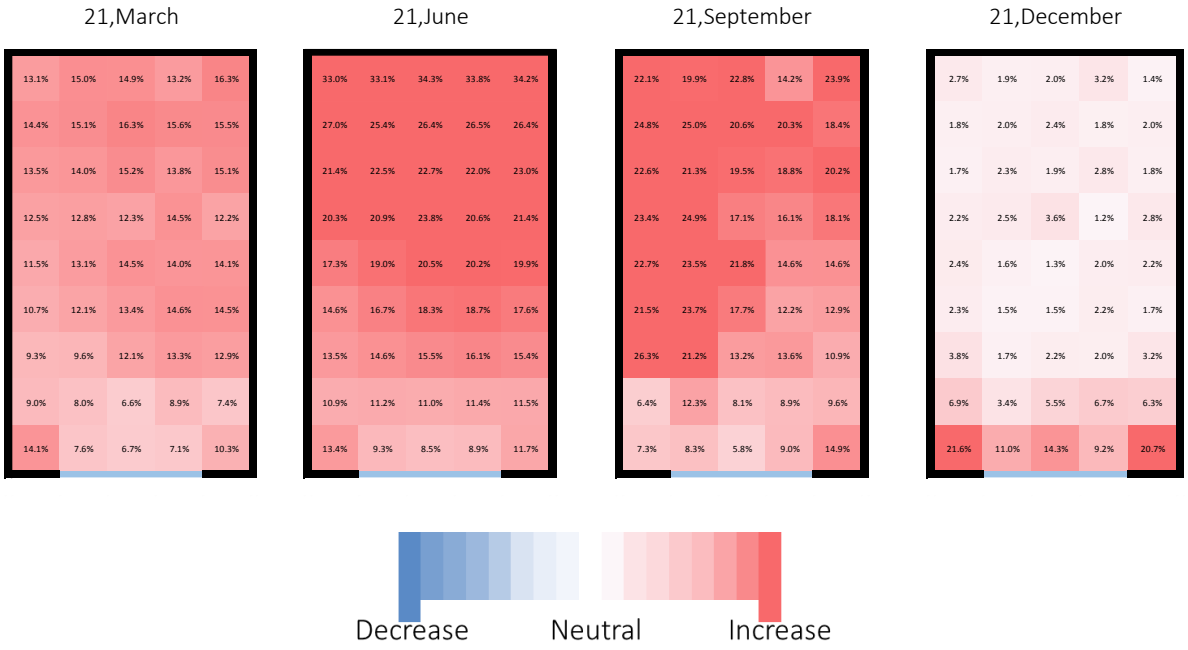


**FIGURE31 THE PERCENTAGE OF DAYLIGHT INCREASE OR DECREASE AT THE EQUINOXES AND SOLSTICES FOR TRIAL 1**

Furthermore, when all the values of both rooms were analyzed together, a graph was produced showing the improvement in daylighting at the points furthest from the window. The graph, in Figure 32, plots the

percentage of improvement versus the time of the year. It indicates an increase in the improvement as we head to the middle of the year reaching a maximum percentage of improvement in illumination in the deepest part of the room of 80% at 12th of July.

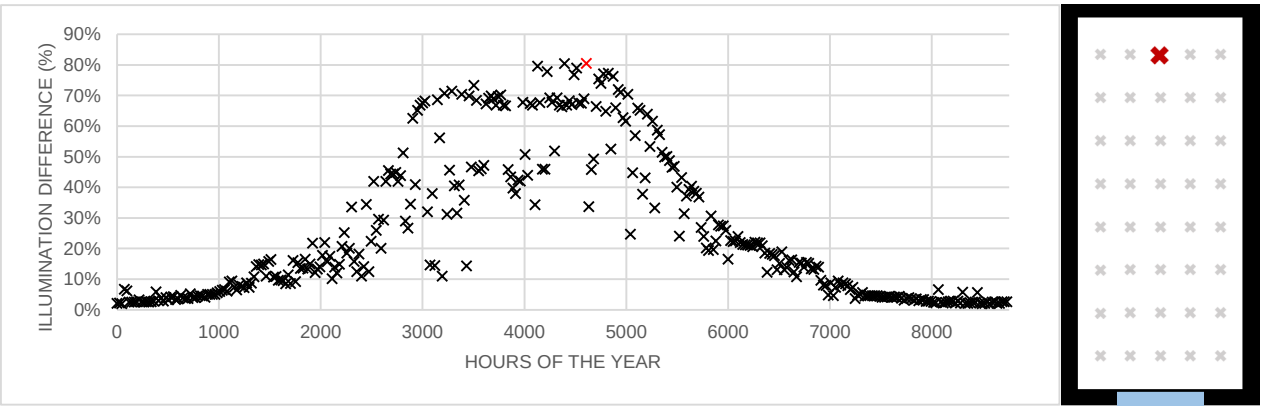


**FIGURE 32THE PERCENTAGE OF IMPROVEMENT OF ILLUMINATION AT NODE 43 AT 12 PM FOR TRIAL 1**

### 4.6.1.3 Dynamic Daylight measures

The produced results from the 5 phase method are generously detailed with hourly data, which nominates the results to be both static and dynamic, varying by the type of analysis carried on and the type of standards used in evaluating the data. Therefore, it is important to utilize the data from the five phase method in generating standard dynamic daylight measures, such as the sDA and ASE which are standardized by the US Illuminating Engineering Society (Illuminating Engineering Society, 2013).

As explained in the literature above, both sDA and ASE portrays the daylighting performance in any space, where the sDA represents how well the space is illuminated by assessing the nodes with more than 300 lux for more than 50% of the time, while the ASE describes the over lighting in a space by measuring how many sensor points or nodes does the room has more than 1000 lux for more than 250 hours annually.

In the following figures, Figure 33 and Figure 34, it is revealed that there is a general improvement of daylight through the sDA and the ASE. Room 1 had an sDA ($sDA_{300/50\%}$) of 67%, which means that the 67% of the points in the room space were illuminated with over 300 lux for more than 50% of the time. On the other hand, the over illumination is not well controlled in room 1, where more than 67% of the nodes in the room were above 1000 lux more than 250 hours during daylight time (i.e. ASE is equal 67%) .

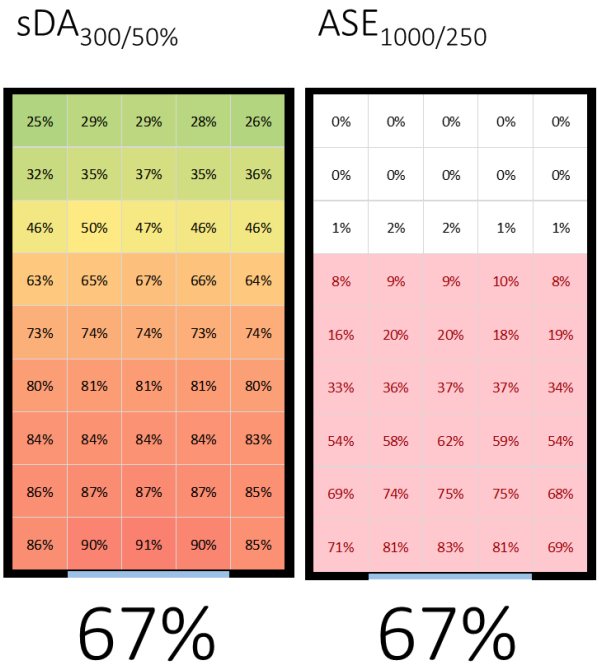


**FIGURE 33SDA AND ASE FOR THE NORMAL WINDOW (ROOM 1)**

As for room 2, a noticeable increase in the spatial Daylight Autonomy was observed while the Annual Sunlight exposure remained the same. The sDA evidently increased by 11% overall, while the parts at the depth of the room had a moderate increase in sDA, and the difference decreases as the distance is closer to the window.


**FIGURE 34SDA AND ASE FOR THE CFS OF TRIAL 1**

### 4.6.2 Second Trial

The second trial involved a more complex fenestration system, with complete geometry of a window retrofitted with the prismatic panel. The prismatic panel is yet glass material with the same properties of the previous

trial. The purpose of this trial is to evaluate the performance of retrofitting the normal glass window with a prismatic panel made from normal optical material, see illustrated in Figure 35.

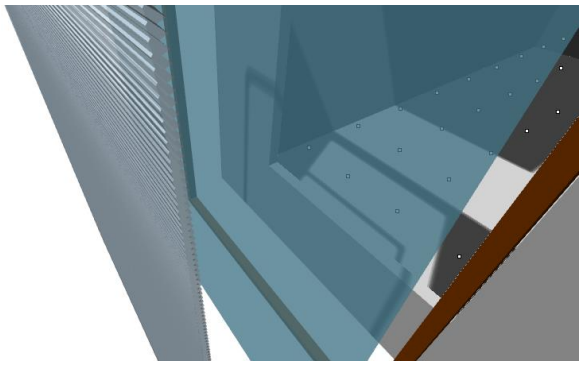

**FIGURE 35 ILLUSTRATION FOR THE LAYERS OF THE CFS IN TRIAL 2**

### 4.6.2.1 Basic Measurements

Taking a quick peek on the overall hourly illuminance values throughout the year, there is no significant difference between Room 1 and Room 2. However, at a closer look at the percentage of increase in illumination in Figure 36, there is a noticeable increase in daylight especially at the depth of the room by 40% in the autumn equinox, with a significant decrease in the illumination near the window area by 32%.

The same behavior occurs at the winter solstice, however the percentage of decrease at the window is much less significant than in autumn, as well as at the depth of the room. At the summer solstice, there is an evident decrease in the illumination near the window; however, the illumination values at the deepest part of the room remains unchanged. Nevertheless, this improvement has shrunk the difference in illumination along the depth of the room.

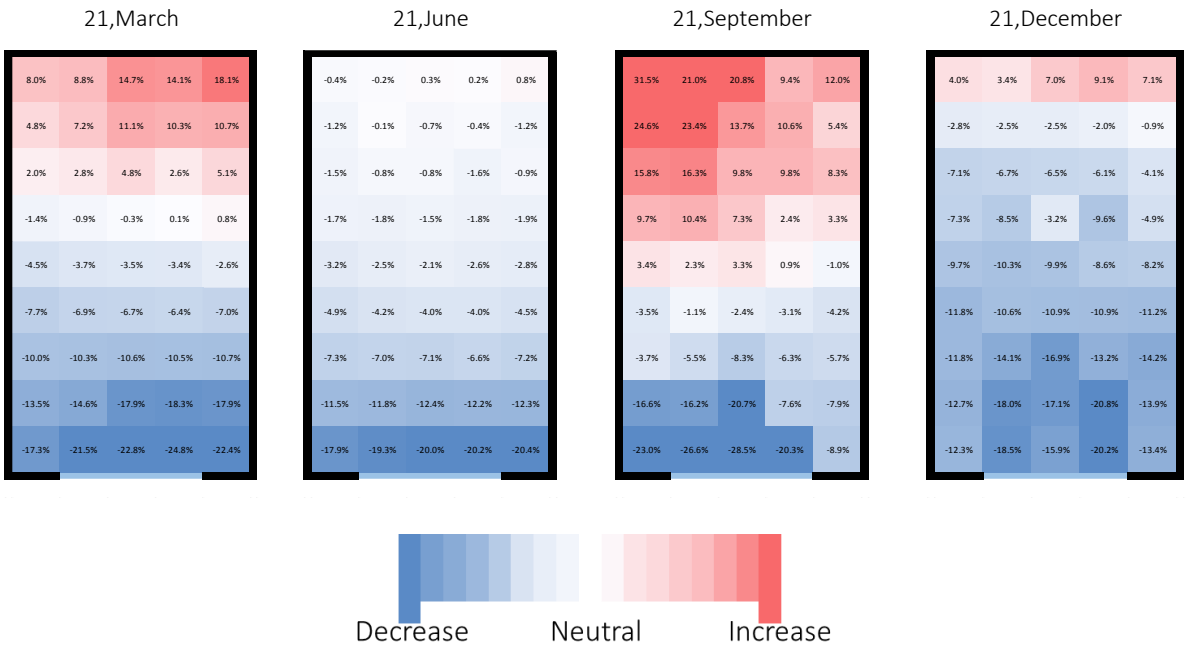


**FIGURE 36THE PERCENTAGE OF DAYLIGHT INCREASE OR DECREASE ON THE EQUINOXES AND SOLSTICES FOR TRIAL 2**

Overall, there is a general percentage of improvement at the deep areas of the room. The improvement is more significant near the autumn season as in Figure 37, where the sun is moderately high, reaching improvements of 52%; however, at spring the improvement is less than autumn although similar angles occur, with a maximum improvement of 41%. While at summer and mid-year the percentage increase in illumination in the farthest points to the window is nearly zero and winter is moderately around 20% improvement.

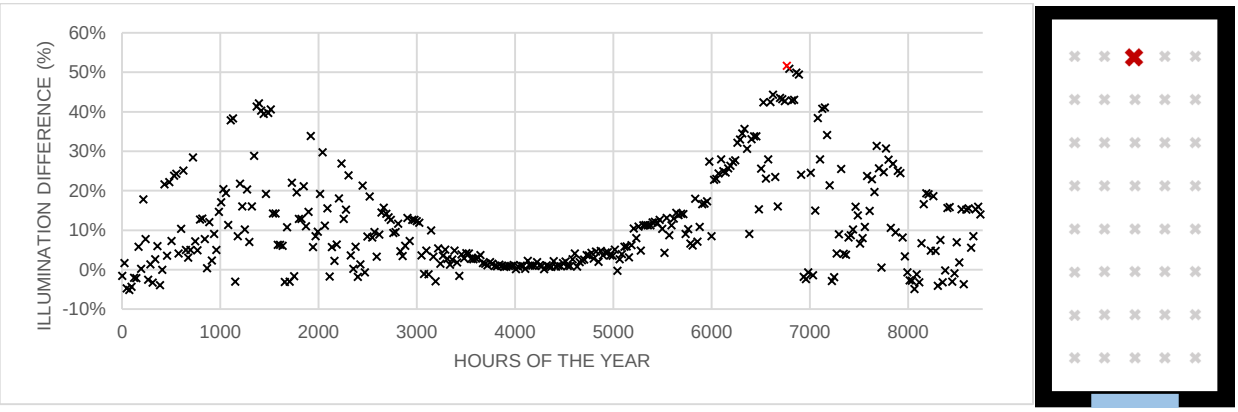


**FIGURE 37THE PERCENTAGE OF IMPROVEMENT OF ILLUMINATION AT NODE 43 AT 12 PM FOR TRIAL 2**

More importantly, a perceptible decrease in daylighting at the nodes near the window is observed by looking at Figure 38. Where it ranges between 33% fall back in illumination at both spring and autumn and a minimum of 7.5% decrease at summer. However, there are some values in the summer with an observable 20% decrease at the area closer to the window.

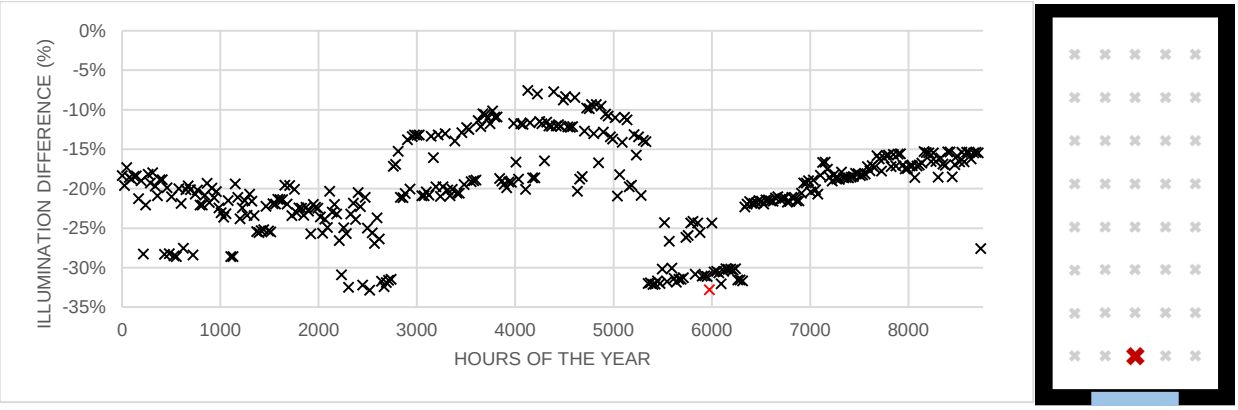


**FIGURE 38THE PERCENTAGE OF IMPROVEMENT OF ILLUMINATION AT NODE 3 AT 12 PM FOR TRIAL 2**

### 4.6.2.2 Dynamic Daylight measures

Figure 39 demonstrates that Room 2, the room having the complex fenestration system, had an sDA of 67% and an ASE of 58%. The previous results indicates that although the overall sDA stayed the same as in Room 1, the proposed design managed to lower the ASE by 7%.

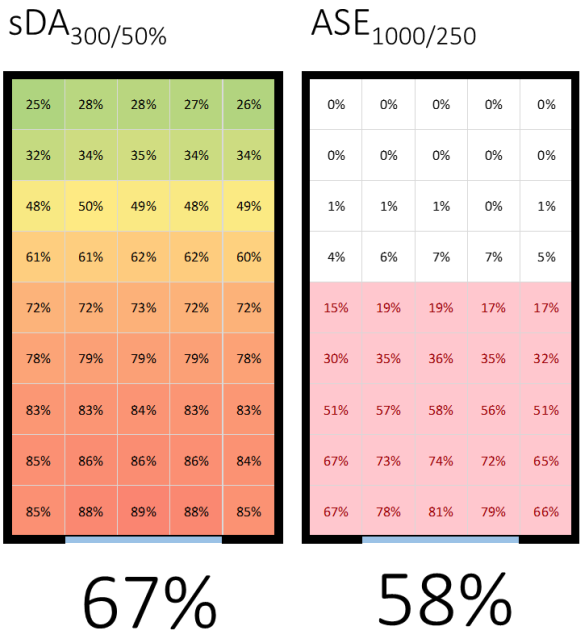


**FIGURE 39SDA AND ASE FOR THE CFS OF TRIAL 2**

### 4.6.3 Third Trial

Another trial was carried out with a more accurate model. This time a translucent material was defined for the prismatic panel. Since the actual properties of plastics would vary from a manufacturing process to the other, a basic translucent material was used.

**TABLE 13 TRANSLUCENT MATERIALS PARAMETERS**

| Parameter | Abbrv. | Value |
|---|---|---|
| **Diffuse Transmission** | $T_d$ | 0.1694 |
| **Specular Transmission** | $T_s$ | 0.5129 |
| **Diffuse Reflection** | $R_d$ | 0.259 |

The previous properties, in Table 13, are translated in form of Radiance material using the following definition:

```
Void trans material_name
0
0
7 R G B Spec_Reflectance Roughness Diffuse_Transmission  Spec_Transmission
```

Where the RGB include the specular reflectance and diffuse reflectance in the following equation (Mead, 2010):

$$R = \frac{C_r}{(1 - R_s) \times (1 - R_s)} \quad (4)$$

$$G = \frac{C_g}{(1 - R_s) \times (1 - R_s)} \quad (5)$$

$$B = \frac{C_b}{(1 - R_s) \times (1 - R_s)} \quad (6)$$

Where;

$$R_s = \frac{T_d + T_s}{(R_d + T_d + T_s)} \quad (7)$$

Therefore this translates to the following in defining the material of the prismatic panel in the BSDF:

```
void transfunc Prismatic_Panel
2 brtd Noise.cal
0
6 0.70 0.70 0.70 0.250 0.500 0.400
```

Normally, the window frame material was defined like the previous trial as well as the normal glass pane was given a glass material with 88% transmission through the following definition:

```
void glassGlass_Panel
0
0
3 0.96 0.96 0.96
```

In GenBSDF, decreasing the number of samples per incident direction using the −c option will increase the variance in the results. This value defaults to 2000 samples distributed over the incoming plane for each of the 145 Klems hemisphere directions. Sampling only 100 ray per patch, which is lower in accuracy, yet, faster in generation time, (3 hours 16 minutes compared to a normal 2000 samples with time of 17 hour and 45 minutes) will give a quick overview on the direction of the results before heading to the more accurate simulation.

```
"genbsdf.exe -c 100 +geom meter materials.rad CFS.rad >CFS_Trial_3.xml"
```

#### 4.6.3.1 Basic Measurements

The 3rd trial showed a decrease in overall illumination than in room 1 with a maximum illumination of 12964 lux. Also the minimum illumination at 12 PM at all times was slightly increased from 156 lux in room 1 to 160 lux in room 2 at the depth of the room.

An improvement in lighting at the depth of the room scored a maximum of 44% improvement at 6th of April at noon. While the proposed design in trial 3 reduced the illumination in front of the window by 25 percent at the same day.

At a point in time analysis level, the proposed design displayed a great deal of improvement in both the depth of the room and in the front of the window, especially at the autumn equinox, where a 38% improvement was observed at the deepest part in the room, while a decrease of the over lighting in front of the window was around 22%.

#### 4.6.3.2 Dynamic Daylight measures

Room 2 achieved a better performance in improving the sDA while maintaining the ASE. Having a significant value of 80% sDA, the 13% increase can be credited by the improvement of the illumination in the deep areas of the room as shown in the previous analysis statement.

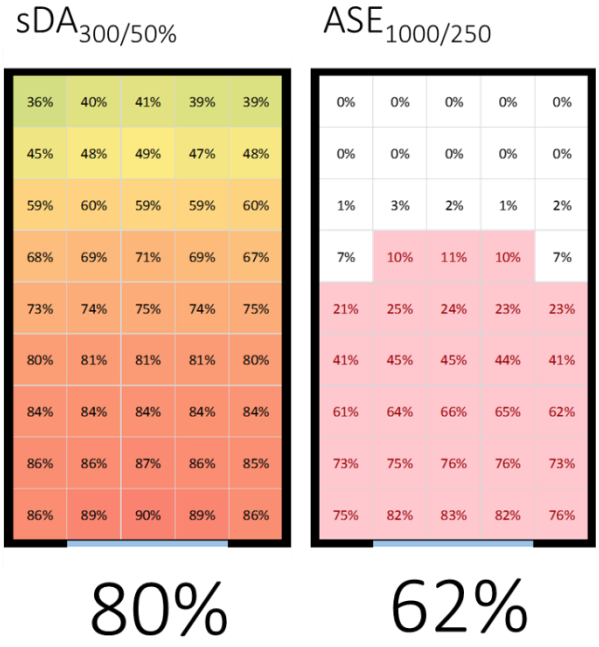


**FIGURE 40SDA AND ASE FOR THE CFS OF TRIAL 3**

## 4.6.4 Fourth Trial

The forth trial was similar to the 3rd trial, the only change was in the number of samples used in the BSDF; using the default ray sampling of 2000 rays per Klems patch, decreases the variation in the results. However, it took 17 hours and 45 minutes to generate the BSDF file for the proposed complex fenestration system design. The following script was written in the genBSDF batch file:

```
"genbsdf.exe -c 2000 +geom meter materials.rad CFS.rad > CFS_Trial_4.xml"
```

### 4.6.4.1 Basic Measurements

An overall decrease in the illumination levels was witnessed in Trial 4, with a maximum illumination level of 12337 lux throughout the year. Moreover, a great improvement in the illumination at the depth of the room, especially near autumn, reaching a significant 49% improvement (at the 13th of October). Also there was an improvement in daylighting near spring equinox recording 44% improvement (at the 4th of March). At the same time, the percentage of lighting in front of the window was decreased up till 27% near autumn and spring too. Even though in summer there were some cases where there was an adequate improvement in the overall illumination in front of the window ranging from 13% to 21% decrease in illumination, the majority of the time the improvement was trivial ,ranging from 2% to 8%, while sometimes there was an increase in the over lighting extending up to 5% increase. However, those cases, the ones which experienced an increase in daylighting were just 3% of the total time.

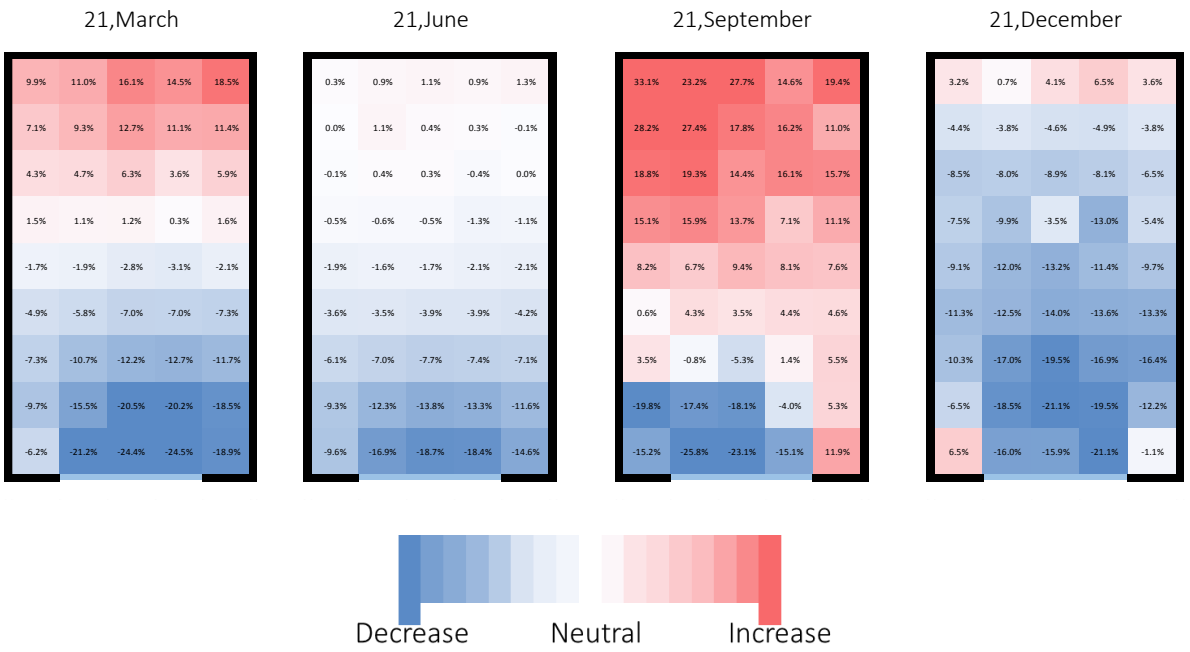


**FIGURE 41 THE PERCENTAGE OF DAYLIGHT INCREASE OR DECREASE AT THE EQUINOXES AND SOLSTICES FOR TRIAL 4**

As for the point in time illumination, the best overall improvement was found in Autumn Equinox, with a 36% increase in daylighting in the deep areas of the room and 22% decrease in daylighting in front of the window. While in summer and winter solstices, similar pattern in the percentage of change in illumination was observed, where it started with a decrease in illumination in front of the window by a value of 16% and 19% for winter and summer solstices respectively .Then, gradually increasing the difference between both rooms 1 and 2 till reaching a slight improvement of illumination at the depth of the room by 4% and 1% for winter and summer solstices respectively.

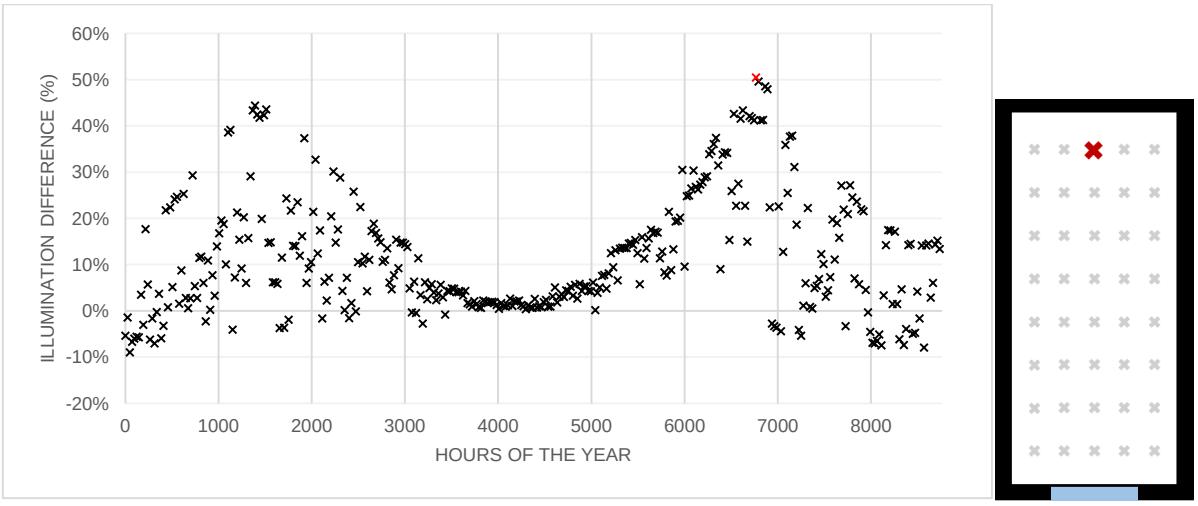


**FIGURE 42THE PERCENTAGE OF IMPROVEMENT OF ILLUMINATION AT NODE 43 AT 12 PM FOR TRIAL 4**

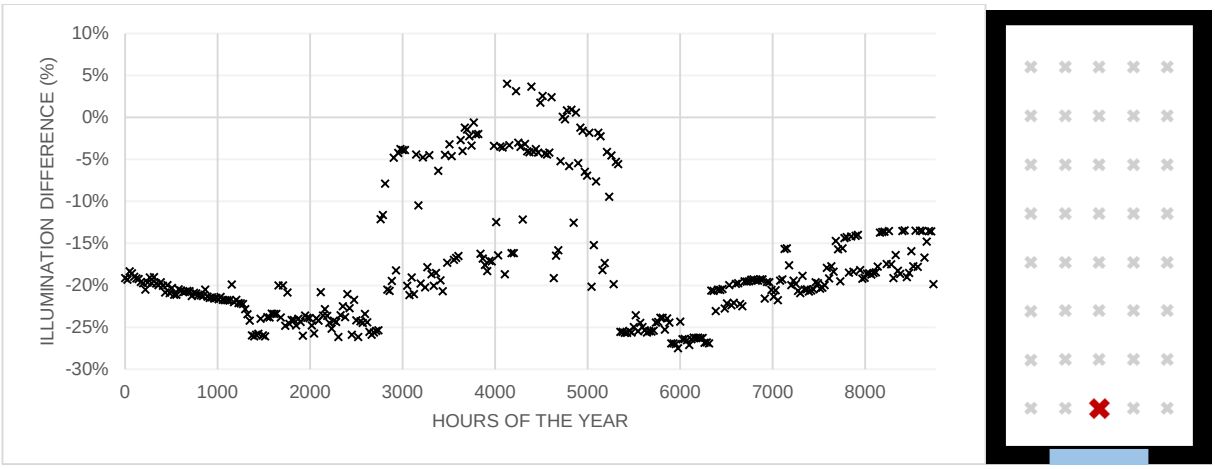


**FIGURE 43THE PERCENTAGE OF IMPROVEMENT OF ILLUMINATION AT NODE 3 AT 12 PM FOR TRIAL 4**

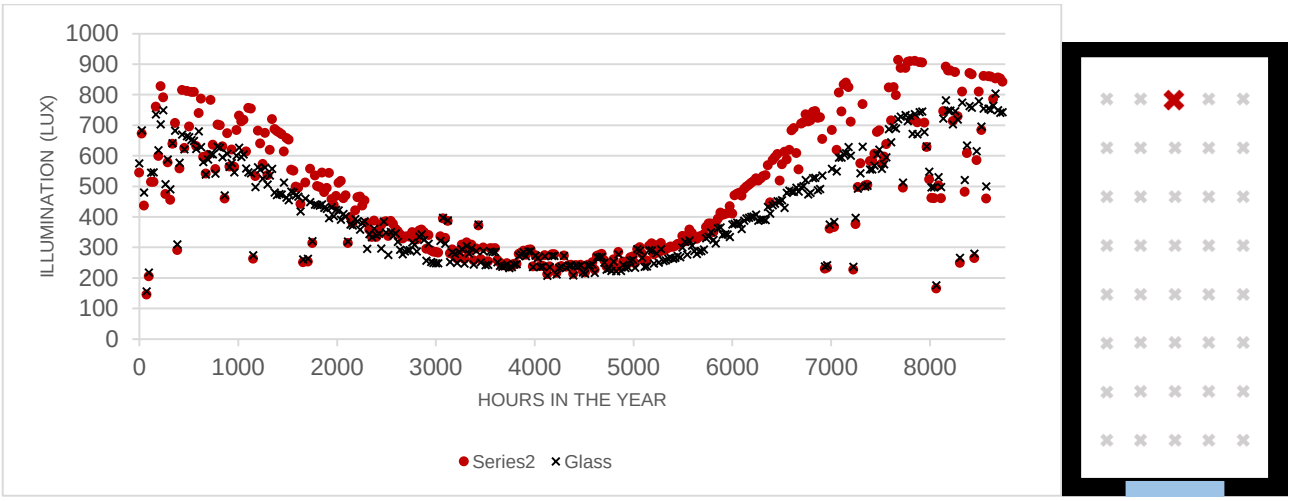


**FIGURE 44THE ILLUMINATION AT 12 PM AT NODE 43 FOR TRAIL 4 VERSUS THE NORMAL GLASS WINDOW**

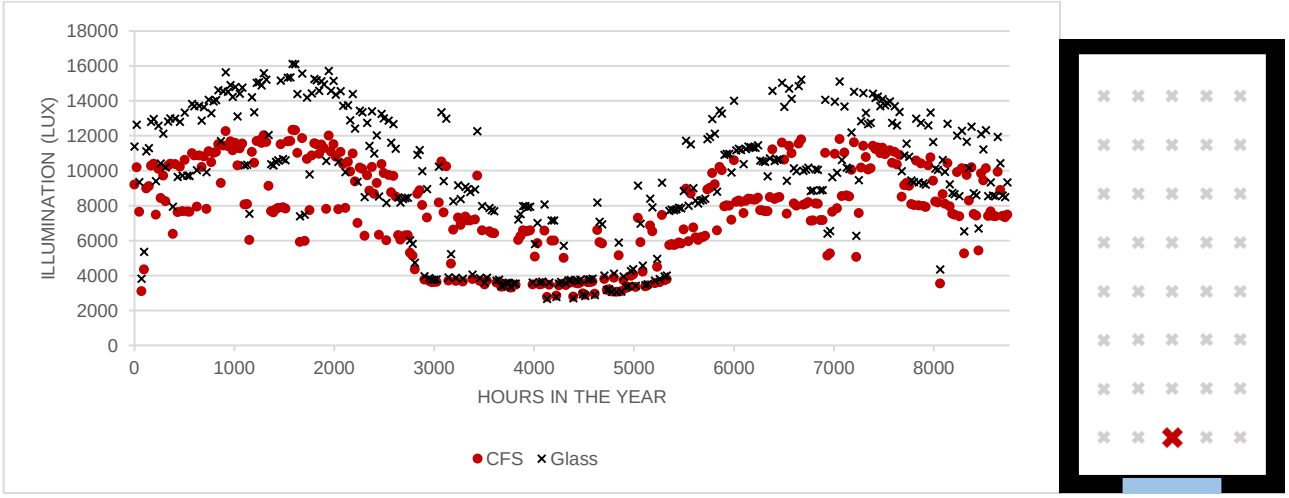


**FIGURE 45THE ILLUMINATION AT 12 PM AT NODE 3 FOR TRAIL 4 VERSUS THE NORMAL GLASS WINDOW**

### 4.6.4.2 Dynamic Daylight measures

Similar to trial 3, room 2 achieved a better performance in improving the sDA by 9%, and for the first time the ASE was also improved having a significant value of 55.6% which resulted in a 7% decrease in ASE than room 1. Figure 46 shows the annual measurements of the fourth trial.

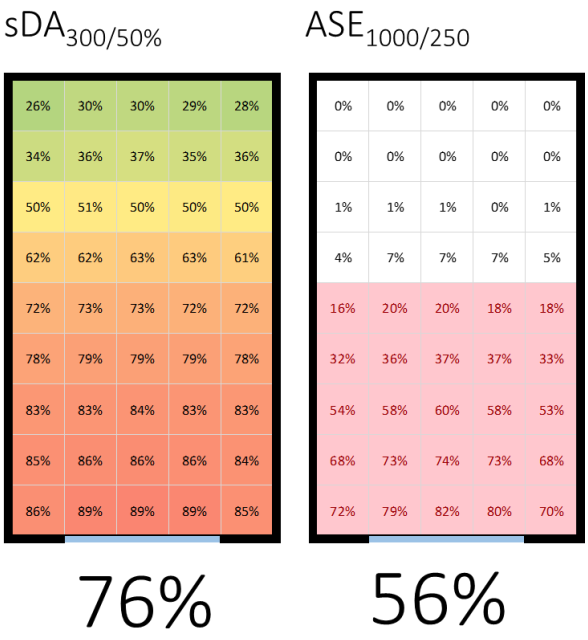


**FIGURE 46 SDA AND ASE FOR THE CFS OF TRIAL 4**

After viewing the overall illuminance for the node in front of the window for both trial 4 and normal glass window, it was observed that improvements mainly occur around the autumn and spring nodes around noon time.

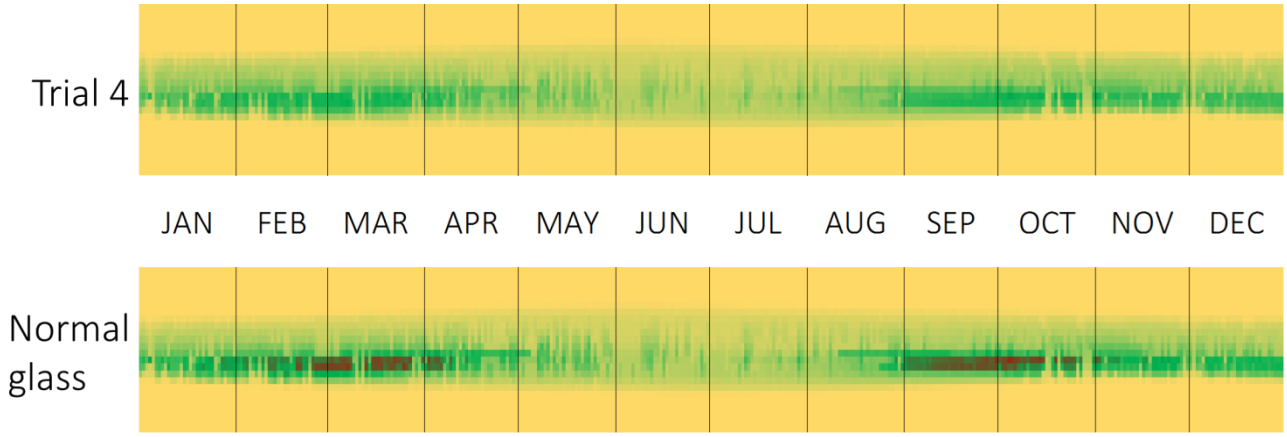


**FIGURE 47 DAILY/HOURLY COMPARISON BETWEEN TRIAL 4 AND NORMAL WINDOW GLASS**

### 4.6.5 Overall trials' results comparison

Most of the designs displayed improvement of lighting in front of the fenestration system, by decreasing the value of illumination at those points. This type of improvement is desirable since the illumination in front of the window can reach up to 17,000 lux throughout the year, so by decreasing the amount of sunlight entering in front of the window, the amount of heat accompanied by the light energy will be reduced likewise.

On the dynamic analysis level, only trial number 4 illustrated improvement in both sDA and ASE. The sDA increased from 67%, with using only a simple glazing window, to 76%, when a retrofitted translucent prismatic panel was used and the ASE decreased 6%. On the other hand, replacing the whole fenestration system with a prismatic panel with a transparent material will demonstrate a more significant improvement in the sDA, however this will be accompanied by more over lighting increasing the ASE by 5%. Nevertheless, retrofitting a normal glass window with a transparent prismatic panel will keep the sDA at the same level, while cause a significant decrease in the ASE by 6%.

**TABLE 14 ALL 4 TRIALS COMPARED TO THE NORMAL WINDOW WITH GLASS BY DIFFERENT DYLIGHTING MEASURES**

| Trial No. | BSDF used | Max. illum | Min. illum | sDA | ASE | Improvement at depth, hour | Improvement at window, hour |
|---|---|---|---|---|---|---|---|
| | | At 12 noon (lux) | | | | | |
| **Glass** | - | 16100 | 156 | 67% | 62% | | |
| **1** | PMMA | 17354 | 166 | 78% | 67% | 80%, 4393 | N/A |
| **2** | Full frame & transparent panel | 12665 | 147 | 67% | 56% | 51%, 6769 | 33%, 5977 |
| **3** | Full frame & translucent prism | 12964 | 160 | 80% | 62% | 44%, 2305 | 25%, 2305 |
| **4** | Accurate translucent prism | 12337 | 145 | 76% | 56% | 49%, 6865 | 27%, 5953 |

### 4.6.6 Overall Time of 5 phase method

#### 4.6.6.1 Computer Specs

To calculate the overall time of the five phase method, the specs of the PC, as shown in Table 15, had to be taken into account in the study in order to benchmark the time each process takes.

**TABLE 15 COMPUTER USED IN THE SIMULATION PROCESS SPECS.**

| Specs | Model |
|---|---|
| **Model Name** | Sony VAIO E-VPCEH16EG |
| **Installed RAM Memory** | 4.00 GB |
| **Processor** | Intel® Core™ i3-2310M CPU @ 2.10 GHz |
| **Operating System** | Windows 7 (64-bit) |

#### 4.6.6.2 Time of computation of each matrix

As seen in Table 16, the overall time for the 5 phase method, if computed in series, would be around 15 hours and 45 minutes. However, since each component can be independently calculated, the total time would be reduced to the maximum time for the computation of components individually; in that case, the daylight matrix would be the increasing or decreasing factor for the whole of the 5 phase method time.

The Direct sun coefficient matrix – involves simulation with proxied geometry of the CFS – would take around 1 hour if the nodes are divided to 5 sets and computed in parallel manner or around 4 hours and 30 minutes if no division of nodes or parallel computation.

**TABLE 16 ACTUAL PROCESSING TIME FOR THE DIFFERENT PHASES**

| Process | Time of computation | |
|---|---|---|
| | Hours | Minutes |
| **Direct sun coefficient matrix** | 4 | 30 |
| **Daylight matrix** | 10 | 42 |
| **Direct Daylight matrix** | - | 55 |
| **Sky matrices** | - | <5 |
| **View matrix** | - | 21 |
| **Direct view matrix** | - | <5 |
| **Compiling the 3 phases** | - | <5 |
| **Total Time** | **15** | **45** |

#### 4.6.6.3 Computation time of BSDFs

The following Table 17 demonstrates the time taken to generate a BSDF, which is used in the direct daylight component and the final summation of the five-phase method. Using a simple PMMA material for the prismatic shape, which is defined in Radiance as a “glass” material, took the least time in computation. Yet, adding a glazing component nearly tripled the time of computation. Furthermore, the introduction of translucent materials in trial 3 and decreasing the number of samples from 2000 to 100 in computation increased the time

of computation to 3 hours and 15 minutes. In the end, using 2000 samples per Klems patch set a record of 17 hours and 44 minutes of computation.

**TABLE 17 COMPUTATIONAL TIME OF THE GENBSDF**

| Trial No. | Trial Description | Material Description | Number of samples per Klems patch | Process | Time of computation | |
|---|---|---|---|---|---|---|
| | | | | | Hours | Minutes |
| **1** | Prism | PMMA* | 2000 | genBSDF | 0 | 30 |
| | Frame | Wood | | | | |
| **2** | Prism | PMMA* | 2000 | | 1 | 26 |
| | Glazing | Glass, 88% | | | | |
| | Frame | Wood | | | | |
| **3** | Prism | Translucent | 100 | | 3 | 15 |
| | Glazing | Glass, 88% | | | | |
| | Frame | Wood | | | | |
| **4** | Prism | Translucent | 2000 | | 17 | 44 |
| | Glazing | Glass, 88% | | | | |
| | Frame | Wood | | | | |

*PMMA has a refractive index similar to that of the PP, it is widely used as an optical material

# CHAPTER 5:

# PHYSICAL MODEL SETUP AND MEASUREMENTS

# Chapter 5: Physical Model Setup and Measurements

## 5.1 Testing Procedure

### 5.1.1 Prismatic Panel Manufacturing using recycled plastic

The proposed plastics used in the prismatic panel are recycled Polycarbonate, recycled Polystyrene and recycled Polypropylene, where consumers' products containing Polypropylene (number 5) were collected as waste product. In the Egyptian market, numerous products use the PP as a part of food packaging, due to its low manufacturing cost, high safety if disposed or recycled and low reaction when used as a food container. Furthermore, PP is very flexible in manufacturing; transparent products can be manufactured from polypropylene, and the degree of transparency can be adjusted by tampering the type of additives used, thermal conditions and pressure during manufacturing.

Therefore, in order to manufacture the prismatic panel using recycled plastic, a number of plastic products such as food containers for PP, food plates of expanded polystyrene (EPS) and construction waste of PC are collected, see Figure 48.

**FIGURE 48 SAMPLES OF DAILY USED PLASTICS, LEFT: POLYPROPYLENE CUP, RIGHT: POLYSTYRENE PLATE**

The consumer PP is then cleaned, by washing and drying before being shredded, to enhance the quality of the final product. It is sometimes recommended to cut the plastic first, or in some cases shred it, before cleaning. Afterwards the plastic undergoes different size reduction steps to create a resin like plastic material to be easily moulded and shaped this is achieved when the plastic is cut into smaller pieces then fed into a shredding machine (shredder) for further cutting. It is recommended to use a horizontal cutting machine since most of the plastic food containers are not thin film plastics and the horizontal cutting machine has blades that are rotating on a horizontal axis. Afterwards “the shredded plastics pass through a grid into a collecting tray” (El Haggar, 2007) (Lardinos & Van de Klundert, 1995).

**FIGURE 49 FINE PELLETS OF PS SHREDDED**

For better quality and greater material density, it is recommended to use an agglomerator which pre heats the plastics and cuts it into small granules. Afterwards, those granules are pelletized, where uniform sized pellets are formed, see Figure 49. Subsequently, the plastic goes through the extrusion phase, “in this phase the plastics undergo mixing, homogenization, compression, plasticization and melt filtration.” (El Haggar, 2007)

#### 5.1.1.1 Forming recycled plastic sheets

In order to form recycled plastic sheets with 4 mm thickness, pressing is carried out on the plastic pellets, where it can either take the form of the final shape or can be produced as a smooth surface, which is done using a hydraulic thermal press.

In order to determine the suitable option, Table 18 summarizes two common methods in producing a recycled plastic prismatic panel with a size of 250 mm x 250 mm x 6 mm. Not only producing the panels on the experiment scale was noted, but also the commercial scale production was taken into consideration in the comparison between the 2 common production methods of plastics.

**TABLE 18 COMPARISON BETWEEN PRESSING AND INJECTION MOULDING IN MANUFACTURING PRISMATIC PANELS**

| Point of comparison | | Pressing | Injection moulding |
|---|---|---|---|
| **Material** | Raw material type | Shredded Recycled Plastic / sheets from die-free injection moulded | Shredded recycled plastic pellets |
| | Raw material quantity | Sheet of 30mm*30mm*6mm | Mass = ρ x V Pellets of mass of approx. 335 gm |
| | Raw material cost (EGP) | Cost of collection / cleaning / shredding of plastic for recycling | |
| **Time (min.)** | Preparing (neglecting first run) | 2 | 2 |
| | Processing | 30 | 3/60=0.05 |
| | Cooling | 5 | 0.5 |
| | Post-cooling | 2(Removing of flashes) | 1(Removing of runners) |
| **Equipment** | Required equipment specifications | Press machine<br>• Capacity of 100 ton<br>• Has water heating and cooling systems (using water) | Injection moulding machine<br>• Shot= 400 gm<br>• clamping pressure= 450 ton<br>• Distance between tie rods= 250mm |
| **Complementary equipment** | Die type | With ejector and heating system | Hot runner |
| | Number of dies | 2 (upper side) + 2 (lower side) | 1 |
| | Estimated cost/ die depending on manufacturing of small-size panel (EGP) | 10,000-12,000 | 30,000-35,000 |
| **Labor** | Skill | More skilled | Less skilled |
| | Estimated cost/ hour (EGP/hr) | 10 | 7 |
| **Product** | Accuracy | High | High |
| | Roughness | Low | Low |
| | Number of products/ day [working hours/ (processing + processing + cooling time)] | 38 [8*60*3/37+50+5] | 192[8*60/2.5] |
| | Cost/ product | 5.78[9.375*37/60] | 0.26[6.25*2.5/60] |
| | Total cost of products/day (EGP) | 219 | 122 |
| **Cost** | Fixed costs (die cost) (EGP) | 12,000 | 30,000 |
| | Variable costs per product (EGP) | 5.78 | 0.64 |

From the previous table, it can be concluded that the injection moulding is a preferable choice for mass production, since injection moulding produces more panels per minute and has lower variable costs and high initial cost. However, for a prototype production, the initial cost of the injection moulding is far higher than the pressing. On the other hand, the fast production rate of the injection moulding is not necessarily needed in the prototype manufacturing also the variable cost difference is negligible compared to the die cost. Therefore, it is highly recommended to go for the pressing in the initial prototyping stages, and if a commercial potential is created, the switch to injection moulding would be advised.

### 5.1.2 Die Manufacturing

The die, which has the designed prismatic shape, is manufactured from raw iron where it was cut and shaped using a wire cutting machine as seen in Figure 50. The wire cutting machine replicates the inserted CAD profile of the shape needed by cutting through the iron blocks.


**FIGURE 50 WIRE CUT MACHINE USED TO SHAPE THE DIE**

The final product was 2 iron blocks each with the shape of one of the sides of the prism design. Both blocks dimensions are 10 cm x 10 cm and depth of 4 cm. Another block of greater dimensions and a hollow core of 10 cm x 10 cm is made in order to enclose both iron blocks as shown in Figure 51 and Figure 52 (a) and (b).

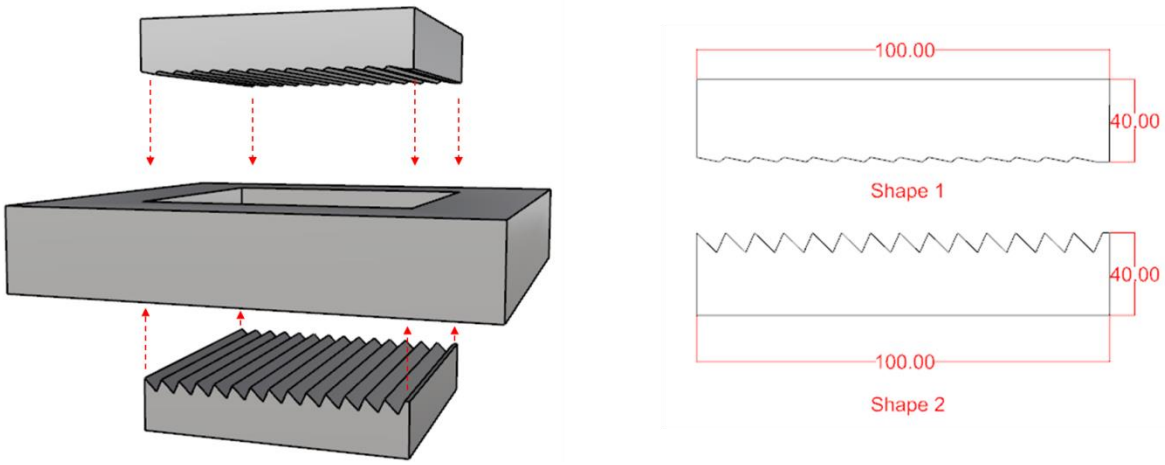


**FIGURE 51 3D MODEL OF THE DIE MANUFACTURED**

### 5.1.3 Plastic Recycling and prism formation

The fine pellets are inserted between two plates as shown in Figure 52(c). Afterwards, the dies are placed on a hydraulic press with heaters installed on the upper and lower plates Figure 52(d). Different pressures and temperatures were tested for each plastic material, in order to reach an acceptable range of optimum settings as shown in Table 19. The final product dimensions are 10 cm x 10 cm and 4 mm thickness.

**TABLE 19 SETTINGS FOR RECYCLING DIFFERENT TYPES OF PLASTICS**

| Material | Temperature (°C) | Pressure (psi) |
|---|---|---|
| PC | 150-170 | 2000 |
| PS | 105-110 | 1500 |
| PP | 120-140 | 2000 |

An extra sample made from acrylic was manufactured, in order to validate the acrylic design simulated on Radiance. The acrylic sample is utilized as a control sample to test the pattern behaviour on a clear acrylic prismatic panel to compare with the recylced plastic panels.

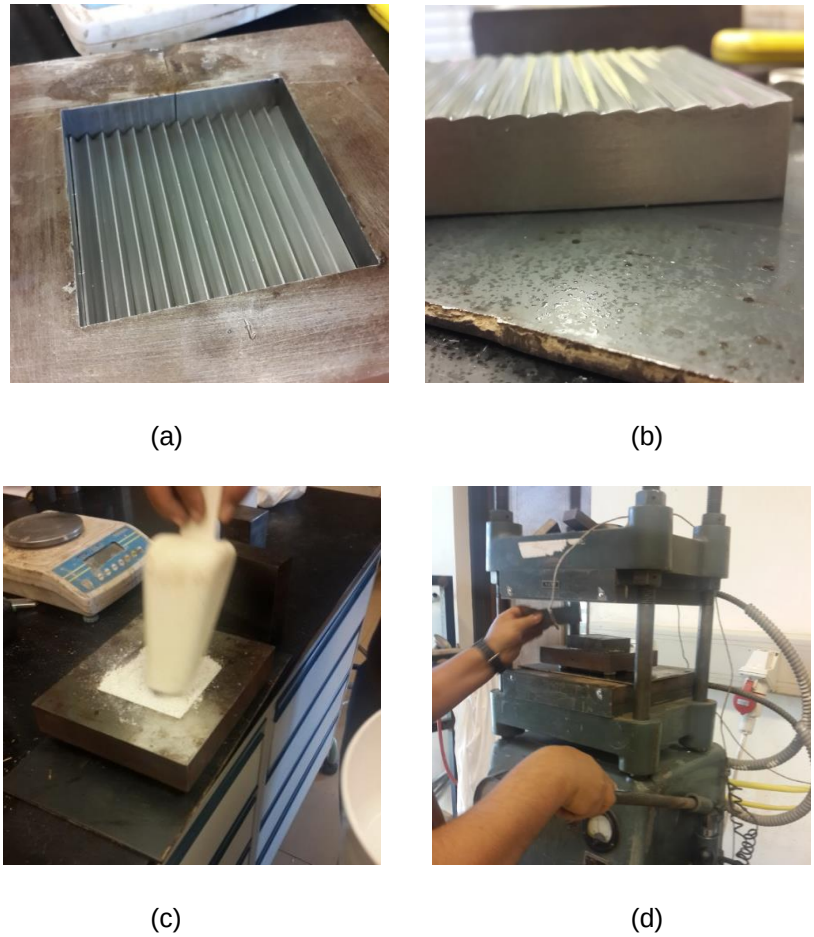

(a) (b)

(c) (d)

**FIGURE 52 (A) DIE PLACED WITHIN A CONTROLLED MOULD (B) THE OTHER DIE (C) PLASTIC RESIN PLACED ON THE DIE (D) HYDRAULIC PRESSING MACHINE WITH HEATERS WHERE THE DIE IS PLACED**

3 samples without any prism design were manufactured to observe their optical and visible properties. All 3 materials are translucent but with different grades. The polycarbonate is the most transparent, visually, while

the polypropylene is hardly transparent. Yet, it can transmit some light. Both polycarbonate and polystyrene developed a brownish colour; however, polypropylene developed a white colour.

**(A) (B) (C)**

**FIGURE 53 THE RECYCLED PLASTIC SAMPLES (A) PC (B) PS (C) PP**

The polycarbonate visual texture indicates the presence of high impurities and incomplete mixing of the polycarbonate pellets, Figure 54(a). However, polystyrene had a clearer texture with little impurities to see, Figure 54(b). On the other hand, polypropylene showed some vine-like impurities which resulted from "un-cooked" PP particles, Figure 54(c).

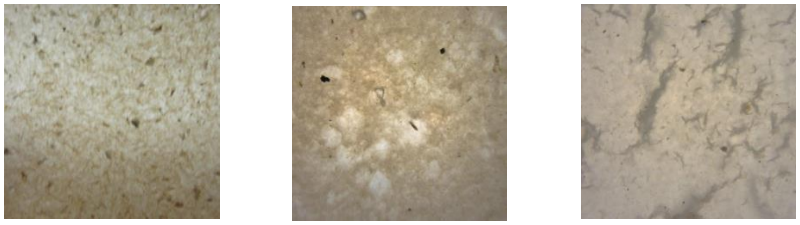

**(A) (B) (C)**

**FIGURE 54 CLOSE-UP OF THE 3 MATERIALS (A) PC (B) PS (C) PP**

## 5.1.4 Diffused Transmission Measurements

The spectrophotometer results at 550 nm are shown in Table 20:

**TABLE 20 DIFFUSED AND SPECULAR TRANSMITTANCE AND REFLECTANCE OF THE DIFFERENT PLASTICS**

| Material | Transmittance | | Reflectance | |
|---|---|---|---|---|
| | Diffused | Specular | Diffused | Specular |
| RPC | 8.6% | 20.0% | 34.0% | 37.4% |
| RPS | 2.5% | 2.8% | 45.1% | 49.6% |
| RPP | 2.2% | 2.4% | 45.5% | 50.0% |

The previous findings resulted from the average values of the material along different points on the surface, since recycled plastic is impure and contains different foreign particles within the medium of the material. Those impurities would affect the overall light transmission of the material.

### 5.1.4.1 Final Products

The final prismatic panels that were produced were the acrylic, polycarbonate and polystyrene panels, see Figure 57. Unfortunately, the polypropylene did not give effective results since all experimental products of the prismatic panel turned out to be nearly opaque which is not valid for further testing.

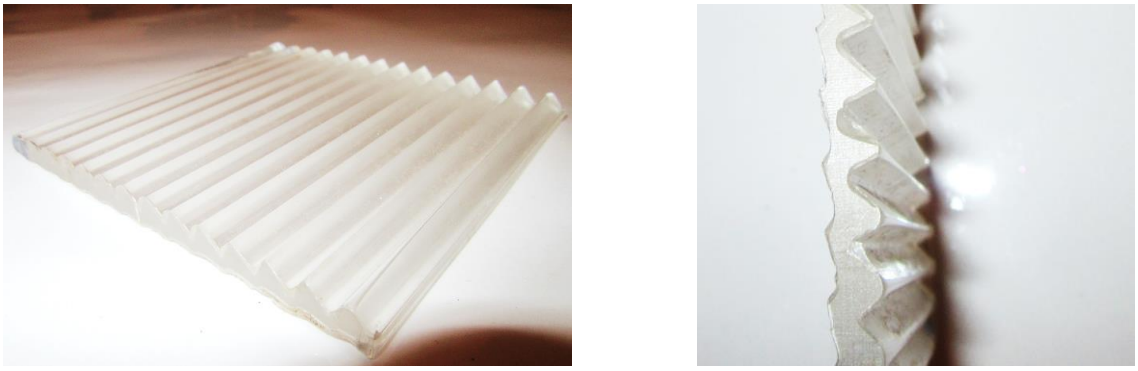

(a) (b)

(c) (d) (e)

**FIGURE 55 (A) ACRYLIC PRISMATIC PANEL (B) SIDE VIEW OF THE PRISM DESIGN (C) FRONT VIEW OF ACRYLIC PANEL (D) FRONT VIEW OF POLYCARBONATE PANEL (E) FRONT VIEW OF POLYSTYRENE PANEL**

## 5.1.5 Room Setup

A 1:10 scale model room was constructed using wooden sheets and structures. The dimensions of the room fabricated is 36 cm x 82 cm x 28 cm. The setup includes 4 Lux meters to measure the illumination at different points of the room in a linear manner. Three lux meters are placed equidistantly on the floor, and the fourth will be placed in the middle of the ceiling. The measurements conducted on the 6$^{th}$ of June 2016 between 10:30 AM to 12:00 PM, in Cairo, Egypt. The room's small size was advantageous since it was easy to tilt the room to simulate a certain solar altitude. The measurements involved solar altitudes from 35° to 75°. The samples included the acrylic, RPS and RPC prismatic pattern. Moreover, a control test is made where the CFS was substituted by a single glass pane with 88% transmission to report the difference between the 4 systems.

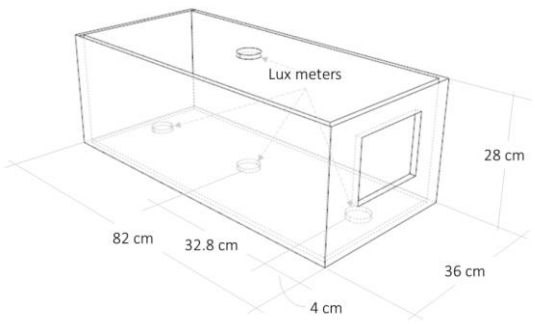


**FIGURE 56 ACTUAL MODEL ROOM DIMENSIONS AND SETUP**

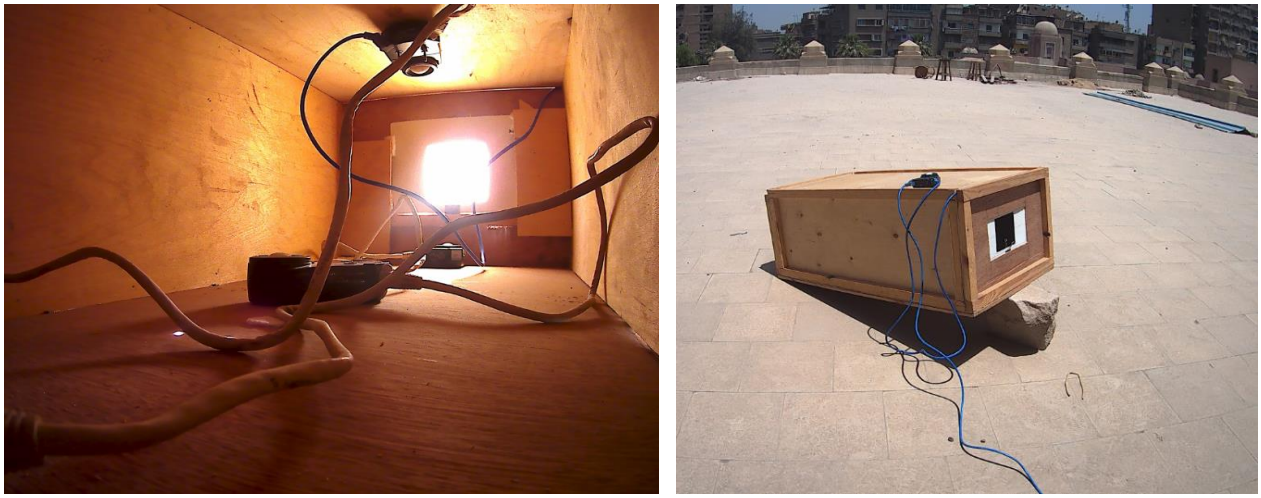

**FIGURE 57 (RIGHT) LUX METERS ARRANGEMENT INSIDE THE MODEL. (LEFT) THE MODEL FACING SOUTH AND TILTED TO MEASURE AT A CERTAIN SOLAR ALTITUDE.**

### 5.1.6 Results

The initial results included the 3 main lux meters on the ground at different solar altitudes with all 4 samples. The following, Figure 58, illustrates the difference in daylighting performance at the 3 main areas in the room at different solar altitudes with 4 different panels. At all solar altitudes, the plain glass sample showed extreme readings at the window lux meter, since sunlight was falling at it directly. While going deeper into the room, a steep fall in the readings was noticed which ranges from numbers above 40,000 lux at the window, whereas less than 200 lux in the middle and deep within the room. The acrylic prismatic sample distinctively decreased the illumination at the window from illumination values as high as 68,000 to values below 10,000, while succeeding in increasing the illumination at the middle and depth of the room at all solar altitudes. As for the RPC, the panel succeeded in lowering the illumination in front of the window area while maintaining similar values of illumination to the plain glass at the middle and deep parts of the room, however this behaviour is noticed at the high solar altitudes only. Whereas at solar altitude 45° and 35° the RPC prismatic panel managed to increase the difference in illumination by at least 100%. Meanwhile, the RPS prismatic panel didn't improve the illumination at the middle or depth of the room at all solar altitudes.

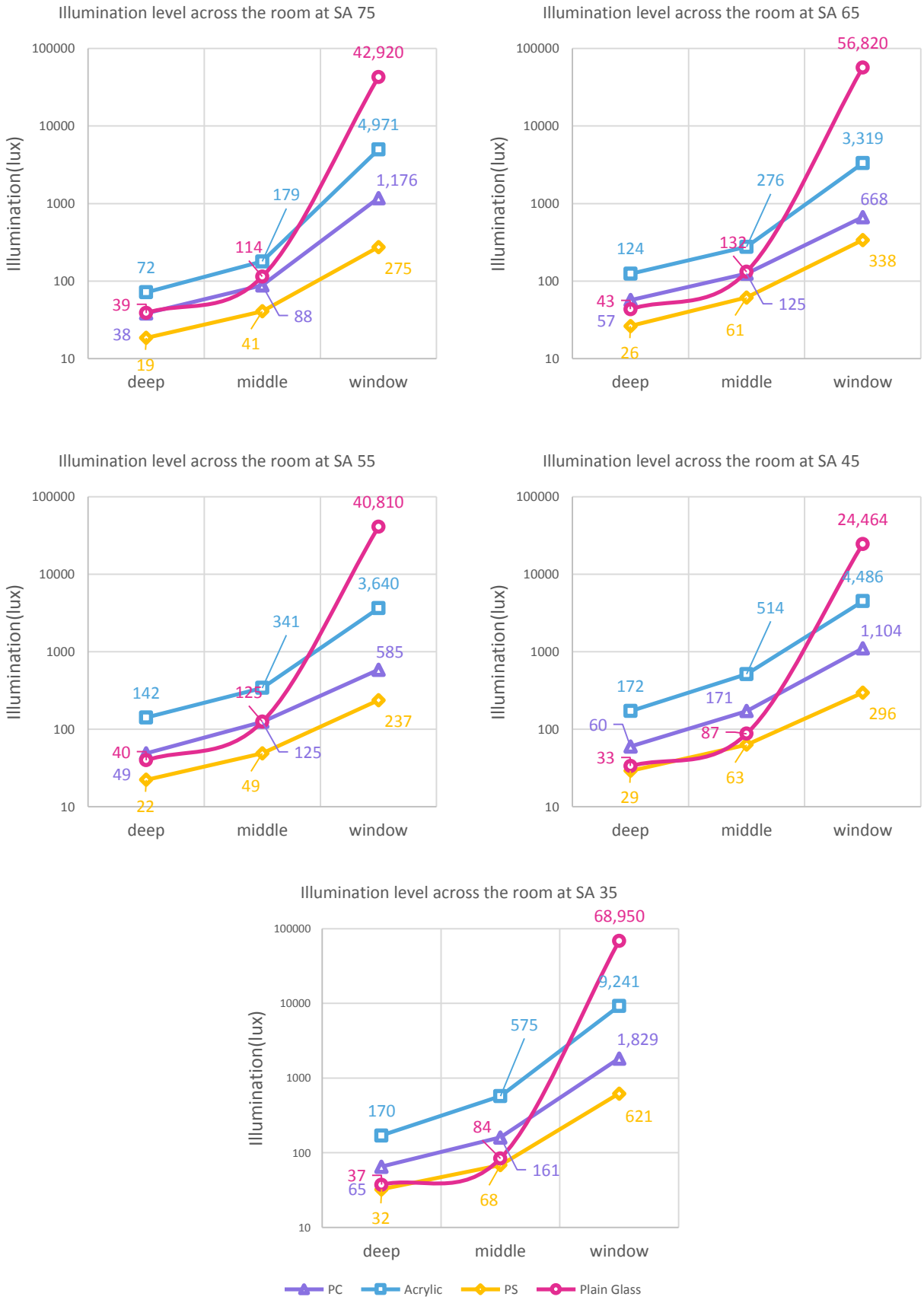


**FIGURE 58 ILLUMINATION ACROSS THE ROOM VERSUS SOLAR ALTITUDES**

Measuring the performance of each panel against different solar altitudes at the deep and near window nodes, the acrylic prismatic panel showed the highest effect on the deep part of the room, where it increased the illumination at all solar altitudes. However, at lower solar altitudes the percentage of increase was the greatest. The RPC also increased the illumination at the depth of the room but with lower impact than the acrylic. On the other hand, the RPS panel did not show any improvement at the deep parts of the room. All panels managed to lower the illumination near the window.

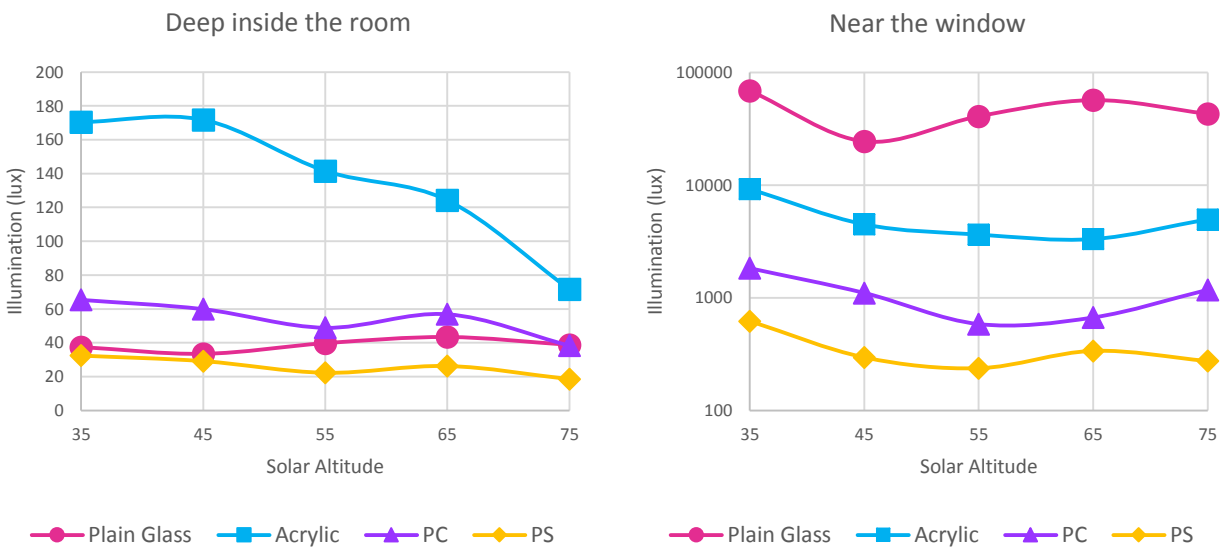


**FIGURE 59 ILLUMINATION AT THE EXTREME POINTS IN COMPARISON WITH THE DIFFERENT SAMPLES**

On another point of view, both the acrylic prismatic panel and RPC prismatic panel were put up against the plain glass panel in a visual comparison. As shown in Figure 60, there is a great difference in the lighting levels between the acrylic prismatic panel and the plain glass panel, where light is observed at the middle part of the room as well as the wall facing the window when using the acrylic prism panel. On the other hand, the RPC shows an improvement of daylighting in the deep parts of the room while eliminating the direct sun near the window. However, a yellowish hue is present in the light entering the room due to the tinted colour in the recycled RPC.

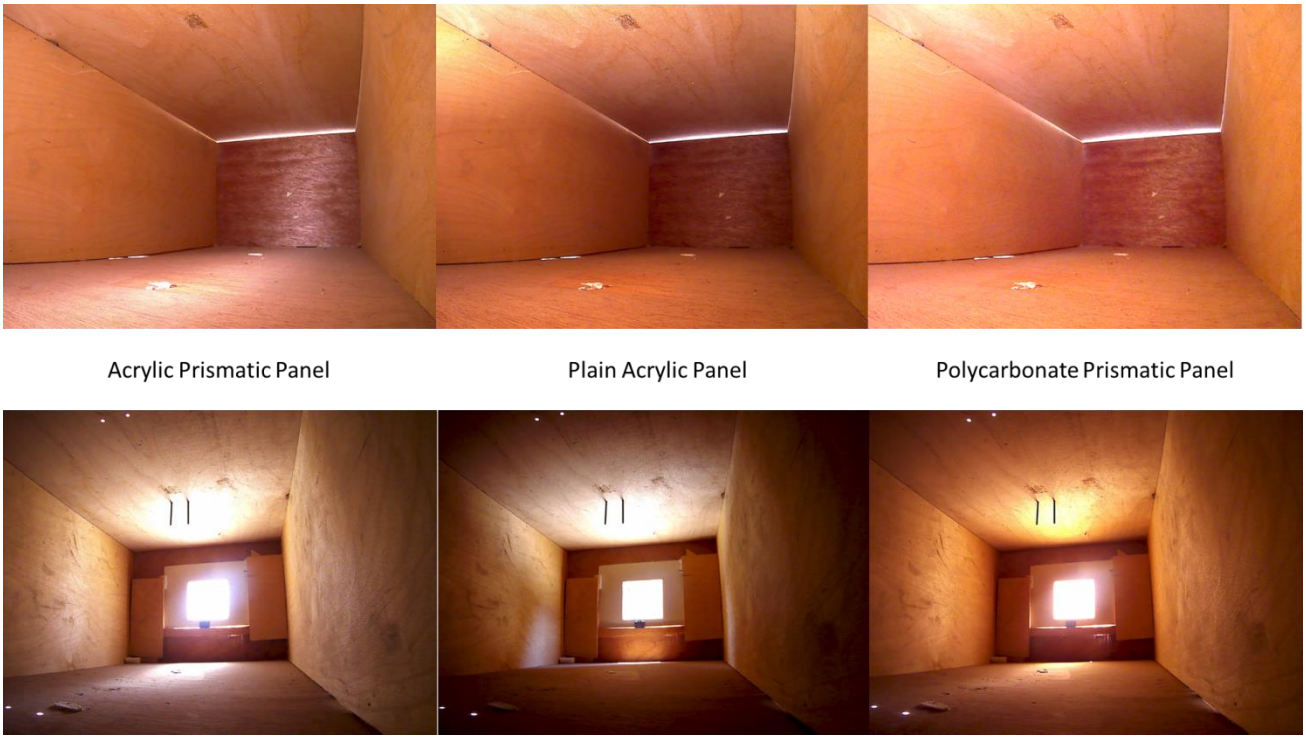


**FIGURE 60 (UPPER) CAMERA VIEW AT DEPTH OF THE ROOM (LOWER) CAMERA VIEW OF THE WINDOW**

## 5.2 Visual light analysis

An extended light behaviour analysis was made on a similar small scale model room, however, it was conducted indoors using a directed artificial light source. The setup consisted of a stand which directs the artificial light source with specific incident angles. And the sample is placed vertically and the interior of the room is captured using a high exposure camera mode.

Figure 61 shows the different samples' behaviour at solar altitudes between 30° and 80°. It is observed that the acrylic panel showed improvement in the illumination inside the space at all solar altitudes, and this improvement is very clear especially in the high solar altitudes such as 80°. The RPC also presented an enhancement in the overall illumination in the room compared to the plain glass, however, the intensity of light is less than the acrylic's. And at solar altitudes 30° and 40° the improvement in the depth of the space seems unnoticeable however, near the window the illumination levels decreased which made the space with more uniform lighting.

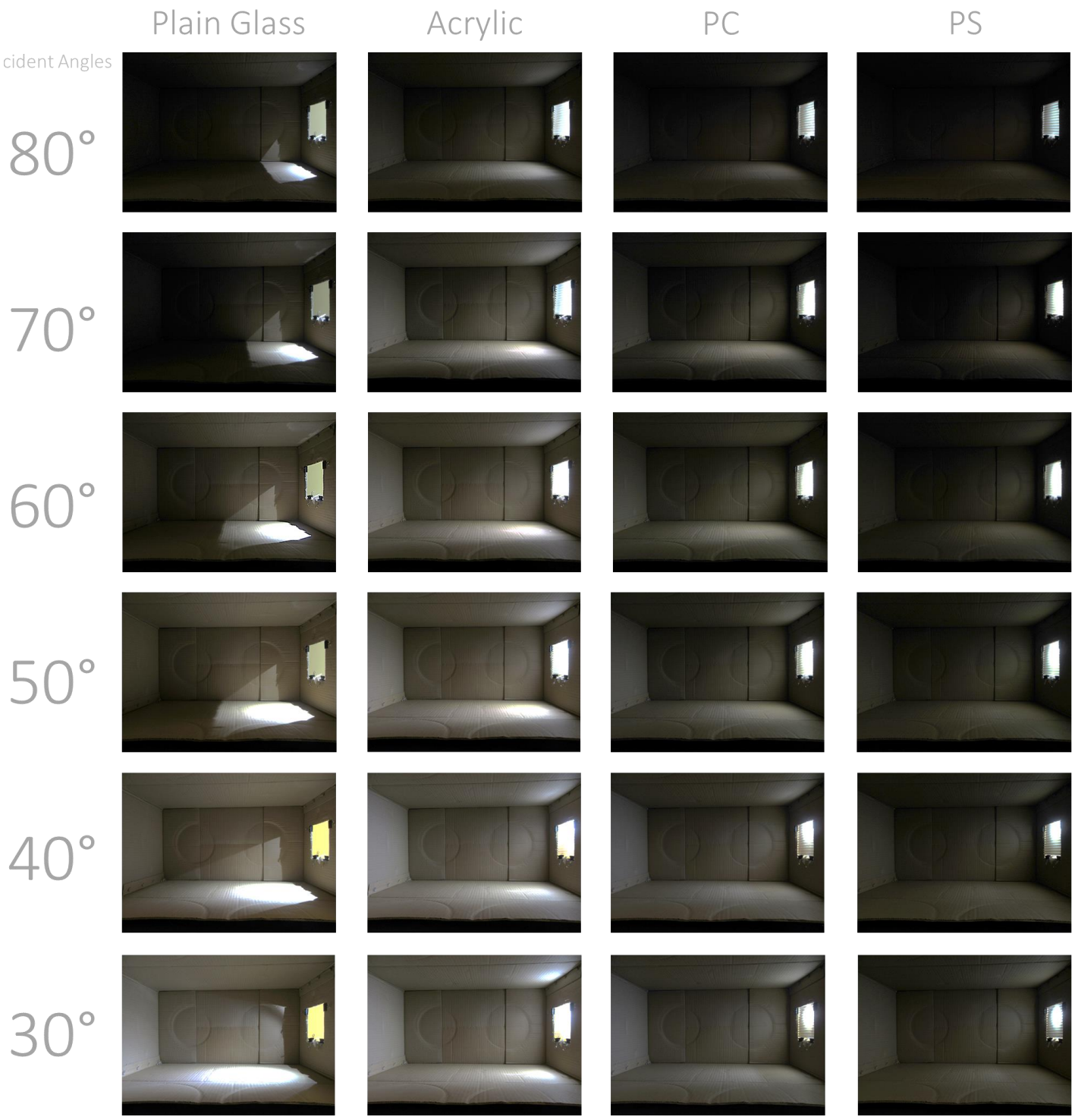


**FIGURE 61 HIGH EXPOSURE IMAGES OF DIFFERENT SAMPLES VERSUS SOLAR ALTITUDES FROM 30° TO 80°**

# CHAPTER 6:
# CONCLUSIONS

# Chapter 6: Conclusions

## 6.1 Main Objective

The objective of this thesis was to investigate the opportunity of designing a complex fenestration system (CFS) using recycled plastic for high altitudes. This target is considered a multi-challenge due to a variety of reasons, which includes but is not exclusive to, inconsistent daylighting, interior heat gain and manufacturing complications.

The main objective was segregated into a set of goals and milestones, by which the methodology of the thesis was constructed upon. Primarily, the main goal was to improve the daylighting performance within the built space, by eliminating the “cave effect” and decreasing the excessive direct sun. At the same time creating an edge in designing more sustainable products with the incorporation of recycled plastic with the complex fenestration system.

### 6.1.1 Specific goal

The proposed system in this thesis constitutes of a CFS that has two main layers, a transparent light transmitting layer and a translucent layer made from recycled plastic and an optimized shape is cut through the latter layer.

The translucent layer, which is made of recycled plastic such as polypropylene PP (number 5) or polystyrene (number 6) or polycarbonate (number 7), have a prismatic profile optimized for regions with high solar altitudes(summer altitudes). The shape optimization objective function targeted solar altitudes from 50° till 80° degrees, in south orientation as shown in Figure 62. However, the final prismatic shape exhibited an improvement in the daylighting for both high and low solar altitudes.

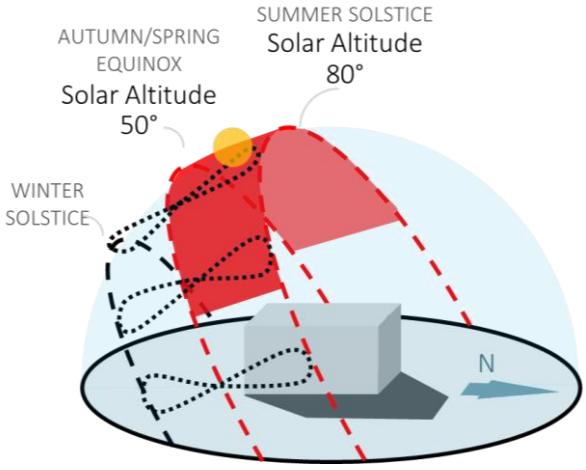


**FIGURE 62 SOLAR PATH DIAGRAM SHOWING THE AREA OF INTEREST FOR THE PROPOSED DESIGN**

## 6.2 Social Gain

The proposed design can be socially beneficial besides its environmental benefits. Cultures similar to the Egyptian culture appreciate privacy, the CFS designed doesn't prevent daylight from entering even though it blocks the view from the outside. Therefore, this feature, though architecturally unappealing, might be socially acceptable. The proposed design can be introduced as a retrofitting component for the window system that can replace curtains or other view blocking techniques, such as the Mashrabiya.

Not only the proposed design can be used as a total coverage for the window system, but the CFS can be utilized to fit a certain part of the fenestration system where it can redirect light deep into spaces and in the same time allow view to the outside, such as in Figure 63. Some facilities would find this setup advantageous such as classrooms.

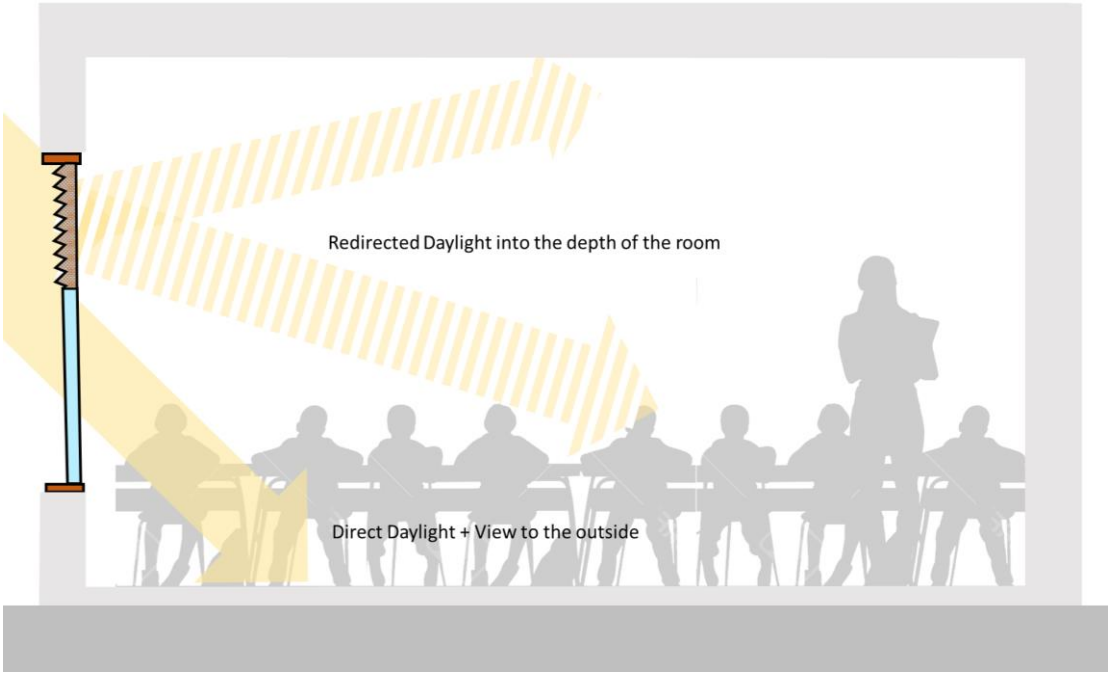


**FIGURE 63 POSSIBLE SETUP FOR THE CFS IN SPACE WITH VIEW TO THE OUTSIDE NEEDED**

Another credit for the designed CFS is the use of recycled materials. Our society has become more open to the idea of using recycled products. Lately, many industries implemented the utilization of plastic waste in their products and even dedicated a whole line for recycled products, such as recycled paper notebooks and bags. Utilizing recycled plastic within the CFS would be perceived as an innovation in design, thus it can be encouraged and funded by governments, NGOs or private industries.

## 6.3 Economic Payback

The proposed design would be of economic benefit as it saves both electric energy that could have been used in lighting deep spaces and plastic waste disposal management which can be of high cost. The amount of illumination compensated by the use of the proposed design within a space can be calculated against the energy which would have been consumed from electric lighting. Also the solar heat energy prevented by using

the proposed design would contribute in great cooling energy savings. On the other hand, the utilization of plastic waste in the design would lead to decrease in the raw material cost used in the design, as well as a decrease in the cost of plastic waste handling and disposal. However, the energy used in creating the product should be taken into consideration for an accurate life cycle cost analysis.

## 6.4 Summary

The objectives were achieved by designing and creating a prismatic panel design which diffuses and redirects sunlight in a way that helps the light to penetrate deeper into the room. Those objectives included eliminating the “cave effect” in deep rooms, utilizing household plastic waste in the CFS design and achieving privacy through blocking the view to the outside by using translucent panels.

The presence of optimum prismatic model for specific design conditions accelerates the achievement of adequate daylighting in poorly lit spaces. This thesis investigated the design of a prismatic panel to enhance the daylight performance within dark spaces in hot arid environments. After the exploration of various solutions and state of the art daylight designing processes, a workflow is created in order to fabricate a prismatic shape of 4 repeating surfaces with specific angles that meets a certain design criteria. The following summarizes the flow of work within the thesis:

- **Mathematical Model:** The design involved uses a mathematical model which makes use of the prismatic pattern surfaces’ refraction and internal reflection, depending on the medium’s refraction index and surfaces’ tilt angles. An optimum design was attained for high solar altitudes, using a target range of solar altitudes from 50° to 80° degrees as the reference for optimization. The optimization process involved altering the tilt angle of the 4 surfaces, which will afterwards create the prismatic pattern along the panel. This initial step ensured that the high solar altitude incident light would be refracted to an upward direction “deflecting” light deep inside the built space while minimizing the light directed downwards.
    - **Conclusion:** The optimization process results produced a prism design with 4 specific angles which resulted in an increase in the angle of deflection of light rays upwards at all solar altitudes between 10° to 80°, while the rays deflected downwards decreased at solar altitudes 50° to 80° with an angle no more than 30°. A four side prismatic array panel was designed using the mathematical model.

- **Raytracing Simulation:** The design was taken through different layers of validation starting with the TracePro® simulation, which included accurate ray tracing of the light incident on the prismatic design, leading to a more accurate representation of the optical behavior of the proposed design. Another point covered using TracePro®, was measuring the power output of the exiting rays at different solar altitudes.
    - **Conclusion:** The design proved to be accurate after validating the mathematical model with the TracePro® simulation, with a standard error of the mean of ±1.03 degrees for the upward rays and ±2.47 for the downward rays.

- **Daylight Simulation:** In order to represent the full optical properties of the materials used in the design Radiance software was employed. Radiance is used to represent the CFS design in a close to a real-environment situation and measure both point-in-time and dynamic daylight measures within a standard room for daylight measurements. The five-phase method, which is the state-of-the-art in dynamic measurements for CFS, was utilized to produce detailed annual illumination for the proposed design and a variety of results from a number of trials, decision makers can determine which type of material can be used for the complex fenestration system design.
    - **Conclusion:** A general improvement of the daylighting levels at the depth of the room was observed, since most of the time the illumination levels at the depth of the room is very low related to the illumination levels at the window area, therefore by increasing the illumination levels in the deep areas of the room and decreasing the daylighting in front of the window, the variance between the start and end of the room is decreased giving more uniform light distribution.

At the end, a physical prototype is in its initial development. The prismatic panel's manufacturing technique was determined to involve the pressing technique, since it is more economical at the current stage; however, injection molding would prove to be a better route in case of mass production. The thesis proposes a technique of real life measuring in order to validate the Radiance result against the real measurements of 1:10 scale.

On a commercial scale, the final fenestration system will consist of multi-layers, in which one layer will be the recycled plastic at certain conditions, with the designed pattern, while the other layer will be a simple glass sheet. The proposed fenestration system is to be cost efficient, in the condition of proper recycling procedure is carried out and the appropriate manufacturing technique is applied. On the other hand, multiple designs can be created, to fill the need of different designing conditions, using the workflow explained above.

## 6.5 Limitations

However, it is expected that the final prototype have some drawbacks that needs to be tackled in further research. Some of those drawbacks are summarized in the aesthetics of the prototype, as translucent reprocessed recycled plastics contains deformities on the macromolecular structure which will be visible to the eye. Moreover, the prototype will be blocking the view to the outside, which is a critical disadvantage that needs to be investigated in further research. At the end, this thesis only covered some of the optical properties of the prototype regardless of other optical behaviors, such as discomfort glare or any of the thermal properties, which needs more research to be done upon.

Due to the limitation in suitable equipment, more optical measurement and verification should be carried out such as in Figure 64.

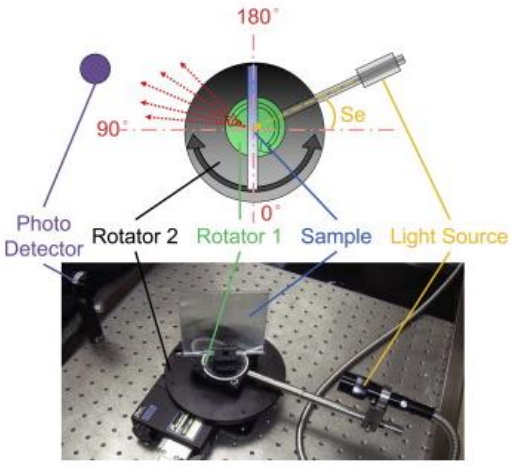


**FIGURE 64 OPTICAL MEASUREMENT DEVICE USED BY (HUANG, ET AL., 2015)**

Even though the physical model will produce the most accurate representation for replicating the behaviour of the CFS in real life whilst testing the Radiance simulations, some limitations still occurred, due to time constrain and manufacturing incapability.

Some of those limitations are:

1. Plastics collected should have their optical properties tested, before recycling as well, to record the opacity, specular transmission, diffused transmission and refractive index and compare it with the recycled plastics resulting from the manufacturing process.
2. Lack of time to measure the spatial Daylight Autonomy and Annual Sunlight Exposure, since those types of measurements require a whole year recording of illumination values.
3. Unavailability of a full scale model (1:1) to test the design. The 1:10 model would lead to uncertainty in the results as many scale-related challenges would arise, for instance, the indirect daylighting intensity and the reflective ground component of the daylight would be affected with different scales.
4. Limited number of lux meters within the room, due to the scale size constrain and financial constraints, the number of lux meters used within the physical model were limited to 4 lux meters.

# APPENDICES

# Appendix A: Mathematical Model

## 1.1 Snell's Law

According to (Vanderwerf, 2010) Snell's law of refraction is used to define the refraction behaviour of a light ray passing from one medium to another. The behaviour is quantified through the angle of incident on a particular medium's surface as shown in Figure 65.

$$n \sin I = n' \sin I' \tag{8}$$

**n =** Refraction Index
**n'=** Refraction Index of medium
**I=** Angle of incidence
**I'=** Angle of incidence at medium

### 1.1.1 Optical Dielectric Materials

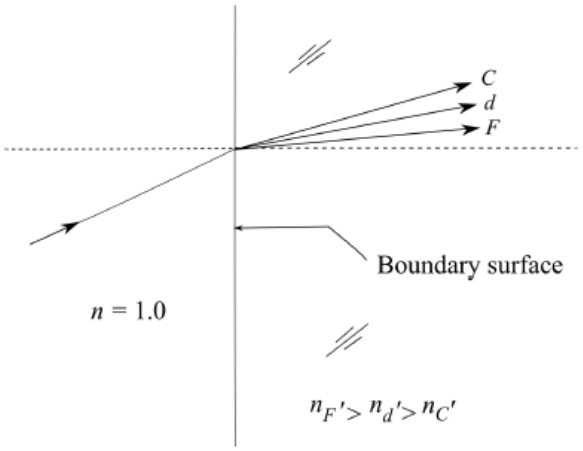


**FIGURE 65 DISPERSION OF REFRACTED LIGHT FOR DIFFERENT GLASS TYPES**

### 1.1.2 Law of reflection

$$K' = K - 2k \cos I \tag{9}$$

**K**= incident ray vector

**K'=** reflected ray vector

**k** = upward vector normal at the reflecting surface

**I**= angle of incidence

For a Cartesian coordinate system, the following equation result:

$$K_i' = K_i - 2\rho k_i \tag{10}$$

Where;

$$\rho = \sum \text{Kiki} = \cos I, \text{ where } (i = x, y, z) \quad (11)$$

## 1.2 Reflection Matrix

$$\begin{pmatrix} K'_x \\ K'_y \\ K'_z \end{pmatrix} = R \begin{pmatrix} K_x \\ K_y \\ K_z \end{pmatrix} \quad (12)$$

Where;

$$R = \begin{pmatrix} 1-2k_x^2 & -2K_xK_y & -2K_xK_z \\ -2K_xK_y & 1-2k_y^2 & -2K_yK_z \\ -2K_xK_z & -2K_yK_z & 1-2k_z^2 \end{pmatrix} \quad (13)$$

Equation (12) defines the reflected ray's direction in 3D space. The reflection matrix can be multiplied to calculate the direction of the exiting ray for consecutive reflecting surfaces.

$$R = (R_n)\ (R_{n-1})\ (\ldots)\ (R_1) \quad (14)$$

### 1.2.1 Intersection Coordinate Matrix

This matrix ensures that the next reflective surface is in a position to intercept the incident ray. The matrix for calculating the intersection coordinates is as follows:

$$\begin{pmatrix} 1 \\ x_n \\ y_n \\ z_n \end{pmatrix} = C \begin{pmatrix} 1 \\ x_{n-1} \\ y_{n-1} \\ z_{n-1} \end{pmatrix} \quad (15)$$

Where C is the intersection-coordinate matrix:

$$\mathbf{C} = \begin{pmatrix} 1 & 0 & 0 & 0 \\ PK_{x(i-1)}/\rho & 1-k_xK_{x(i-1)}/\rho & -k_yK_{x(i-1)}/\rho & -k_zK_{x(i-1)}/\rho \\ PK_{y(i-1)}/\rho & -k_xK_{y(i-1)}/\rho & 1-k_yK_{y(i-1)}/\rho & -k_zK_{y(i-1)}/\rho \\ PK_{z(i-1)}/\rho & -k_xK_{z(i-1)}/\rho & -k_yK_{z(i-1)}/\rho & 1-k_zK_{z(i-1)}/\rho \end{pmatrix} \quad (16)$$

Where ***i***= 1, 2, 3 …

**P**= the perpendicular distance from surface i to the origin

Computation of the coordinate matrix C for a surface requires knowledge of the preceding surface coordinates and the direction cosines of the incident ray. For a sequence of several reflecting surfaces, the mirror coordinate matrices can be multiplied to calculate the coordinates of the final ray at a defined surface:

$$C = (C_n)\ (C_{n-1})\ (\ldots)\ (C_1) \quad (17)$$

## 1.3 Refraction Matrix

From the definition of the reflection matrix for a mirror, we can derive a definition of a refraction matrix for refraction at a boundary between mediums different refractive indices.

The direction cosines of the refracted ray are:

$$K'_x = \left(\frac{n}{n'}\right) K_x + k_x \left[\rho' - \left(\frac{n}{n'}\right)\rho\right], \tag{18}$$

$$K'_y = \left(\frac{n}{n'}\right) K_y + k_y \left[\rho' - \left(\frac{n}{n'}\right)\rho\right], \tag{19}$$

$$K'_z = \left(\frac{n}{n'}\right) K_z + k_z \left[\rho' - \left(\frac{n}{n'}\right)\rho\right], \tag{20}$$

$$\rho = \cos I = \sum K_i k_i, \textit{ where } i = (x,y,z) \tag{21}$$

$$\rho' = \cos I' = \sqrt{1 - \left[\left(\frac{n}{n'}\right)\sin I\right]^2} \tag{22}$$

The previous equations can be added in a matrix form becoming:

$$\begin{pmatrix} 1 \\ K'_x \\ K'_y \\ K'_z \end{pmatrix} = \mathcal{R} \begin{pmatrix} 1 \\ K_x \\ K_y \\ K_z \end{pmatrix} \tag{23}$$

Where R is the refraction matrix, defined as:

$$\mathcal{R} = \begin{pmatrix} 1 & 0 & 0 & 0 \\ k_x\left[\rho' - \left(\frac{n}{n'}\right)\rho\right] & \left(\frac{n}{n'}\right) & 0 & 0 \\ k_y\left[\rho' - \left(\frac{n}{n'}\right)\rho\right] & 0 & \left(\frac{n}{n'}\right) & 0 \\ k_z\left[\rho' - \left(\frac{n}{n'}\right)\rho\right] & 0 & 0 & \left(\frac{n}{n'}\right) \end{pmatrix} \tag{24}$$

Since both Refraction and Reflection matrices are not in the same order, they cannot be multiplied together directly, therefore a modified reflection matrix in the fourth order, same as the refraction matrix is introduced as R'.

Where,

$$R' = \begin{pmatrix} 1 & 0 & 0 & 0 \\ -2k_x\rho & 1 & 0 & 0 \\ -2k_y\rho & 0 & 1 & 0 \\ -2k_z\rho & 0 & 0 & 1 \end{pmatrix} \tag{25}$$

Therefore,

$$\begin{pmatrix} 1 \\ K'_x \\ K'_y \\ K'_z \end{pmatrix} = R' \begin{pmatrix} 1 \\ K_x \\ K_y \\ K_z \end{pmatrix} \tag{26}$$

## 1.4 External and Internal Reflections at Optical Surfaces

Both Brewster reflection and total internal reflection are important considerations in many prism designs.

### 1.4.1.1 External Reflection

The reflection parameters of light depend on whether the ray is incident on a medium of higher or lower refractive index.

$$I_{Brew} = \tan^{-1}\left(\frac{n'}{n}\right) \tag{27}$$

### 1.4.1.2 Internal Reflection

$$I_{crit} = \sin^{-1}\left(\frac{n'}{n}\right) \tag{28}$$

# Example

## Givens

- Solar Altitude input from 10° to 80° with increments of 10°.
- Surfaces 1 to 4 are randomly generated for the first iteration.
- The process is divided into 2 scenarios 1 and 2 where scenario 1 includes rays entering the prism from surface 1 and exiting either from 2 or 3 and scenario 2 includes rays entering from surface 4, as in Figure 1Figure 66.

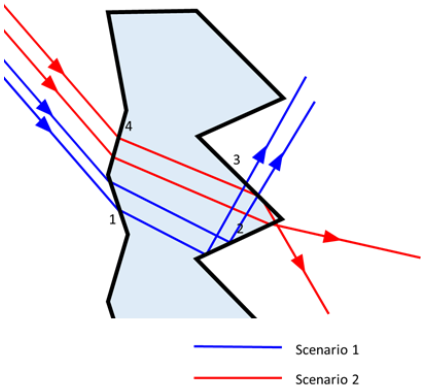


**FIGURE 66 ILLUSTRATION OF SCENARIO 1 AND 2**

## Surface 1: Scenario 1 (Solar Altitude 10°)

Solar Altitude (Absolute incident angle) = 10°

Normal Surface angle = -9.9°

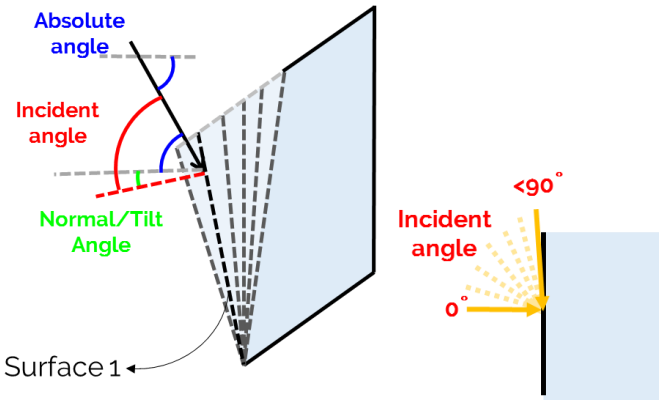


**FIGURE 67 SURFACE 1 INCIDENT ANGLE**

If 0° < Incident angle < 90°; Use refraction law.

If Incident angle < 0° or Incident angle > 90°; Regenerate a new Normal Surface angle.

Incident angle = Normal Surface angle – Solar Altitude = 10 – (-9.9) = 19.9° → Use Refraction Law.

**Refraction Law**

$$\begin{pmatrix} 1 \\ K'_x \\ K'_y \\ K'_z \end{pmatrix} = \mathcal{R} \begin{pmatrix} 1 \\ K_x \\ K_y \\ K_z \end{pmatrix}$$

$$\mathcal{R} = \begin{pmatrix} 1 & 0 & 0 & 0 \\ k_x\left[\rho' - \left(\frac{n}{n'}\right)\rho\right] & \left(\frac{n}{n'}\right) & 0 & 0 \\ k_y\left[\rho' - \left(\frac{n}{n'}\right)\rho\right] & 0 & \left(\frac{n}{n'}\right) & 0 \\ k_z\left[\rho' - \left(\frac{n}{n'}\right)\rho\right] & 0 & 0 & \left(\frac{n}{n'}\right) \end{pmatrix}$$

$$K(Solar\ Altitude) = \begin{bmatrix} 1 \\ 0.17 \\ 0 \\ 0.98 \end{bmatrix}$$

$$\rho' = \cos I' = \sqrt{1 - \left[\left(\frac{n}{n'}\right)\sin I\right]^2}$$

$$k(Normal\ Surface\ angle) = \begin{bmatrix} 1 \\ -0.17 \\ 0 \\ 0.98 \end{bmatrix}$$

$$\rho' = \sqrt{1 - \left[\left(\frac{1.0003}{1.5}\right)\sin 19.9\right]^2} = 0.9737$$

$n' = Refractive\ index\ of\ material$ = 1.5

$n = Refractive\ index\ of\ air$ = 1.0003

$$\rho = \cos I = \sum K_i k_i$$

$I' = Output\ Incident\ Angle$

$$\rho = \cos 19.9 = 0.93$$

$$K' = \begin{bmatrix} 1 \\ 0.05 \\ 0 \\ 1.00 \end{bmatrix} = 3.15°$$

## Surface 2: Scenario 1 (Solar Altitude 10°)

Absolute incident angle (from surface 1 K') = 3.15°

Normal Surface angle = 74.34°

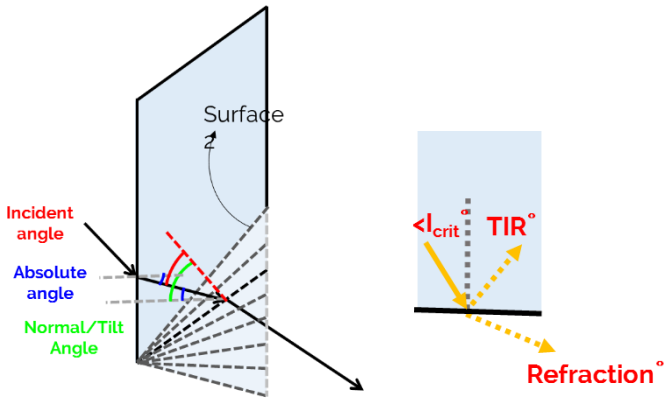


**FIGURE 68 SURFACE 2 INCIDENT ANGLE**

If Incident angle < $I_{crit}$; Use Refraction law.

If Incident angle > $I_{crit}$ ; Use Reflection law.

$$I_{crit} = \sin^{-1}\left(\frac{n'}{n}\right) = \sin^{-1}\left(\frac{1.5}{1.0003}\right) = 41.68°$$

Incident angle = Normal Surface angle – Solar Altitude = 71.19° > 41. Use Reflection Law.

**Reflection Law**

$$\begin{pmatrix} 1 \\ K'_x \\ K'_y \\ K'_z \end{pmatrix} = R' \begin{pmatrix} 1 \\ K_x \\ K_y \\ K_z \end{pmatrix} \qquad R' = \begin{pmatrix} 1 & 0 & 0 & 0 \\ -2k_x\rho & 1 & 0 & 0 \\ -2k_y\rho & 0 & 1 & 0 \\ -2k_z\rho & 0 & 0 & 1 \end{pmatrix}$$

$$\rho = \cos I = \sum K_i k_i$$

$$\rho = \cos 71.19 = 0.32$$

$$K' = \begin{bmatrix} 1 \\ -0.57 \\ 0 \\ 0.82 \end{bmatrix} = -34.46°$$

## Surface 3: Scenario 1 (Solar Altitude 10°)

Absolute incident angle (from surface 2 K') = -34.46°

Normal Surface angle = -33.16°

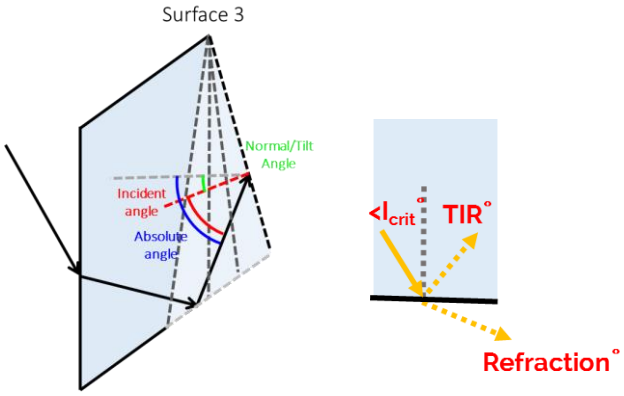


**FIGURE 69 SURFACE 3 INCIDENT ANGLE**

If Incident angle < $I_{crit}$; Use Refraction law.

If Incident angle > $I_{crit}$ ; Failed case.

Incident angle = -34.46 – (-33.16) = 1.29° < Incident angle. ∴ Refraction occurs

Use refraction Law:

K = 35.11°

**TABLE 21 TABLE WITH ALL INCIDENT OUTPUT ANGLES FROM SURFACES 1 2 AND 3 FOR SCENARIO 1**

| SOLAR ALTITUDE | | SURFACE 1 | SURFACE 2 | SURFACE 3 | FINAL |
|---|---|---|---|---|---|
| | | -9.99 | 74.34 | -33.17 | EXITING RAY |
| 10 | Absolute | 3.15 | -34.46 | 35.11 | 35.11 |
| | Incident | 20.00 | 71.19 | 1.29 | |
| 20 | Absolute | 9.42 | -40.74 | 44.41 | 44.41 |
| | Incident | 30.00 | 64.92 | 7.57 | |
| 30 | Absolute | 15.31 | -46.63 | 52.67 | 52.67 |
| | Incident | 40.00 | 59.03 | 13.46 | |
| 40 | Absolute | 20.63 | -51.95 | 59.52 | 59.52 |
| | Incident | 50.00 | 53.71 | 18.78 | |
| 50 | Absolute | 25.17 | -56.48 | 64.84 | 64.84 |
| | Incident | 60.00 | 49.17 | 23.31 | |
| 60 | Absolute | 28.68 | -60.00 | 68.60 | 68.60 |
| | Incident | 70.00 | 45.66 | 26.83 | |
| 70 | Absolute | 30.92 | -62.23 | 70.83 | 70.83 |
| | Incident | 80.00 | 43.42 | 29.06 | |
| 80 | Absolute | 31.69 | -63.01 | 71.57 | 71.57 |
| | Incident | 90.00 | 42.65 | 29.84 | |

# Appendix B: Five-Phase Method

1. Model the Room/Environment

2. Model on a separate layer a surface that indicates the fenestration glazing system in relation to the inner side of the room and assign “Glow” material and rename it to *viewmtxsrf*. N.B. Make sure the normal direction of the surface is facing the inside of the room

3. Model another surface that has a relation with the sky and the outer side of the room, while having its normal direction facing outside the room. Assign this surface “Glow” material also and name it *daymtxsrf.*

4. Insert points which will act as illuminance sensor points in the Radiance simulation afterwards.

5. Model the geometry of the fenestration system in place.

6. Copy the fenestration system, rotate it around the X axis for 90° degrees in clockwise direction and move it under the horizontal line (Z-axis) of your model space and export the geometry alone to create a BSDF, where the Z positive is the outside of the space and Z negative is the inside.

7. Extract the previous geometry and use it to generate a BSDF function for the geometry (.xml file)

   ```
   “genbsdf.exe materials.rad CFS.rad >CFS.xml”
   ```

8. Setup the Daylight and View matrices files using radiance’s *rfluxmtx* command
   a. As for the Daylight matrix make sure to include the receiver file (which is a simple geometry representing the position of the complex geometry. Also include the sky geometry and environment along with the rest of the model and its materials.

      ```
      “rfluxmtx.exe -ab 2 -ad 5000 -lw 1e-4 -c 10000 CFS.rad sky.rad
      materials.rad model.rad > daylight.dmx”
      ```

   b. Concerning the View Matrix a sender file should be included “with glow materials” along with the model and model materials.

      ```
      “rfluxmtx.exe -n 4 -faa -I+ -ab 6 -ad 50000 -lw 2e-5 -y 20
      <points.rad - bot.rad materials.rad model.rad > view_matrix.vmx”
      ```

9. After obtaining a daylight and view matrices as well as a BSDF file, generate a sky matrix of the location of your model using one of the suitable weather files.

   ```
   “gendaymtx.exe Cairo.wea > cairo.smx”
   ```

10. Having all three matrices and a BSDF file, combine them together by the “Rmtxop” function using the following line to ensure the results are in the form of illuminance.

    ```
    “rmtxop.exe view_matrix_without_glow.vmx CFS.xml daylight.dmx Cairo.smx |
    rmtxop.exe -fa -c 47.4 119.9 11.6 - > final_3phase.txt”
    ```

11. Generate the daylight and view matrices with the direct flux component only:
    a. First, the room's surfaces should be converted into black material to avoid specular reflection of rays

       "xform.exe –m black room.rad > room_black.rad"

    b. Direct Daylight matrix can be generated using a zero ambient bounces scene and black materials on the room surfaces

       "rfluxmtx.exe -ab 0 -ad 50000 -lw 1e-5 -c 10000 CFS.rad sky.rad materials.rad model_black.rad > daylight_d.dmx"

    c. View matrix with direct component only, however the direct view matrix will be created with 1 ambient bounce

       "rfluxmtx.exe -faa -I+ -ab 1 -ad 20000 -lw 1.52e-5 -y 45 <points.pts - viewsurf.rad materials.rad room_black.rad > viewmatrix_direct.vmx"

    d. Generate the direct Sky component using the –d command within the gendaymtx

       "gendaymtx.exe -d cairo.wea > cairo_direct.smx"

    e. Combine the 3 matrices generated above along with the BSDF file

       "rmtxop.exe view_direct\viewmatrix_direct.vmx genbsdf\CFS.xml daylight_direct\daylight_d.dmx sky\cairo_direct.smx | rmtxop.exe -fa -c 47.4 119.9 11.6 -t - > i_ds3ph.txt"

12. Afterwards create the radiance scene description for the more accurate direct sun coefficient as well as the sky with sun only component, where a sky with all the sun's energy in a single patch is created.
    a. For the direct sun coefficient, the proxied geometry of the BSDF can be used in the model for more accurate representation of the scene, especially if it will be visualized.

       "rcontrib.exe < points.pts -I -ab 1 -ad 65536 -lw 1.52e-5 -dc 1 -dt 0 -dj 1 -st 1 -ss 0 -faa -e MF:1 -f reinhart.cal -b rbin -bn Nrbins -m solar room_suns.oct > directsun.dsmx"

    b. For the sky sun component, use the *-5* command with the *gendaymtx* to create the desired sky description

       "gendaymtx.exe -5 -d -m 1 cairo.wea > cairo_direct_m1.smx"

    c. Combine both terms together to form the direct sun related matrix

       "rmtxop.exe sun_coefficent\directsun.dsmx sky\cairo_direct_m1.smx | rmtxop.exe -fa -c 47.4 119.9 11.6 -t - > i_ds5ph.txt"

13. Having all three final matrices, combine them together by the "Rmtxop" function followed by another command line to ensure the results are in the form of illuminance.

       "rmtxop.exe i_3ph.txt + -s -1 i_ds3ph.txt + i_ds5ph.txt > Final_5ph.txt"

# BIBLIOGRAPHY

# Bibliography


Alstan, J. (2014). DIVA for Rhino. *Software*. Retrieved from www.diva4rhino.com

Andersen, M., Bodart, M., Culter, B., Kleindienst, S., Lee, J., & Yi, L. (2008). An intuitive daylighting performance analysis and optimization approach. *Building Research & Information, 36*(6).

Asdrubali, F., & Baldinelli, G. (2009). Theoretical modelling and experimental evaluation of the optical properties of glazing systems with selective films. *Building Simulation, 2*(2), 75-84. doi:10.1007/s12273-009-9112-5

Basurto, C., Kampf, J., & Scartezzini, J. (2015). Annual Performance Assessment of Complex Fenestration Systems in Sunny Climates Using Advanced Computer Simulations. *Journal of Daylighting*, 32-43.

Bueno, B., Wienold, J., Katsifaraki, A., & Kuhna, T. (2015). A Radiance-based modelling approach to assess the thermal and daylighting performance of complex fenestration systems inoffice spaces. *Energy and Buildings*, 10-20. doi:10.1016/j.enbuild.2015.02.038

Building Technologies Program. (2014, July 31). *The RADIANCE 4.2 Synthetic Imaging System*. (Lawrence Berkeley National Laboratory) Retrieved March 25, 2016, from Radiance Site http://radsite.lbl.gov: http://radsite.lbl.gov/radiance/refer/ray.html

Bülow-Hübe, H. (2001). *Energy-Efficient Window - Effects on Energy Use and Daylight.* Doctoral Dissertation, Lund University.

Buß, T., Teisseire, J., Mazoyer, S., & Sondergard, E. (2013, February). Controlled angular redirection of light via nanoimprinted disordered gratings. *Applied Optics, 52*(4), 709-716.

Carlos, O., Myriam, A., & Jan, H. (2012, July). State of the art in lighting simulation for building science: A literature review. *Journal of Building Performance Simulation, 5*(4), 209-233. doi:10.1080/19401493.2011.558211

Carmody, J. (2007). High performance windows and facades. *EcoBuild Federal Conference.* Washington, DC: Center for Sustainable Building Research (CSBR).

Chan, Y., & Tzempelikos, A. (2012). A hybrid ray-tracing and radiosity method for calculating radiation transport and illuminance distribution in spaces with venetian blinds. *Solar Energy, 86*(11), 3109–3124. doi:10.1016/j.solener.2012.07.021

Cheung, H., & Chung, T. (2008). A study on subjective preference to daylit residential indoor environment using conjoint analysis. *Building and Environment, 43*(12), 2101-2111. doi:10.1016/j.buildenv.2007.12.011

*CODE V Optical Design Software*. (2014). Retrieved from Synopsys: https://optics.synopsys.com/codev/

Cuce, E., & Riffat, S. (2015). Vacuum tube window technology for highly insulating building fabric: an experimental and numerical investigation. *Vacuum, 111*, 83-91. doi:10.1016/j.vacuum.2014.10.002

Cuttle, C. (1983). People and windows in workplaces. *Proceedings of the people and physical environment research conference*, (pp. 203-212). Wellington, New Zealand.

Dávila, C. (2014). *On advanced daylighting simulations and integrated performance assessment of complex fenestration systems for sunny climates.* Lausanne: École Polytechnique Fédérale De Lausanne.

Edmonds, I., & Pearce, D. (1999). Enhancement of crop illuminance in high latitude greenhouses with laser-cut panel glazing. *Solar Energy, 66*(4), 255-265.

Egyptian Energy Effeciency for Building Code Comittee. (2006). *Egyptian Energy Effeciency for Building Code.* Housing and Building National Research Center, Egyptian Ministry of Housing and Development. Cairo, Egypt: Housing and Building National Research Center.

El Haggar, S. (2007). *Sustainable Industrial Design and Waste Management.* Elsevier.

El-Henawy, S., Mohamed, M., Mashaly, I., Mohamed, O., Galal, O., Taha, I., . . . Safwat, A. (2014). Illumination of dense urban areas by light redirecting panels. *Optics Express, 22*(S3), A895-A907. doi:10.1364/OE.22.00A895

*Fabric energy efficiency for zero carbon homes - A flexible performance standard for 2016*. (2014). Retrieved 04 15, 2016, from ZeroCarbonHub: www.zerocarbonhub.org

Fang, Y., Hyde, T., Arya, F., & Hewitt, N. (2013). *A novel building component hybrid vacuum glazing: a modelling and experimental validation.* ASHRAE Trans.

Fernandez-Balbuena, A., Vázquez-Moliní, D., Garcia-Fernandez, B., Garcia-Botella, A., & Bernabeu, E. (2009). Skylight: a hollow prismatic CPC. *SPIE 7423, Nonimaging Optics: Efficient Design for Illumination and Solar Concentration VI.* San Diego, CA. doi:10.1117/12.825818

Frost, K., Eto, J., Arasteh, D., & Yazdanian, M. (1996). The national energy requirements of residential windows in the U.S. *ACEEE Proceedings on energy efficiency in buildings.* Pacific Grove, Canada.

Furniss, J. (2015). Alternative framings of transnational waste flows: reflections based on the Egypt–China PET plastic trade. *Area, 47*(1), 24–30. doi:10.1111/area.12160

García-Fernández, B., Vázquez-Molini, D., & Fernández-Balbuena, A. (2011). Lighting quality for aluminum and prismatic light guides. *SPIE 8170, Illumination Optics II.* Marseille, France: SPIE. doi:10.1117/12.896814

Granqvist, C. (1995). *Handbook of inorganic electrochromic materials.* Amsterdam: Elsevier.

Han, K., & Kim, J. (2011). Reflectance modulation of transparent multilayer thin films for energy efficient window applications. *Materials Letters, 65*(15-16), 2466–2469. doi:10.1016/j.matlet.2011.05.006

Han, Z., Boa, Y., Wu, W., Liu, Z., Liu, X., & Tian, Y. (2012). Evaluation of thermal performance for vacuum glazing by using three-dimensional finite element model. *2nd Annual Meeting on Testing and Evaluation of Inorganic Materials*, *492*, pp. 328-332. Changsha, China. doi:10.4028/www.scientific.net/KEM.492.328

Hasan, M., Abdul Malek, A., Haseeb, A., & Masjuki, H. (2010). Investigations on TiO2 and Ag based single and multilayer films for window glazings. *Journal of Engineering and Applied Sciences, 5*(9), 22-28. Retrieved from https://www.scopus.com/record/display.uri?eid=2-s2.0-78649729580&origin=inward&txGid=0

Hee, W., Alghoul, M., Bakhtyar, B., Elayeb, O., Shameri, M., Alrubaih, M., & Sopian, K. (2015). The role of window glazing on daylighting and energy saving in buildings. *Renewable and Sustainable Energy Reviews, 42*, 323-343.

Hopkinson, R. (1963). *Architectural Physics - Lighting.* London: Her Majesty's Stationery Office.

Housing and Building Research Center. (2006). *Code: ECP 306-2005 Egyptian Code for building energy conservation.* Cairo, Egypt: Housing and Building Research Center.

Huang, T., Hocheng, H., Chou, T., Yang, W., Ting, C., Cheng, K., & Hsieh, C. (2015). Design and fabrication of sunlight-redirecting and infrared-insulating microstructure. *Energy and Buildings, 90*, 114-126. doi:10.1016/j.enbuild.2014.12.051

IEC 61966-2-2. (2003). *Multimedia systems and equipment - Colour measurement and management - Part 2-1: Colour management - Default RGB colour space - sRGB*, 51. Retrieved from http://www.colour.org/tc8-05/Docs/colorspace/61966-2-1.pdf

Ihm, P., Nemri, A., & Krarti, M. (2009). Estimation of lighting energy savings from daylighting. *Building and Environment, 44*(3), 509-514. doi:10.1016/j.buildenv.2008.04.016

Illuminating Engineering Society. (2013). IES: LM-83–12. *Approved Method: IES spatial daylight autonomy (sDA) and annual sunlight exposure (ASE)*.

International Telecommunication Union. (2015, June 17). BT.709-6. *Parameter values for the HDTV standards for production and international programme exchange*. Retrieved from https://www.itu.int/rec/R-REC-BT.709/en

Iskandar, L. (2003). Integrating local community-based waste management into international contracting. *Solid waste collection that benefits the urban poor.* Dar as salaam.

Kämpf, J., & Scartezzini, J. (2011). GERONIMO: the CFS Daylighting Wizard. *4th VELUX Daylight Symposium.* Lausanne, Switzerland.

Kämpf, J., Basurto, C., & Scartezzini, J. (2011). *Visualization of the impact of complex fenestration systems based on Radiance.* Retrieved from http://leso.epfl.ch/page-75134-fr.html

Kischkoweit-Lopin, M. (1997). Architektur auf der Sonnenspur. *HEW (Hrsg.).* Hamburg, Germany.

Kischkoweit-Lopin, M. (2002). An Overview of Daylighting Systems. *Solar Energy, 73*(2), 77-82. doi:10.1016/S0038-092X(02)00036-1

Klammt, S., Neyer, A., & Muller, H. (2012, April). Microoptics for efficient redirection of sunlight. *Applied Optics, 51*(12), 2051-2056. doi:10.1364/AO.51.002051

Klems, J. (1994). A new method for predicting the solar heat gain of complex fenes-tration systems. Overview and derivation of the matrix layer calculation. *Proceedings of the ASHRAE Winter Meeting*, *100*, pp. 1065-1072. New Orleans, LA.

Lardinos, I., & Van de Klundert, A. (1995). Plastic Waste: Options for Small-Scale Resource Recovery. *Urban Solid Waste Series 2.* Amsterdam: The TOOL Publications.

Lim, Y., Kandar, M., Ahmad, M., Ossen, D., & Abdullah, A. (2012). Building façade design for daylighting quality in typical government office building. *Building and Environment, 57*, 194-204. doi:10.1016/j.buildenv.2012.04.015

Mardaljevic, J., Heschong, L., & Lee, E. (2009, September). Daylight metrics and energy savings. *Lighting Research and Technology, 41*(3), 261-283. doi:10.1177/1477153509339703

McNeil, A. (2013, September 11). The Five-Phase Method for Simulating Complex Fenestration with Radiance. Retrieved from Radiance-Online: www.radiance-online.org

Mcneil, A. (2013). *The Three-Phase Method for Simulating Complex Fenestration with Radiance.*

Mcneil, A. (2015, August 18). Putting Radiance to Work - Modeling Glass Block. *14th International Radiance Workshop*. Philadelphia, USA. Retrieved from http://www.radiance-online.org/community/workshops/2015-philadelphia

McNeil, A., Jonsson, C., Appelfeld, D., Ward, G., & Lee, E. (2013). A validation of a ray-tracing tool used to generate bi-directional scattering distribution functions for complex fenestration systems. *Solar Energy, 98*(C), 404–414. doi:10.1016/j.solener.2013.09.032

McNeil, A., Jonsson, J., & Appelfeld, D. (2011). Validation of genBSDF. *10th International Radiance Workshop.*

Mead, D. (2010). 'Trans' Materials Modeling and Specifying a Next Generation. *9th International Radiance Workshop.* Freiburg, Germany.

Moeck, M., & Selkowitz, S. (1996). A computer-based daylight systems design tool. *Elsevier, 5*, 193-209.

Nabil, A., & Mardaljevic, J. (2005). Useful daylight illuminance: a new paradigm to access daylight in buildings. *Lighting Research and Technology, 37*(1), 41-59. doi:10.1191/1365782805li146ed

Nassar, K., Safwat, A., Darwish, A., El-Henawy, S., Mashaly, I., Mohamed, O., & Mohamed, M. (2014). Designing a Light Redirecting System for Southern Skies. *Proceedings of the 2014 Building Simulation and Optimization Conference*, (pp. 1-7).

Nicholls, R., & Dennis Hall, K. (2004). *Green Building Bible: In Depth Technical Information and Data on the Strategies and Systems Needed to Create Low Energy, Green Buildings* (Vol. 2). Green Building Press.

Ochoa, C., Aries, M., & Hensen, J. (2011). State of the art in lighting simulation for building science: a literature review. *Building Performance Simulation*.

*OSLO*. (2001). Retrieved from Lambda Research Corporation: http://www.lambdares.com/oslo

Padiyath, R. (2013). *Daylight Redirecting Window Films.* 3M Company. St. Paul, MN: 3M Company.

Papaefthimiou, S., Leftheriotis, G., & Yianoulis, P. (2001). Advanced electrochromic devices based on WO3 thin films. *Electrochim Acta, 46*, 2145-50.

Paule, B., Flourentzou, F., & Bauer, M. (n.d.). *Estia. Mise en oeuvre du développement durable dans l'environnement construit.* Retrieved from Estia: www.estia.ch

Perez, R., Seals, R., & Michalsky, J. (1993). All-Weather Model for Sky Luminance Distribution, preliminary. *Solar Energy, 50*(3), 235-245.

Perez-Lombard, L., Ortiz, J., & Pout, C. (2008). A review on buildings energy consumption information. *Energy and Buildings, 40*(3), 394-398. doi:10.1016/j.enbuild.2007.03.007

*Product Information SGG LUMITOP.* (2008). Retrieved from Saint-Gobain Glass: http://uk.saint-gobain-glass.com/upload/files/sgg_lumitop_.pdf 2008

Reinhart, C., & Andersen, M. (2006, July 7). Development and validation of a Radiance model for a translucent panel. *Energy and Buildings, 38*(7), 890-904. doi:10.1016/j.enbuild.2006.03.006

Reinhart, C., & Breton, P.-F. (2009). Experimental validation of 3Ds Max design 2009 and Daysim 3.0 in Building Simulation. *Eleventh International IBPSA Conference 2009.* Glasgow, Scotland: IBPSA.

Reinhart, C., & Fitz, A. (2006). Findings from a survey on the current use of daylight simulations in building design. *Energy and Buildings,, 38*(7), 824-835.

Reinhart, C., & Walkenhorst, O. (2001). Dynamic RADIANCE-based daylight simulations for a full-scale test office with outer venetian blinds. *Energy & Build, 33*(7), 683–697.

Reinhart, C., & Wienold, J. (2016). DAYSIM. *Software for daylight prediction*. Retrieved 2016, from http://www.daysim.com/

Reinhart, C., Jakubiec, J., & Ibarra, D. (2013). Definition of a Reference Office for Standardized Evaluations of Dynamic Façade and Lighting Technologies. *13th Conference of International Building Performance Simulation Association.* Chambéry.

Robinson SJ, C. R. (1989). Evacuated windows-theory and practice. *Proceeedings of the ISES Solar World Congress.* Kobe, Japan: International Solar Energy Society.

Rousseau, M. (1988). *Building Science Insight.* Technical Report.

Rubbert, F. (1999). Sundirecting Glazing - A New Development in Daylighting for Deep Plan Offices. *Glass in Buildings* (pp. 85-90). Bath, UK: University of Bath.

Sabry, H., Sherif, A., & Gad Elhak, M. (2012). Utilization of Combined Daylighting Techniques for Enhancement of Natural Lighting Distribution in Clear-Sky Residential Desert Buildings. *PLEA.* Lima, Peru.

Sadineni, S. B., Madala, S., & Boehm, R. F. (2011). Passive building energy savings: A review of building envelope components. *Renewable and Sustainable Energy Reviews, 15*(8), 3617–3631. doi:10.1016/j.rser.2011.07.014

Scartezzini, J.-L. (1994). Laboratoire de Lumiere Naturelle, Programme Interdisciplinaire LUMEN, Projet OFEN. *Université de Genève, Ecole Polytechnique Fédérale de Lausanne.* Lausanne: Ecole Polytechnique Fédérale de Lausanne.

Scientific Polymer, Inc. (2013). *Refractive Index of Polymers by Index*. Retrieved from Scientific Polymer, Inc.: http://scientificpolymer.com/technical-library/refractive-index-of-polymers-by-index/

Shell, K., Brown, S., Schuetz, M., Davis, R., & French, R. (2011). Design and performance of a low-cost acrylic reflector for a ~7x concentrating photovoltaic module. *SPIE 8108, High and Low Concentrator Systems for Solar Electric Applications VI.* San Diego, CA: SPIE. doi:10.1117/12.897763

Sherif, A., Sabry, H., Elzafarany, A., Gadelhak, M., Arafa, R., & Aly, M. (2015). The Impact of Hospital Intensive Care Unit Window Design on Daylighting and Energy Performance in Desert Climate. *ICEESD 2015 : 18th International Conference on Energy, Environment and Sustainable Development*, *1.* Paris, France.

Sherif, A., Sabry, H., Wagdy, A., & Arafa, R. (2015). Daylighting in Hospital Patient Rooms: Parametric Workflow and Genetic Algorithms for an Optimum Façade Design. *BS2015: 14th Conference of International Building Performance Simulation Association (IBPSA).* Hyderabad, India: IBPSA.

Sherif, A., Sabry, H., Wagdy, A., Mashaly, I., & Arafa, R. (2016, March 27). Shaping the slats of hospital patient room window blinds for daylighting and external view under desert clear skies. *Solar Energy, 133*, 1-13. doi:10.1016/j.solener.2016.03.053

Stokes, M., Anderson, M., Chandrasekar, S., & Motta, R. (1996, November 5). *A Standard Default Color Space for the Internet - sRGB.* Retrieved from https://www.w3.org/Graphics/Color/sRGB

Sullivan, R., & Selkowitz, S. (1985). Window Performance Analysis in a Single-family Residence. *Lawrence Berkeley National Laboratory*, 1-22.

Thanachareonkit, A. (2008). Comparing physical and virtual methods for daylight performance modelling including complex fenestration systems. *LESO-PB*.

Thanachareonkit, A., Lee, E., & McNeil, A. (2013). Empirical assessment of a prismatic daylight-redirecting window film in a full-scale office testbed. *IESNA 2013.* Huntington Beach, CA: IESNA.

*TracePro*. (2014, November). Retrieved from Lambda Research Corporation: http://www.lambdares.com/tracepro

Tripathi, D. (2002). *Practical Guide to Polypropylene.* Smithers Rapra. Retrieved April 22, 2016, from http://site.ebrary.com/lib/aucairo/detail.action?docID=10236790#

*Validation case test CIE-171-2006.* (2013, February). Retrieved from http://www.dialplus.ch/#!df/cvwa

van Hoof, J., Westerlaken, A., Aarts, M., Wouters, E., Schoutens, A., Sinoo, M., & Aries, M. (2012). Light therapy: Methodological issues from an engineering perspective. *Technology and Health Care, 20*, 11-23.

Vanderwerf, D. (2010). *Applied Prismatic and Refrective Optics.* Bellingham, Washington USA: SPIE.

Vilaplana, F., & Karlsson, S. (2008). Quality Concepts for the Improved Use of Recycled Polymeric Materials: A Review. *Macromolecular Materials and Engineering, 293*(4), 274-297. doi:10.1002/mame.200700393

*Visible Transmittance (VT or Tvis)*. (2015, April 22). (Lawrence Berkeley National Laboratory, University of Minnesota) Retrieved April 22, 2016, from Commercial Windows: http://www.commercialwindows.org/vt.php

Vlachokostas, A. (2012, November). Liquid filled prismatic louver façade for enhanced indoor natural lighting in commercial buildings. *Optical Nanostructures and Advanced Materials for Photovoltaics.*

Walze, G., Nitz, P., Ell, J., Georg, A., Gombert, A., & Hossfeld, W. (2005). Combination of microstructures and optically functional coatings for solar control glazing. *Solar Energy Materials and Solar Cells, 89*(2-3), 233-248. doi:10.1016/j.solmat.2004.11.016

Walze, G., Nitz, P., Ell, J., Georg, A., Gombert, A., Bläsi, B., & Hoßfeld, W. (2005). Combination of Microstructures and Optically Functional Coatings for Solar Control Glazing. *Solar Energy Materials and Solar Cells, 89*(2-3), 233-248.

Ward, G., & Shakespeare, R. (2004). *Rendering With Radiance: The Art And Science Of Lighting Visualization.*

Ward, G., Mistrick, R., Lee, E., McNeil, A., & Jonsson, J. (2013). Simulating the Daylight Performance of Complex Fenestration Systems Using Bidirectional Scattering Distribution Functions within Radiance. *The Journal of the Illuminating Engineering Society of North America, 7*(4), 241-261. doi:10.1080/15502724.2011.10732150

*Zemax*. (2014). Retrieved from Zemax, LLC: http://www.zemax.com/

Zoller, F. (1924). *German Patent No. 387655.*